Characterization of proteasome shuttling factors and their impact on misfolded proteins in age-related neurodegenerative diseases

Thesis

to obtain the academic degree of

Doctor medicinae (Dr.med.)

submitted to the Faculty of Medicine of

Martin Luther University Halle-Wittenberg

by Judith-Elisabeth Riemer

Supervisors:

Prof. Rüdiger Horstkorte, Institute of Physiological Chemistry, Martin Luther University Halle-Wittenberg, Germany

Prof. Heidi Olzscha, Institute of Molecular Medicine, Medical School Hamburg (MSH), Hamburg, Germany

Reviewers:

Prof. Dr. Niko Hensel, Halle (Saale)

Prof. Dr. Tobias Piegeler, Leipzig

Date of the defense: 02.10.2024

Table of Contents

I. Index of Figures

II. Abbreviation Index

ANOVA	Analysis of variance
APS	Ammonium persulfate
BCA	Bicinchoninic acid
BrdU	5-bromo-2'-deoxyuridine
BSA	Bovine serum albumin
CO-IP	Coimmunoprecipitation
CRISPR	Clustered Regularly Interspaced Short Palindromic Repeats
DMEM	Dulbecco's Modified Eagle's Medium
DMSO	Dimethyl sulfoxide
DTT	Dithiothreitol
EDTA	Ethylenediaminetetraacetic acid
EGTA	Ethylene glycol-bis(β-aminoethyl ether)-N,N,N′,N′-tetraacetic acid
FBS	Fetal bovine serum
GFP	Green fluorescent pigment
HA-Tag	Human influenza hemagglutinin-Tag
HD	Huntington's Disease
HDACi	Histone deacetylase inhibitor
HR23A/B	Human homolog of Rad23A /Rad23B
Htt	Huntingtin
IB	Inclusion body
IF	Immunofluorescence
IP	Immunoprecipitation
KO	Knockout
MHC	Major histocompatibility complex
N/C ratio	Nuclear/cytoplasmic ratio
NER	Nucleotide excision repair
PBS	Phosphate buffered saline
PI	Propidium iodide
PMSF	Phenylmethylsulfonylfluoride
PQC	Protein quality control
PTM	Post translational modification
Rad23A/B	UV excision repair protein RAD23 homolog A/B
SAHA	Suberoylanilide hydroxamic acid
SDS	Sodium dodecyl sulfate
SH-SY5Y	Human neuroblastoma cell
TEMED	Tetramethylethylendiamine
TRIS	Tris(hydroxymethyl)aminomethane
U2OS	Human bone osteosarcoma epithelial cell
Ub	Ubiquitin
UbA	Ubiquitin-Associated
UbL	Ubiquitin-Like
UPS	Ubiquitin Proteasome System
WB	Western Blot
WT	Wild type

1. Introduction

1.1. Protein quality control

Human cells are in a constant state of equilibrium, in which proteins are newly synthesized and degraded. This state of protein homeostasis is also called proteostasis. For it to be realized, cells need mechanisms that control processes concerning translation of new proteins and protein quality control.

In an average human cell, more than 10,000 different proteins are synthesized, each with a specific native structure and function. Proteins are macromolecules consisting of an amino acid sequence, which is encoded in their genes. After translation, this polypeptide chain is folded to form secondary and tertiary structures and eventually native conformation. Considering the Anfinsen hypothesis (Anfinsen 1973), this process follows the global free energy minimum resulting in the ultimate native confirmation of a protein, which is also the most thermodynamically stable (Varela, England, and Cavagnero 2019) (see figure 1). However, due to the high number of possible conformations of each protein, the process of protein folding is prone to errors.

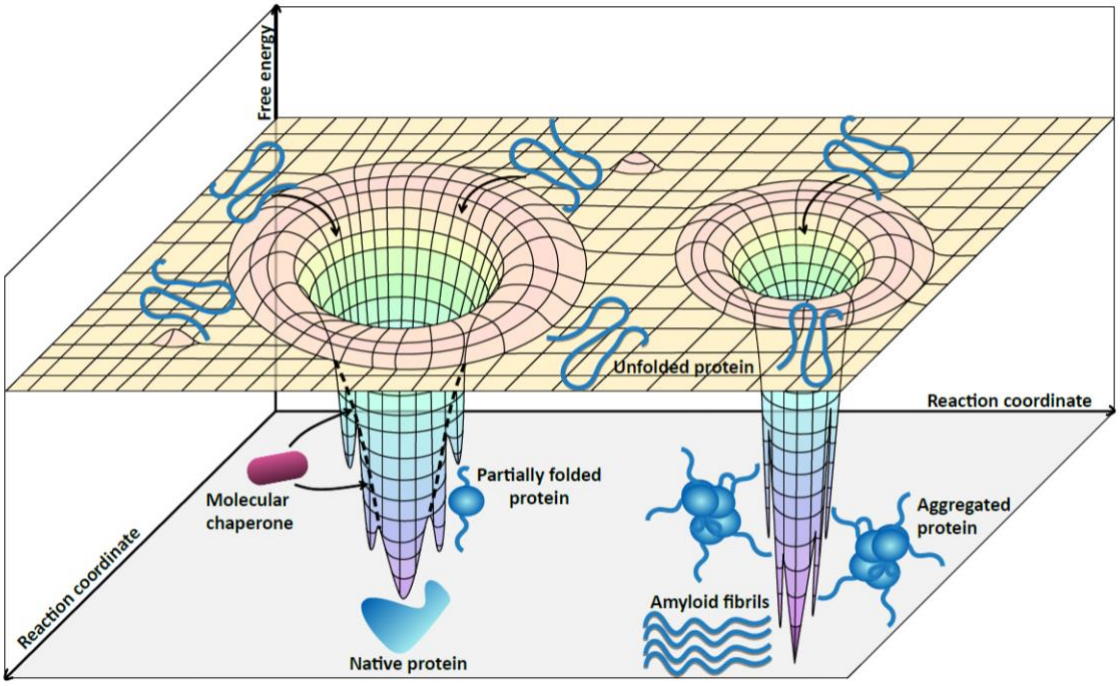

Figure 1: Protein folding and misfolding energy landscape.

During protein folding, unfolded proteins may have to surpass high free energy stages to “fall” into the folding funnel and reach their native conformation, thereby minimizing their free energy level. Molecular chaperones help to prevent trapping of partially folded proteins in low energy states. In case of protein misfolding, aggregated proteins can reach low free energy states and even form highly stable amyloid fibrils. (Adapted from book chapter: **Riemer** et al. 2021 “Protein folding and misfolding: Deciphering mechanisms of age-related diseases” in book “Proteostasis and Proteolysis”)

There are different systems in place to ensure correct protein folding. Molecular chaperones play a key role as they monitor correct protein translation and facilitate the folding process starting at the ribosome. As the nascent chain emerges, molecular chaperones help protect exposed hydrophobic residues and prevent protein misfolding or PTMs that tag the protein for degradation (Hartl 1996). Protein degradation itself is achieved through the Ubiquitin-Proteasome-System (UPS) or autophagy.

The UPS is a system in which proteins get targeted for degradation with polyubiquitin chains. This can be due to misfolding or damage of the protein, or in line of regulatory processes to prevent an imbalance or unproductive surplus of proteins. In this case, Ubiquitin (Ub) molecules are added in a process called ubiquitination, which will be described in more detail below (see section 1.3). Ub-molecules can then be recognized by Ub-receptors that are part of the proteasome. This leads to the start of the degradation process where the protein is threaded through the proteasome and cleaved into polypeptides (Ross and Pickart 2004). Those oligomeric peptides can further be used to synthesize new proteins or to be presented on a major histocompatibility complex I (MHC I) at the cell's surface, which plays a key role in immune response. There are Ub-receptors that are integral part of the proteasome subunits, which can detect Ub-structures near the proteasome. However, there are also non-integral or soluble Ub-receptors which can detect ubiquitinated proteins that are further away and shuttle them towards the proteasome. These receptors can also be called proteasome shuttling factors.

1.1.1. Proteasome shuttling factors HR23A and HR23B

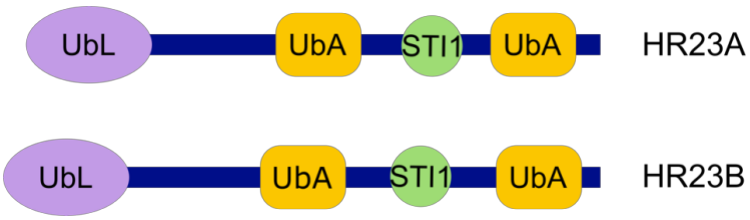

Figure 2: Schematic structure of HR23A and HR23B.

Structural domains of protein shuttling factor HR23A and HR23B. Both proteins contain one UbL, 2 UbA and one STI domain (also XPC binding domain). (Adapted from poster: Kulka, L., **Riemer, J.-E.** et al. 2020 at Cold Spring Harbour conference: Protein homeostasis in health and disease)

Proteasome shuttling factors are proteins that can bind ubiquitinated proteins and facilitate their transport towards the proteasome. In order to do so, they contain Ubiquitin-Like domains (UbL) which can directly interact with the Rpn10 subunit of the proteasome (Heinen et al. 2011) and activate it at the same time, influencing the rate of protein degradation (Collins and Goldberg 2020). The other crucial structure are Ubiquitin-

associated domains (UbA), which can bind polyubiquitin chains (Su and Lau 2009) that for example are attached to proteins that are targeted for degradation.

The shuttling factors that were investigated in this study are human Rad23A (HR23A) and human Rad23B (HR23B) (Elsasser et al. 2004), homologues of Rad23, a protein discovered in *Saccharomyces cerevisiae* for its function in nucleotide excision repair (NER) (Sugasawa et al. 1996). Both proteins contain two C-terminal UbA domains and one N-terminal UbL domain (see figure 2). Additionally, they each contain a stress inducible domain (STI) (or xeroderma pigmentosum C protein (XPC) binding domain) (Kim et al. 2005). HR23A consists of 363 amino acids and is therefore smaller than HR23B with 409 amino acids (Yokoi and Hanaoka 2017). Also, it was shown that HR23B exists in 10 fold higher concentration in human cells compared to HR23A (Okuda et al. 2004).

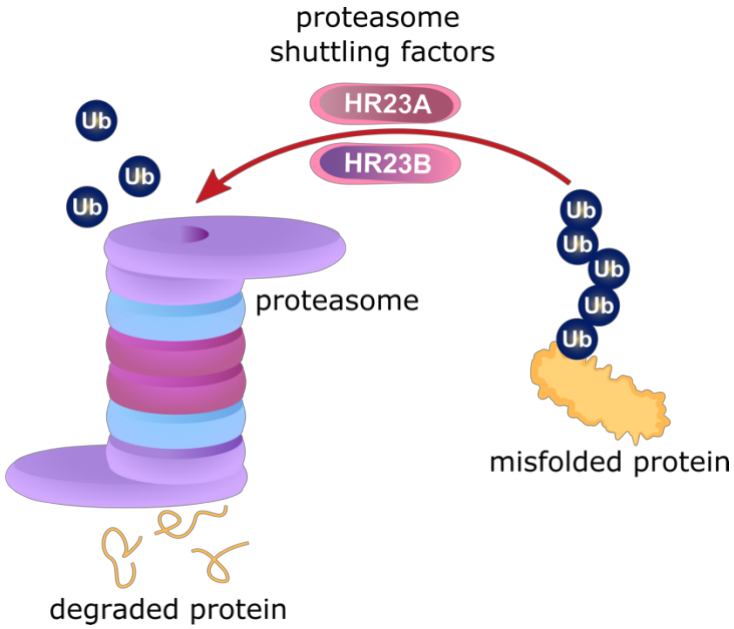

Figure 3: Proteasome shuttling factors facilitate the degradation of misfolded proteins.

Proteasome shuttling factors HR23A and HR23B mimic soluble proteasome receptors and facilitate the transport of ubiquitinated proteins towards the proteasome. The polyubiquitin chain is detached and the target protein degraded. (Adapted from poster: Kulka, L., **Riemer**, J.-E. et al. 2020 at Cold Spring Harbour conference: Protein homeostasis in health and disease)

As mentioned above, HR23A and HR23B are human homologues of Rad23, a protein involved in NER. In 1996 Sugasawa et al. found that is forms a complex with XPC and stabilizes it during its function in DNA repair (Sugasawa et al. 1996). This function was also discovered in HR23A and HR23B and is mostly linked to the STI domain (Araki et al. 2001). Later, HR23A and HR23B's functions in the UPS and in protein quality control were discovered. It has been shown that HR23A and HR23B can facilitate the transport

of misfolded proteins towards the proteasome (New et al. 2013) and interaction with prominent examples of misfolded proteins have been established (Haenig et al. 2020).

What is not yet known is what impact this function has on misfolded proteins in age-related neurodegenerative diseases, whether HR23A and HR23B can replace each other's function and how these proteins influence the general state of proteostasis in a cell.

1.2. Protein misfolding, aggregation and age-related proteinopathies

Due to changes in the amino acid chain or the cellular environment of a protein, the folding dynamic may change and protein misfolding can occur. Misfolded protein species can originate from native proteins but also develop out of intermediate folding stages (Clark 2004). The free energy of a protein is determined by intramolecular interactions of amino acid residues. Any change in the amino acid chain due to mutations, PTMs or non-genetic alterations can therefore influence the folding funnel and possibly create a new global free energy minimum. This way, proteins can get trapped in new, partially folded stable states. Multiple partially folded or misfolded proteins can interact and lead to the formation of aggregates as they often expose hydrophobic residues on their surface (Liu and Eisenberg 2002). On top of that, through nucleation processes, these aggregates can also initiate the development of pre-amyloid oligomers, which can grow into mature amyloid fibrils. Amyloid fibrils are highly organized and consist of cross β structures, a perpendicular arrangement of β-strands along the fibril axis. These aggregates or amyloid structures can be even more stable than native proteins, making spontaneous disassociation into monomers unlikely (Lashuel et al. 2002).

With age, PQC systems can deteriorate in function, increasing their likelihood to reach capacity. As a consequence, protein misfolding and aggregation can occur increasingly and cause pathogenic effects. This becomes apparent when investigating protein-misfolding diseases also called proteinopathies. Here, protein misfolding leads to a number of different toxic processes including aberrant synaptic signalling, neuroinflammation or oxidative stress (Sweeney et al. 2017). These mechanisms are very diverse and seem to differ depending on the misfolded protein itself. Prominent examples of this include alpha synuclein in Parkinson's disease (PD), amyloid-β and Tau in Alzheimer's disease and Htt in Huntington's disease (HD).

1.2.1. Huntington's Disease (HD)

Huntington's disease is a proteinopathy belonging to the group of tandem repeat disorders which affects 4-10/100,000 people and is characterized by abnormal motor movements (chorea), personality changes, dementia and early death. Research has found that a mutation in the Htt gene (also known as IT-15 gene) occurs, increasing the amounts of CAG repeats. This results in an elongated glutamine stretches in exon 1 of Htt, the protein it is coding for. When a certain threshold of glutamine repeats is passed (>36 repeats) (Chen and Wolynes 2017), it leads to a change in folding behavior and ultimately to misfolding and aggregation of the protein. Htt itself is a large protein with an estimated mass of 350 kDa. It is expressed in all human cells, with higher expression levels in brain tissue. It has been linked to several functions, especially involving brain development, interactions with apoptotic cascades and cytoskeletal-related proteins, although its primary function remains unclear (Barron, Hurley, and Parsons 2021).

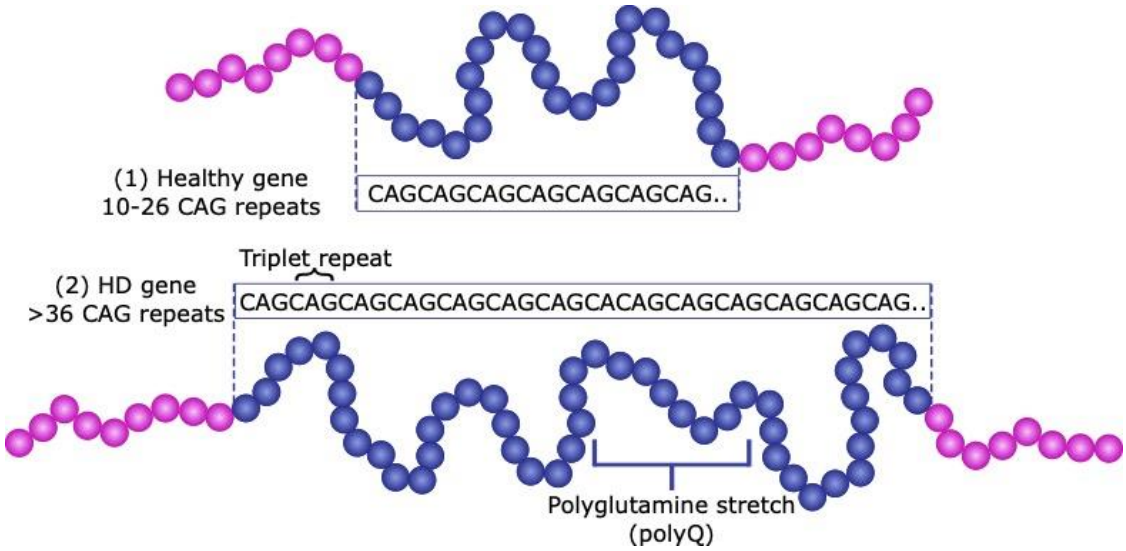

Figure 4: Htt with physiological and pathological number of glutamine repeats.

In the mutated IT-15 gene, CAG repeats increase, leading to a pathological elongation of the polyglutamine stretch in Htt. At a threshold of > 36 repeats, this leads to misfolding of the protein and the development of HD. This figure depicts the simplified structures of a part of exon 1 of Htt with a (1) physiological number of glutamine repeats and (2) a pathological number of glutamine repeats. (Adapted from poster: Kulka, L., **Riemer**, J.-E. et al. 2020 at Cold Spring Harbour conference: Protein homeostasis in health and disease)

Aggregated Htt forms inclusions and has been shown to interfere with neuronal functions, which can be toxic for the cell. The exact pathogenesis of HD is multifactorial and still subject of a lot of research. It has been found that the formation of aggregates and insoluble protein inclusions are vital for the onset and progression of symptoms of HD (Shacham, Sharma, and Lederkremer 2019). On top of that, the CAG repeat length even influences the age of onset. Andrew et al. have shown that the age of onset, which

is usually between 35-50yrs is inversely proportional to the CAG-repeat length (Andrew 1993).

Subject of further investigations is the toxicity of soluble compared to stable amyloid fibrils of Htt. Some theories suggest that the formation of amyloid structures and organization in inclusions might be a protective mechanism of the cell, because it reduces the amount of toxic soluble Htt species (Arrasate et al. 2004). It further has been found that cell toxicity in neurons does not correlate with the number of inclusions (Saudou et al. 1998).

Although most hypotheses focus on the toxicity of mutated Htt, due to its connection to neuroprotective mechanisms, the possibility of toxic loss of Htt function is also subject of research. Complete knockout of wild type (WT) Htt in mice for example lead to embryonic death (Nasir et al. 1995), which shows how vital it is in embryonic development.

1.3. Post translational modifications

During and after translation, proteins can get modified. These modifications are called post-translational modifications (PTMs) and can change the folding dynamic and function of a protein. Common PTMs that will be investigated in this study include acetylation and ubiquitination.

Ubiquitination is a PTM which plays a vital part in the UPS and autophagy. The modification of proteins with single or multiple Ub molecules can target them for degradation (Komander and Rape 2012). The process is highly regulated and occurs with the help of three different enzymes, E1, E2 and E3 ligases (Pickart 2001). Here, Ubiquitin molecules are mostly covalently attached to lysine(*K*)-48-residues, but linkage may also occur on methionine or cysteine residues (Komander and Rape 2012).

The second PTM this study is focusing on is acetylation, which is one of the most prevalent PTMs. Here, acetyl groups can either get added to lysine residues or to the *N*-terminus of a protein. *K*-acetylation can occur post- or co-translationally and is executed through histone acetyltransferases. Removal of acetyl groups can be achieved by histone deacetylases (HDACs). The term “histone”-acetyltransferases/ deacetylases refers to the fact that these enzymes mainly act on histone proteins and therefore play a part in the regulation of transcription. They do, however, modify all other kinds of proteins as well. Generally, the additional acetyl groups lead to a neutralization of the positively charged amino acid lysine. This change can influence the relaxation of chromatin and therefore on transcription but can also alter folding behavior of a protein (Olzscha et al. 2017).

Histone deacetylase inhibitors (HDACi) suppress the function of HDACs, which leads to hyperacetylation. One example of a pan-HDACi is the drug Vorinostat (the commercial name for suberoylanilide hydroxamic acid (SAHA)), which has been approved for the treatment of primary cutaneous t-cell lymphoma (Mann et al. 2007). Treatment of cells with this HDACi has been shown to induce aggregation of Htt and furthermore impairment of the UPS (Olzscha et al. 2017; New et al. 2013). Interestingly, the previously mentioned proteasome shuttling factor HR23B has been shown to be a sensitivity marker for HDACi treatment (Khan et al. 2010). It could be observed that high levels of HR23B lead to more rapid apoptosis whereas cells with lower HR23B levels were more likely be degraded via autophagy (New et al. 2013).

2. Aims of research

The aim of this study is to investigate whether the proteasome shuttling factors HR23A and HR23B can recognize misfolded proteins in age-related neurodegenerative diseases and facilitate their proteasomal degradation. For this purpose, the protein Htt will be investigated in its physiological and pathological form. The expression of Htt will be established in human cells and aggregate formation will be verified by different aggregate stains. It is to be investigated whether HR23A and HR23B influence aggregate morphology and distribution. On top of that a possible protein-protein interaction between the shuttling factors and Htt will be researched.

Concerning the further characterization of HR23A and HR23B, their role in proteostasis and their influence on cell morphology and cell cycle will be investigated. In this context, the influence of PTMs, especially acetylation, will be analyzed using HDACi treatment. It is to be researched whether HR23A and HR23B modulate the effect of HDACi treatment on proteostasis. Furthermore, it will be explored whether acetylation at lysine residues which might compete with ubiquitination leads to a modulation of the degradation of misfolded proteins.

Human cell cultures such as the U2OS cell line (human bone sarcoma epithelial cells) will be used as a model for the study. In these cells, the protein Htt, as well as the proteasome shuttling factors HR23A and HR23B will be co-expressed. In addition, CRISPR/Cas9 generated U2OS knockout cell lines of HR23A and HR23B will be investigated in this context and further characterized. Protein biochemical methods will be used to analyze the distribution and expression of HR23A and HR23B in the different cell lines, as well as their influence on cell morphology, cell cycle and translation rate. The analysis of morphology and distribution of Htt aggregates will be performed by immunofluorescence and filter retardation assay. Evidence of an interaction between the proteasome shuttling factors and pathological Htt will be analyzed using CO-IP. To investigate the influence of acetylation on the function of HR23A and HR23B, cells are treated with the pan-HDAC inhibitor Vorinostat.

3. Material and methods

3.1. Materials

3.1.1. Equipment and expendables

Cell culture equipment	Source
Centrifuge Universal 320	Andreas Hettich GmbH & Co. KG, Tuttlingen, Germany
Countess™ Automated Cell Counter	Thermo Fisher Scientific Inc., Waltham, USA
GFL Waterbath 1003	GFL Gesellschaft für Labortechnik mbH, Burgwedel, Germany
Heraeus HeraCELL incubator	Thermo Fisher Scientific Inc., Waltham, USA
Sterile bench Aura 2000 M.A.C.	EUROCLONE S.p.A., Milan, Italy

Expendables	Source
Cannula BD Microlance™ 3 (27G)	Becton Dickinson GmbH, Heidelberg, Germany
Cannula sterican®, 20G	B. Braun SE, Melsungen, Germany
Cell culture cryogenic tubes	Nunc™/ Thermo Fisher Scientific Inc., Waltham, USA
Cell culture microplate cover	Greiner Bio-One International GmbH, Kremsmünster, Austria
Cell culture microplate, 96 well	Greiner Bio-One International GmbH, Kremsmünster, Austria
Cell scraper 28 cm	Greiner Bio-One International GmbH, Kremsmünster, Austria

Cellstar® cell culture dish (10 cm, 14.5 cm)	Greiner Bio-One International GmbH, Kremsmünster, Austria
Cellstar® cell culture flask (250 ml, 550 ml)	Greiner Bio-One International GmbH, Kremsmünster, Austria
Countess™ cell counting chamber slide	Thermo Fisher Scientific Inc., Waltham, USA
Coverslip Menzel™ 24x60 mm	VWR International, Radnor, USA
Erlenmeyer flask DURAN® 500 ml	Schott AG, Mainz, Germany
Filter Easystrainer™ for 50ml falcons (40 µm)	Greiner Bio-One International GmbH, Kremsmünster, Austria
Filter Filtropur S (0,22 µm)	Sarstedt AG & Co. KG, Nümbrecht, Germany
Glass flask KIMAX™ (50 ml, 100 ml, 250 ml, 500 ml, 1 l)	Thermo Fisher Scientific Inc., Waltham, USA
Gloves Vasco® Nitril non-sterile	B. Braun SE, Melsungen, Germany
Microplates for Operetta® CLS™ PhenoPlate™ (96-Well)	PerkinElmer Inc., Waltham, USA
Nunc™ Lab-Tek™ Chamber Slide System (8-well)	Thermo Fisher Scientific Inc., Waltham, USA
Pasteur pipettes glass (230 mm)	Dr. Ilona Schubert Laborfachhandel, Leipzig, Germany
Pipette tips (5-300 µl)	Brand GmbH & Co. KG, Wertheim, Germany
Pipette tips gel loader (1-200 µl)	Sarstedt AG & Co. KG, Nümbrecht, Germany
Pipette tips SafeSeal filter (10 µl, 200 µl, 1 ml)	Biozym Scientific GmbH, Hessisch Oldendorf, Germany

Pipettes glass (2 ml, 5 ml, 10 ml, 20 ml)	HBG Henneberg-Sander GmbH, Gießen-Lützellinden, Germany
Pipetting aid Automatic-Sarpette®	Sarstedt AG & Co. KG, Nümbrecht, Germany
Reaction tube (15 ml, 50 ml)	Greiner Bio-One International GmbH, Kremsmünster, Austria
Reaction tube rack	A. Hartenstein GmbH, Würzburg, Germany
Reaction tubes (1.5 ml, 2 ml)	Sarstedt AG & Co. KG, Nümbrecht, Germany
Reaction tubes SafeSeal 1.5 ml	Sarstedt AG & Co. KG, Nümbrecht, Germany
Whatman™-Paper (3 mm)	Cytiva, Marlborough, USA

Membranes	Source
Amersham™ Protran® Western-Blotting-Membrane, Nitrocellulose (0.45 µm)	Cytiva, Marlborough, USA
Cellulose acetate Membrane filter (0.22 µm)	Sterlitech Corporation Auburn, USA

Microscopes	Source
Axiovert 100	Carl Zeiss AG, Oberkochen, Germany
Operetta CLS analysis system	PerkinElmer Inc., Waltham, USA
Telaval 31	Carl Zeiss AG, Oberkochen, Germany

Microplate reader	Source
Clariostar® microplate reader	BMG Labtech GmbH, Ortenberg, Germany

Flow cytometer	Source
ChemiDoc™ MP Imaging System	Bio-Rad Laboratories Inc., Hercules, USA

Immunoblot Imaging System	Source
BD Accuri C6	Becton Dickinson GmbH, Heidelberg, Germany

Sonifier	Source
Sonopuls™ Ultrasonic Homogenizer Mini20	BANDELIN electronic GmbH & Co. KG, Berlin, Germany

Mixers	Source
Heating magnetic stirrer FB15001	Thermo Fisher Scientific Inc., Waltham, USA
Vortex Genie 2	Sigma-Aldrich, St. Louis, USA
Vortex mixer MS2	IKA®-Werke GmbH & Co. KG, Staufen, Germany

pH meter	Source
HI2210	Hanna® Instruments Inc., Woonsocket, USA

PAGE equipment	Source
Bio-Dot® Apparatus	Bio-Rad Laboratories Inc., Hercules, USA
Dual Cool C.B.S. Scientific DCX-700	Thermo Fisher Scientific Inc., Waltham, USA
Gel Doc XR+ system	Bio-Rad Laboratories Inc., Hercules, USA
Mini Gel tank	Thermo Fisher Scientific Inc., Waltham, USA
Mini vertical system C.B.S. Scientific EBX-700	Thermo Fisher Scientific Inc., Waltham, USA
Novex™ WedgeWell™ 4-20% Tris-Glycine gel	Thermo Fisher Scientific Inc., Waltham, USA
Universal heat sealer ES 300	Geho Pack Service GmbH, Heidgraben, Germany

Pipettes	Source
Eppendorf Reference 2 Variable Volume Pipettor, volumes: 0.5-10 µl, 2-20 µl, 10-100 µl, 100-1000 µl	Sigma-Aldrich, St. Louis, USA
Transferpipette multi-channel pipettor 30-300 µl	Brand GmbH & Co. KG, Wertheim, Germany

Scales	Source
MC1	Sartorius AG, Göttingen, Germany
MXX-2001	Sartorius AG, Göttingen, Germany

Spectrophotometer	Source
NanoDrop 2000	Thermo Fisher Scientific Inc., Waltham, USA

3.1.2. Chemicals and reagents

Chemical/ reagent	Source
0.5% Trypsin EDTA (10x)	Biozym® Scientific GmbH, Hessisch Oldendorf, Germany
2-mercaptoethanol	Carl Roth GmbH + Co. KG, Karlsruhe, Germany
5-Sulfosalicylic acid	Carl Roth GmbH + Co. KG, Karlsruhe, Germany
Acetic acid	Carl Roth GmbH + Co. KG, Karlsruhe, Germany
Agar-Agar	Carl Roth GmbH + Co. KG, Karlsruhe, Germany
Agarose standard	Carl Roth GmbH + Co. KG, Karlsruhe, Germany
Albumin Fraction V	Carl Roth GmbH + Co. KG, Karlsruhe, Germany
Ammonium persulfate (APS)	Carl Roth GmbH + Co. KG, Karlsruhe, Germany
Ampicillin	Carl Roth GmbH + Co. KG, Karlsruhe, Germany
Bromophenol blue	SERVA Electrophoresis GmbH, Heidelberg, Germany
Cycloheximide C1988-1G	Sigma-Aldrich, St. Louis, USA
Dimethyl sulfoxide	Sigma-Aldrich, St. Louis, USA
Dimethylformamide	Sigma-Aldrich, St. Louis, USA

DMEM (Dulbecco's modified Eagle's medium) Gibco™	Thermo Fisher Scientific Inc., Waltham, USA
Enhanced chemiluminescence (ECL) Select™ Western Blotting	GE Healthcare, Chicago, USA
Ethanol	Merck KGaA, Darmstadt, Germany
Ethidium bromide solution (1%)	AppliChem GmbH, Darmstadt, Germany
Ethylene glycol-bis(β-aminoethyl ether)-N,N,N′,N′-tetraacetic acid (EGTA)	Merck KGaA, Darmstadt, Germany
Ethylenediaminetetraacetic acid (EDTA)	Carl Roth GmbH + Co. KG, Karlsruhe, Germany
Fetal bovine serum (FBS) Gibco™	Thermo Fisher Scientific Inc., Waltham, USA
GeneJuice® Transfection Reagent	Merck KGaA, Darmstadt, Germany
Glycerol	Carl Roth GmbH + Co. KG, Karlsruhe, Germany
Glycine	Carl Roth GmbH + Co. KG, Karlsruhe, Germany
Hepes	Merck KGaA, Darmstadt, Germany
Hoechst H33258	Merck KGaA, Darmstadt, Germany
Kanamycin	Carl Roth GmbH + Co. KG, Karlsruhe, Germany
L-glutamine	Merck KGaA, Darmstadt, Germany
Lysogeny Broth Base (LB Broth Base)	Thermo Fisher Scientific Inc., Waltham, USA

MG 132	Merck KGaA, Darmstadt, Germany
Milk powder	Carl Roth GmbH + Co. KG, Karlsruhe, Germany
Monopotassium phosphate	Carl Roth GmbH + Co. KG, Karlsruhe, Germany
Mounting media Dako	Agilent Technologies Inc., Santa Clara, USA
N-Ethylmaleimide	Sigma-Aldrich, St. Louis, USA
Natriumorthovanadate	Bio-Techne® Corporation, Minneapolis, USA
Nonylphenoxypolyethoxyethanol (NP-40)	Merck KGaA, Darmstadt, Germany
Paraformaldehyde	Carl Roth GmbH + Co. KG, Karlsruhe, Germany
Penicillin-G	Sigma-Aldrich, St. Louis, USA
Phenylmethylsulfonylfluoride (PMSF)	Sigma-Aldrich, St. Louis, USA
Ponceau (S) solution	Carl Roth GmbH + Co. KG, Karlsruhe, Germany
Potassium chloride	Sigma-Aldrich, St. Louis, USA
Propidiumiodide	Sigma-Aldrich, St. Louis, USA
Protease Inhibitor Cocktail	Sigma-Aldrich, St. Louis, USA
Puromycin P8833	Sigma-Aldrich, St. Louis, USA
Rotiphorese® Gel 30 (37,5:1)	Carl Roth GmbH + Co. KG, Karlsruhe, Germany
SOC Outgrowth-Medium	New England Biolabs®, Ipswich, USA
Sodium acetate	Carl Roth GmbH + Co. KG, Karlsruhe, Germany

Sodium deoxycholate	Carl Roth GmbH + Co. KG, Karlsruhe, Germany
Sodium dodecyl sulfate (SDS)	Carl Roth GmbH + Co. KG, Karlsruhe, Germany
Streptomycin	Sigma-Aldrich, St. Louis, USA
Suberanilohydroxamic acid (SAHA)	Hölzel Diagnostika Handels GmbH, Köln, Germany
Tetramethylethylen-1,2-diamine (TEMED)	SERVA Electrophoresis GmbH, Heidelberg, Germany
Trichloroacetic acid	Carl Roth GmbH + Co. KG, Karlsruhe, Germany
Triton X-100	SERVA Electrophoresis GmbH, Heidelberg, Germany
Trypan Blue stain 0.4%	Thermo Fisher Scientific Inc., Waltham, USA
Tween 20	Carl Roth GmbH + Co. KG, Karlsruhe, Germany
X-34	Prof. Dr. Heidi Olzscha, Institute for Biochemistry, Medical School Hamburg

3.1.3. Media and stock solutions

3.1.3.1. Lysis buffers

Cytosolic lysis buffer pH 7.4		**Nuclear lysis buffer** pH 7.4		**Radio immune precipitation assay (RIPA) lysis buffer** pH 7.5	
20 mM	Hepes	0.1%	TBS-Tween	150 mM	Sodium chloride
10 mM	KCl	1%	NP40	50 mM	Tris-HCl
2 mM	$MgCl_2$	0.5%	Sodium desoxycholate	0.5% (w/v)	Sodium desoxycholate
1 mM	EDTA	0.1%	SDS	1% (v/v)	NP-40
1 mM	EGTA			1 mM	EDTA

TNN lysis buffer pH	
50 mM	TrisHCl
0.5%	NP-40
150 mM	NaCl
20 mM	MgCl2

3.1.3.2. Media and stock solutions

Blocking solution		**Blotting Buffer** pH 8.5		**Culture media for U2OS, $HR23B^{KO}$, $HR23A^{KO}$**	
1x PBS		H_2O		DMEM	
1-5% (w/v)	BSA or milk powder	10 mM	TRIS	10%(v/v)	FBS
		150 mM	Glycerol	1% (v/v)	P/S
		10% (v/v)	Ethanol	1% (v/v)	L-glutamine

Cryoconservation media		**Fixing solution**		**5x Laemmli SDS sample buffer**	
FBS		1x PBS		H_2O	
10% (v/v)	DMSO	4%(w/v)	Paraformaldehyde	1% (w/v)	SDS
				63 mM	Tris-HCl
				25%	Glycerol
				5% (v/v)	2-mercapto-ethanol
				0.01% (w/v)	Bromophenol blue

10x Phosphate buffered saline (PBS) pH 7.4		**Permeabilizing solution**		**Ponceau (S) solution**	
H_2O		1x PBS		H_2O	
8% (w/v)	Sodium chloride	0.5% (v/v)	Triton-X-100	0.2% (w/v)	Ponceau (S)
0.2% (w/v)	Potassium chloride			0.3% (v/v)	Trichloro-acetic acid
1.15% (w/v)	Na_2HPO_4			0.3% (v/v)	Sulfosalicylic acid
0.2% (w/v)	KH_2PO_4				

Protease inhibitors		**Running buffer for SDS-PAGE**		**SDS Collecting Gel**	
1:500	Protease inhibitor cocktail	H_2O		H_2O	
500 µM	PMSF	192 mM	Glycine	4%	Acrylamide
100 µM	Sodium ortho-vanadate	25 mM	TRIS pH 8.5	377 mM	TRIS pH 6.8
5 µM	SAHA	0.1% (w/v)	SDS	0.05% (w/v)	SDS
5 µM	MG132			0.8% (v/v)	APS
400 µM	N-ethyl-maleimide			0.08% (v/v)	TEMED

SDS Separation Gel	TRIS buffered saline (TBS) pH 7.6	TBS-Tween
H_2O	H_2O	1x TBS
10 or 12% Acrylamide	0.1% Tween20	0.1% Tween20
124 mM TRIS pH 8.8	2.4% (w/v) TRIS	
0.05% (w/v) SDS		
0.4% (v/v) APS		
0.1% (v/v) TEMED		

3.1.4. Enzymes

Enzyme	Source
RNase	Sigma-Aldrich, St. Louis, USA

3.1.5. Cell lines

Cell line	Description	Source
$HR23A^{KO}$	Stable HR23A knockout cell line generated using CRISPR Cas9 in U2OS cells	Diana Panfilova, AG Olzscha, Institute for Physiological Chemistry, Martin-Luther-University, Halle-Wittenberg
$HR23B^{KO}$	Stable HR23B knockout cell line generated using CRISPR Cas9 in U2OS cells	Diana Panfilova, AG Olzscha, Institute for Physiological Chemistry, Martin-Luther-University, Halle-Wittenberg
U2OS cells ATCC-Number: HTB-96	Humane bone osteosarcoma cells	American Type Culture Collection (ATCC) Manassas, USA

3.1.1. Bacteria

Bacteria	Source
DH5-α competent *E. coli*	New England Biolabs®, Ipswich, USA

3.1.2. Plasmids

Name	Vector	Construct	Antibiotic resistance	Source
pcDNA3	pcDNA3	Empty	Ampicillin	Thermo Fisher Scientific Inc., Waltham, USA
Htt20Q	pcDNA3	Exon 1 Htt 20Q HA-Tag	Ampicillin	Prof. Dr. Heidi Olzscha, Institute for Biochemistry, Medical School Hamburg
Htt97Q	pcDNA3	Exon 1 Htt 97Q HA-Tag	Ampicillin	Prof. Dr. Heidi Olzscha, Institute for Biochemistry, Medical School Hamburg
peGFP	peGFP C1.1	Empty	Kanamycin	Clontech Laboratories Inc., Mountain View, USA
GFP-Htt23Q	peGFP	Exon 1 Huntingtin 23Q GFP-Tag	Kanamycin	Addgene, Watertown, USA
GFP-Htt74Q	peGFP	Exon 1 Huntingtin 74Q GFP-Tag	Kanamycin	Addgene, Watertown, USA

3.1.3. Test systems

Test system	Source
Pierce™ BCA Protein Assay Kit	Thermo Fisher Scientific Inc., Waltham, USA
PROTEOSTAT® Protein Aggregation Kit	Enzo Life Sciences Inc., Lausen, Switzerland
PureLink™ HiPure Plasmid Maxiprep Kit	Thermo Fisher Scientific Inc., Waltham, USA
Zyppy™ plasmid miniprep Kit	Zymo Research Europe GmbH, Freiburg, Germany

3.1.4. Antibodies

3.1.4.1. Primary antibodies

Antibody	Species	Concentration	Order #	Source
β-Tubulin	Mouse	1:2000 (WB) Milk 1% (w/v)	MA5-16308-HRP	Thermo Fisher Scientific Inc., Waltham, USA
Actin ab 5	Mouse	1:5000 (WB) Milk 1% (w/v)	612657	Becton Dickinson GmbH, Heidelberg, Germany
Amyloid fibrils	Rabbit	1:1000 (WB) Milk 1% (w/v)	ab126468	Abcam®, Cambridge, Great Britain
GAPDH	Mouse	1:5000 (WB) Milk 1% (w/v) 1:80 (IF)	sc 47724	Santa Cruz Biotechnology Inc., Dallas, USA
GFP HRP	Mouse	1:1000 (WB) Milk 1% (w/v) 8 µg (IP)	11814460001	Merck KGaA, Darmstadt, Germany
HA	Mouse	1:50 (IF)	2367S	Cell Signaling Technology®, Danvers, United States of America

HA	Rabbit	1:50 (IF)	H6908	Merck KGaA, Darmstadt, Germany
Histon H3	Rabbit	1:1000 (WB) Milk 1% (w/v)	14-494	Cell Signaling Technology®, Danvers, USA
HR23A	Rabbit	1:50 (IF) 1:500 (WB) Milk 1% (w/v)	HPA026 418	Merck KGaA, Darmstadt, Germany
HR23B	Rabbit	1:1000 (WB) Milk 1% (w/v) 1:100 (IF) 2-4 µg (IP)	ab86781	Abcam®, Cambridge, Great Britain
IgG Isotype Control	Rabbit		31235	Thermo Fisher Scientific Inc., Waltham, USA
IgG Isotype Control	Mouse		31903	Thermo Fisher Scientific Inc., Waltham, USA
Oligomer fibrils A11	Rabbit	1:1000 (WB) Milk 1% (w/v)	AHB005 2	Thermo Fisher Scientific Inc., Waltham, USA
Puromycin clone 12D10	Mouse	1:2000 (WB) Milk 1% (w/v)	MABE3 43	Merck KGaA, Darmstadt, Germany

3.1.4.2. Secondary antibodies

Antibody	Species	Concentration	Order #	Source
Anti-mouse FITC	Goat	1:800 (IF)	A16067	Thermo Fisher Scientific Inc., Waltham, USA
Anti-rabbit Dylight 649	Goat	1:300 (IF)	611-143-122	Biomol GmbH, Hamburg, Germany
Anti-rabbit FITC	Goat	1:800 (IF)	65-6111	Thermo Fisher Scientific Inc., Waltham, USA

TrueBlot Mouse: Anti Mouse IgG	Rat	1:5000 (WB)	18-8817-33	Rockland Immunochemicals, Inc., Philadelphia, USA
TrueBlot Rabbit: Anti Rabbit IgG	Rat	1:5000 (WB)	18-8816-33	Rockland Immunochemicals, Inc., Philadelphia, USA

3.1.5. Size standards

Size standard	Source
GeneRuler™ 100bp DNA ladder	Thermo Fisher Scientific Inc., Waltham, USA
PageRuler™ Plus prestained protein ladder	Thermo Fisher Scientific Inc., Waltham, USA

3.1.6. Software

Software	Source
BD Accuri C6 Analysis Software	Becton Dickinson GmbH, Heidelberg, Germany
BD FACSDiva™ Software, Version 9.0	Becton Dickinson GmbH, Heidelberg, Germany
Chromas 2.6.6	Technelysium Pty Ltd., South Brisbane, Australia
Endnote™ 20.2 for Macintosh	Clarivate Analytics, Philadelphia, USA
Harmony high content analysis software version 4.8	PerkinElmer Inc., Waltham, USA
Image Lab™, Version 6.0.1	Bio-Rad Laboratories Inc., Hercules, USA
ImageJ, Version 1.53a	National Institutes of Health, Bethesda, USA

Inkscape version 1.0.1	Inkscape.org
Microsoft Office 2021 (Excel, PowerPoint, Word)	Microsoft® Corporation, Redmond, USA
MARS Analysis Software, version 3.20 R2	BMG Labtech GmbH, Ortenberg, Germany
NanoDrop™ 1000, version 3.3	Thermo Fisher Scientific Inc., Waltham, USA
Origin Pro 2019	Originlab Corporation, Northampton, USA
Quantity One®, version 4.6.2	Bio-Rad Laboratories Inc., Hercules, USA
ZEN (blue edition), version 2.3 SP1	Carl Zeiss AG, Oberkochen, Germany

3.2. Methods

3.2.1. Molecular biological methods

3.2.1.1. Transformation of competent cells

The transformation of competent *E. coli* was attained using the heat shock method. Here, 25 µl of competent cells were incubated with 0.2 µg plasmid DNA for 20 min on ice. Then heat shock was performed at 40°C for 50s. Cells were then set on ice for 2 min and transferred to 500 µl of pre-heated super optimal broth with catabolites (SOC) media and incubated at 37°C for 60 min under soft shaking. 20 µl of the solution were then plated onto ampicillin or kanamycin containing LB-agar dishes and incubated at 37°C overnight.

3.2.1.2. Plasmid preparation

Plasmid preparation was performed using either mini-preparation Kit (see 3.1.8) or Maxi-preparation Kit (see 3.1.8) for the DNA yield required. Colonies of competent *E. coli* were selected using a toothpick and incubated in 3 ml (mini preparation) or 200 ml (maxi preparation) LB-media with ampicillin or kanamycin in concentration of 100 mg/ml at 37°C and 300 RPM overnight. The DNA extraction was performed as depicted in the manufacturer's instructions. DNA was diluted in ddH_2O and the concentration was determined using Nanodrop spectrophotometer. Sequencing was performed by the company SeqLab using 12 µl of an 80 ng/µl solution. Analysis of the sequencing data was performed using Chromas.

3.2.1.3. Restriction digest of plasmids

Restriction digest of plasmids pcDNA3, 20QHtt and 97QHtt was performed using restriction enzyme ECO RI-HFm, which has one cleavage sight in pcDNA3 and none in the insert sequences. 50 µl of reaction solution were assembled using the components water, cut smart buffer (1:10), 1 µg DNA of each plasmid and restriction enzyme (10U). The solution was incubated for 1 h at 37°C. Consequently, heat shock was performed at 65°C for 20 min, which leads to enzyme deactivation. The samples were loaded onto a 1% agarose gel to perform DNA electrophoresis.

3.2.1.4. DNA agarose electrophoresis

In this method, DNA fragments are separated along an electrical gradient depending on their size. The chosen agarose concentration of the gel is calculated dependent on the size of the tested DNA fragments. In this case, 50 ml of 1% agarose gel was used.

0.5 g of agarose was mixed in 50 ml TAE buffer (see 3.1.3.2), brought to a boil and stirred until the mixture was even. 1 µl of ethidium bromide was added per 50 ml gel. The gel was cooled shortly, then poured into gel chamber and the well comb was set in place.

15 µl samples were prepared using similar amounts of DNA each and 10x sample buffer in dilution 1:10. The gel chamber was filled with 1x TAE-buffer until reaching the loading line and the well comb was removed. DNA gene ruler was used as size standard and samples were loaded accordingly. Voltage was applied at 80 V for 1 h.

3.2.2. Protein biochemical methods

3.2.2.1. Cell lysis of mammalian cells

Cells were grown to 80-100% confluency and harvested using either a cell scraper or trypsin EDTA solution after previously washing the cells with PBS. The cells were collected in a falcon tube and centrifuged at 500 g for 3 min. The pellet was washed once with PBS and transferred to an Eppendorf tube. The cells were centrifuged at 2,000 g for 3 min, the supernatant discarded, and the pellet resuspended in cold lysis buffer. A variety of lysis buffers were used for different experiments as described in 3.1.3.1. If not stated otherwise, 100 µl of RIPA lysis buffer was used. Samples were then incubated at 4°C on a rotating disk for 1 h. Afterwards, lysates were pulled through a fine needle (27G) and centrifuged at 4°C and 16,000 g for 10 min. The supernatant was then transferred to a new pre-cooled tube and protein concentration was measured. All protein solutions were stored at -20°C.

3.2.2.2. Protein concentration measurement via BCA assay

Protein concentration was measured using the bicinchoninic acid (BCA) assay and the absorbance of different samples was measured according to manufacturer's instructions at λ = 562 nm. A series of different dilutions of bovine serum albumin (BSA) 2 mg/ml was used as a protein standard curve. Dilutions were established using ddH_2O in following concentrations: 2.0, 1.5, 1.0, 0.75, 0.5, 0.25, 0.125, and 0.025 mg/ml. Measured lysates were diluted in a ratio of 1:5 with ddH_2O and protein concentrations were determined using the quadratic equation of the standard curve.

3.2.2.3. SDS PAGE

The sodium dodecyl sulfate polyacrylamide (SDS) gel electrophoresis was established in 1970 by Ulrich Laemmli and is used to separate proteins under denaturizing conditions according to their mass (Laemmli 1970). When applying an electrical current, proteins travel towards the anode, with different speeds depending on their molecular weight.

Equal protein amounts were incubated with 5x Laemmli sample buffer at 95°C for 5 min and a minimum of 20 µg were loaded onto polyacrylamide gels. Gels consisted of 4% collecting gel and 10 or 15% separating gel. For the first 10 min, a voltage of 110V was applied, followed by an increase to 160V. As a size standard PageRuler™ Plus prestained protein ladder was used.

3.2.2.4. Western Blot analysis

In order to detect different proteins, already separated proteins from the SDS PAGE were transferred and immobilized on a nitrocellulose membrane (Burnette 1981). After equilibration of both the nitrocellulose membrane and Whatman paper with the transfer buffer (see 3.1.3.2) the sandwich blot was assembled with specific caution to avoid air inclusions. The transfer then occurred under cooling and mixing of the transfer buffer and under applied electric current of 300 mA for 80 min. The membrane was hereafter stained with Ponceau S solution for 5 min and visualized. Afterwards, the membrane was incubated in blocking solution for a minimum of 30 min. The primary antibody was diluted in same blocking solution (see 3.1.9.1) and the membrane was incubated with it for either 2 h at room temperature or overnight at 4°C on a rotation disk. Afterwards, the antibody solution was removed using 3 wash steps with 1x TBS for 10 min on a rocking platform and the secondary antibody solution was applied (3.1.9.2). It was incubated for 1.5 h at room temperature and removed with 2 further wash steps with 1x TBS-T and 1 wash step with 1x TBS for 10 min. Chemiluminescence could be detected with the ChemiDoc™ MP Imaging System. Since secondary antibodies are tagged with a peroxidase, the chemiluminescent reaction is possible when applying substrate solution GE Healthcare Amersham™ ECL Western-Blot-reagent to the membrane. In this case, 1 ml of a 1:1 peroxide:luminol solution was used.

3.2.2.5. Cytoplasmic nuclear extraction assay

In this assay, different types of lysis buffers were used to separate nuclear from cytoplasmic protein fractions and analyze the distribution of HR23B across those cellular compartments. $1x10^6$ cells U2OS cells were seeded on each 10 cm petri dish and incubated at 37°C 5% CO_2 for 24 h. The cells were then harvested using 2 ml of 1x trypsin EDTA and the pellet was lysed with 100 µl cytosolic lysis buffer (see 3.1.3.1) for 45 min at 4°C on a rotating disk. Samples were centrifuged at 1,000 g and 4°C for 5 min and the supernatant transferred to another tube and incubated in ultrasonic bath for 2 min. Samples were centrifuged at 16,000 g and 4°C for 10 min and supernatant resembled cytoplasmic protein fraction.

The remaining pellet was washed twice with ice cold 1x TBS and centrifuged at 16,000 g for 10 min and the supernatant discarded. Then cells were resuspended in 100 µl of nuclear lysis buffer (3.1.3.1) pulled through a fine needle (27G) several times and incubated for 30 min on ice. Samples were then sonified with 10% intensity and 5 pulses over 10 s) and then centrifuged at 16,000 g and 4°C for 10 min. The supernatant resembled the nuclear protein fraction.

For analysis in Western Blot, protein concentrations were determined using BCA Assay (see 3.2.2.2) and equal amounts of both nuclear and cytoplasmic protein fraction were combined to create total protein fraction. 12% gels were used for the histone blot and 10% gels for all other blots. In WB, double the amount of total protein solution was loaded to achieve total protein amount. Purity of cytosolic and nuclear protein fraction was tested using anti-β-tubulin antibody as a cytosolic protein and anti-histone H3 antibody as a nuclear protein. HR23B localization within the cell was analyzed using anti-HR23B antibody (for concentrations see 3.1.9.1). Images were quantified using ImageLab software and normalized on total protein amount.

3.2.2.6. Puromycin incorporation assay

The puromycin incorporation assay is a non-radioactive method to determine translatory rates in cells. The principal of this assay relies on the structural similarity of the antibiotic puromycin to tRNAs and its function to get incorporated into nascent chains produced at the ribosome. This process terminates elongation and the consequent analysis of puromycin intensity in cell lysates can be used to determine the translatory rate of the cell (Schmidt et al. 2009).

To ensure even confluency of cells, the seeding amount of different cell lines has to be adjusted according to their replication dynamics. In this case, $1x10^6$ cells of U2OS WT cells, and $1.5x10^6$ cells of $HR23A^{KO}$ and $HR23B^{KO}$ cell lines were seeded onto two 10 cm petri dishes each. Cells were incubated at 37°C and 5% CO_2 for 24 h. In order to harvest the cells, they were washed 1x with PBS and then incubated with 2 ml of 1x trypsin EDTA for 5 min, then resuspended with an equal amount of media and transferred to an Eppendorf tube. Samples were centrifuged at 500 g for 3 min and the pellet was resuspended in 1 ml media. The cell amount was counted using an automated cell counter and equal concentration of cells ($1x10^6$ cell in 1 ml media) were established for each sample. As controls, U2OS WT cells were used. Control 1 resembles no addition of puromycin, control 2 preincubation with 250 µM cycloheximide for 30 min. The different samples were incubated with puromycin at 37°C for exactly 10 min each. Following two steps of centrifugation at 2,000 g for 3 min and washing with warm PBS. The resulting pellet was then shock frosted in liquid nitrogen and lysed using RIPA buffer for 1 h at

4°C. Protein concentrations were measured using BCA assay (see 3.2.2.2) and equal amounts of each sample were analyzed using puromycin antibody in Western Blot (see 3.1.9.1 and 3.2.2.4). Actin served as a loading control.

3.2.2.7. Co-Immunoprecipitation

To perform co-immunoprecipitation assay 5x10^6 U2OS cells were seeded on 15 cm petri dishes. After incubation at 37°C and 5% CO_2 for 24 h, cells were harvested using cell scraper and washed 1x with PBS. Cell lysis was then performed using TNN lysis buffer (see 3.1.3.1) with protease inhibitors. 2 ml were added to sample and incubated at 4°C for 3 h under rotation. Lysates were pulled through a 27G needle, centrifuged at 4°C and 16,000 g for 10 min and the protein concentration was measured using BCA protein assay (see 3.2.2.2). Agarose beads were prepared with 4 wash steps using TNN lysis buffer and centrifugation at 8,000 g for 1 min. Equal amounts of lysate were used to perform the immunoprecipitation with the target antibody as well as the IgG control. Samples were prepared as follows: 100 µl Protein A agarose beads + 4 µg GFP antibody/ IgG mouse antibody + 700 µl lysate. This mixture was incubated at 4°C on a rotating disk overnight. Then, samples were centrifuged at 8,000 g for 1 min and the supernatant was saved as depletion. The samples were then washed 4 times using TNN lysis buffer and centrifuged at 8,000 g after each step. The proteins were then eluted using 5x Laemmli loading buffer heated to 95°C. Samples were vortexed and centrifuged to 16,000 g twice and supernatants saved as IP. Lysate, depletion and IP samples were analyzed in SDS PAGE and Western Blot using anti-GFP antibody and anti-HR23B antibody (see 3.1.9.1). As secondary antibody TrueBlot Goat-anti-mouse and Goat-anti-rabbit antibodies were used in a concentration of 1:5000 (see 3.1.9.2). GAPDH served as a loading control.

3.2.2.8. Filter retardation assay

To analyze the amount of Htt and its composition in different aggregate or oligomeric species a filter retardation assay was performed. The principle is the filtration of protein lysates through different membranes with distinct pore sizes. Lysates are pulled through a cellulose acetate (CA) membrane, which can filter aggregated proteins (Sin et al. 2018), using a vacuum pump that is connected to the filtering apparatus. The remaining proteins in the lysate were blotted onto a nitrocellulose (NC) membrane, similarly to the one used in WB analysis. This way, aggregates and amyloid structures can be detected on the CA membrane, but not on the NC membrane and oligomeric species can pass the CA membrane and are therefore detectable on the NC membrane. In preparation of the assay, U2OS cells were seeded on 10 cm petri dishes (10^6 cells each) and transfected with different Htt constructs using GeneJuice® (see 3.2.3.4). Following

constructs were used: H_2O, peGFP, GFP-Htt23Q, GFP-Htt74Q. Cells were then harvested and lysed using RIPA buffer (see 3.1.3.1) with added protease inhibitors. Protein concentration was measured using BCA assay (see 3.2.2.2) and different dilutions of the lysates were established. Both membranes were cut to the dimensions of the filter apparatus (12x8 cm) and watered with PBS for 10 min. The apparatus was assembled, and the NC membrane was placed underneath the CA membrane under specific caution to avoid any air inclusions. The vacuum pump was connected, and wells were washed with 200 µl PBS. The suction was adjusted accordingly to ensure controlled movement of liquids through the membranes. Then 10 µl of each sample and replicate was added directly onto the first membrane and vacuum applied. Samples were washed twice with 200 µl PBS. Membranes were then set out to dry and eventually incubated in specific blocking solution for 1 h at room temperature (see 3.1.9.1). Later, primary antibody was added and incubated at 4°C overnight. The secondary antibody was added after several wash steps with TBS and the chemiluminescent signal was visualized similarly to Western Blot analysis (see 3.2.2.4).

3.2.3. Cell biological methods

3.2.3.1. Cultivating adherent cell lines

U2OS cells were cultivated in Dulbecco's modified Eagle's media (DMEM) with 10% FBS, 1% penicillin/ streptomycin and 1% L-glutamine at 37°C and 5% CO_2. Cells were split every 2-3 days, when reaching 80-90% confluency. Media was removed and cells were washed with 1x PBS and then incubated with appropriate amount of 1x trypsin EDTA solution at 37°C for 5-10 min. Detachment of cells was verified using light microscopy and cells were suspended in new DMEM media to stop the reaction. Cells were diluted 1:2 and transferred to new cell culture flask or dish. PCR was regularly performed to check for mycoplasma DNA.

3.2.3.2. Cryopreservation of mammalian cell lines

To preserve adherent mammalian cells, they were stored in cryoconservation media at -150°C. To achieve that, cells were washed and detached from the culture flask as described above (3.2.3.1), resuspended in 1 ml freezing media (see 3.1.3.2) and stored in cryovials. The number of cells in a 550 ml culture flask was stored in 3 cryovials. These were then stored at -20°C for 3 h, then at -80°C for 24 h and finally at -150°C. For defrosting, 37°C warm culture media was prepared, and cells were taken out of storage. They were put in the incubator at 37°C to defrost quickly and then suspended in 15 ml

warm culture media per cryovial. Cells were centrifuged to remove remnants of cryoconservation media. Then, cells were resuspended in 10 ml culture media and stored in medium culture flask at 37°C and 5% CO_2.

3.2.3.3. Determining cell count

The cell count was determined using Countess™ cell counting chamber and a trypan blue staining. 9 µl of detached cells was resuspended in 1 µl or trypan blue and the solution was put onto a counting slide. Total amount of cells, dead cells and alive cells were measured according to their staining.

3.2.3.4. Transfection of mammalian cells using GeneJuice®

The transfection of U2OS cells was performed using the reagent GeneJuice®. Cells were cultivated and seeded in necessary number on a petri dish or microscopy slide. To create the reagent mixture, serum free (Optimem) media was used in which GeneJuice® was added with a ratio of 1:25. The sample was vortexed and incubated for 5 min at room temperature. DNA was added in ratio 1:2 to GeneJuice®. The sample was then mixed gently and incubated for 15 min at room temperature. To conclude, the sample was then gently applied onto cultivated cells in a ratio of 1:10 of new cultivating media.

3.2.3.5. Cell preparation for flow cytometry and cell cycle analysis

Cells were seeded on to 6-well plates in appropriate concentration. Culture media was collected in a flow cytometry tube, to gather dead and subG1 phase cells. Then, cells were washed 1x with PBS and the trypsin-EDTA solution was added. The detached cells were added into the FACS tube and centrifuged at 360 g. After decanting the supernatant, cells were washed 1x with PBS and the centrifugation step was repeated. The supernatant was again discarded, and cells were resuspended flicking the tube in remaining PBS. To fixate the cells 1 ml of ice cold 70% ethanol in PBS was added dropwise while vortexing the solution. The samples were incubated overnight at 4°C.

For staining the cells, they were centrifuged at 360 g for 1 min and washed with PBS. After a second centrifugation step, the supernatant was decanted and cells resuspended in remaining PBS. Add 1 ml of PBS staining buffer containing RNase in concentration 100 µg/ml and propidium iodide (PI) in dilution 1:25. Cells were incubated in the dark for 20 min at 4°C.

3.2.3.6. Cell cycle analysis of U2OS and HR23A/BKO cell lines using flow cytometry

Cell cycle analysis was performed using flow cytometry and PI staining. PI stains the cell's nuclear chromatin and the intensity of its signal is therefore equivalent of the DNA content of a cell (Krishan 1975). The different phases of the cell cycle are characterized by varying DNA-contents which allows the categorization of the cells into the correspondent phase.

3x 10^5 cells of each cell line ($HR23A^{KO}$, $HR23B^{KO}$ and U2OS) were seeded onto 6-well-plates and treated with either 0 µM (DMSO), 2.5 µM, 5 µM or 10 µM SAHA for 24 h. Afterwards, cells were prepared for flow cytometry and stained for cell cycle analysis as described in 3.2.3.5. Cells were then read on FACS using a limit of 20,000 ungated events and slow speed. For the analysis 4 different blots were used: 1. Forward scattered light (FSL) / Side scattered light (SSL) to gate cells that are not debris, 2. / 3. FL2-A (PI excitation) in linear and logarithmic calculation, 4. Dot blot to exclude aggregates FL2-A (x) and FL2-H (y). The data was analyzed using BD Accuri C6 Analysis Software and statistically evaluated using Origin Pro.

3.2.3.7. Fluorescent microscopy

To perform an immunofluorescent staining, cultivating media was removed from the cell culture and cells were washed with PBS. Fixation was performed using 4% paraformaldehyde (PFA) in PBS for 45 min. The samples were washed with PBS and cells were permeabilized adding 0.5% (v/v) Triton X-100 (PBS) for 30 min. Samples were washed twice using PBS and 1% bovine serum albumin was added as blocking reagent and incubated for 30 min. In the following step, the primary antibody was diluted in 1% BSA (dilutions see table 3.1.9.1), added to the sample and incubated for 2 h at room temperature. Next, the sample was washed three times in PBS on a rocking platform for 10 min each. The secondary antibodies were diluted accordingly in PBS (see table 3.1.9.2), added to the sample and incubated for 1.5 h at room temperature under strict light protection. As nuclear stains either Hoechst (1:2000) or PI (1 µg/ml) were used and added to the secondary antibody mixture. Afterwards, the sample was washed with PBS three times. When using Proteostat® for aggregate staining it was added in dilution 1:2500 for 30 min. The sample was again washed three times for 15 min using PBS on a rocking platform. Consequently, the sample was treated with 4% PFA for another 15 min. Slides were then dipped in distilled water three times and mounting media and coverslip was added. All immunofluorescent staining were stored in the dark at 4°C.

Samples were visualized under application of immersion oil using immunofluorescence microscope with 63x magnification.

3.2.3.8. Analysis of CSA of Htt aggregates using ImageJ software

Using immunofluorescent staining (protocol see 3.2.3.7) Htt aggregates in U2OS, HR23A^{KO} and HR23B^{KO} cells were visualized. To measure the cross-sectional area of these aggregates ImageJ software was used. This way, aggregates were be measured individually using the IF images obtained, which were set to equal scales. There were less IF images of HR23A^{KO} samples compared to the other cell lines, which resulted in a corresponding difference in number of aggregates measured. The statistical analysis of this data was performed using Origin Pro.

3.2.3.9. Quantitative analysis of immunofluorescent images using Operetta

To analyze a high number of immunofluorescent images automatically, Operetta high content analysis system was used. Cells were seeded onto a 96 well plate using 15,000 U2OS WT cells and 20,000 HR23A/B^{KO} cells for each well. The cells were transfected using GeneJuice® with 20Q and 97Q Htt and pcDNA3 (see 3.2.3.4) and IF staining was performed as described in 3.2.3.7. Two IgG controls were carried along for each experiment using IgG anti-mouse and IgG anti-rabbit. For the analysis of the cross-sectional area of Htt aggregates, the aggregate/cell ratio and the nuclear/ cytoplasmic ratio, following antibodies were used: anti-HA antibody to visualize Htt, anti-GAPDH-antibody to visualize the cytoplasm and cell borders. Proteostat® was used as an aggregate stain and Hoechst to visualize the nucleus. As secondary antibodies DyLight and FITC were used (for exact concentrations see 3.1.9.1 and 3.1.9.2). The number and size of Htt aggregates could then be measured using the feature “find spots” in the harmony high content imaging and analysis software. Cells borders and cytoplasmic areas were detected using the feature “find cytoplasm” and the anti-GAPDH channel. “Find nucleus” was used to count and measure nuclei and their cross-sectional area using the Hoechst channel. Statistical analysis was performed using Origin Pro.

3.2.4. Data analysis

All gathered data was analysed and depicted in graphs using Origin Pro software (Version 2019). If not noted otherwise, mean values and their standard deviations are shown. Statistical analysis was either performed using Student’s T or One-Way or Two-Way ANOVA (analysis of variance) and consecutive Tukey test. Results were considered

significant when $p < 0.05$. P-values are indicated by stars in all figures, (*) $p < 0.05$, (**) $p < 0.01$ and (***) $p < 0.005$. N.s. indicates $p > 0.05$.

4. Results

4.1. Subcellular localization and expression levels of HR23A and HR23B

4.1.1. Investigating cytoplasmic and nuclear protein fractions

The first part of this study focused on the gaining deeper understanding about the proteasome shuttling factors HR23A and HR23B and characterize them and their role in proteostasis U2OS cells. One of the first questions concerned the expression of HR23A/B within the different cellular compartments. Pia Fangmann had shown that HR23B may play a role in protein quality control of ribosomal proteins (data not published), which raised the question whether it is expressed in the nucleus. To investigate HR23B's subcellular localization, cytoplasmic nuclear extraction assays were performed (protocol see 3.2.2.5). The different protein fractions were then analyzed using WB and anti-HR23B, anti-histone-H3 and anti-β-tubulin antibody (protocol 3.2.2.4).

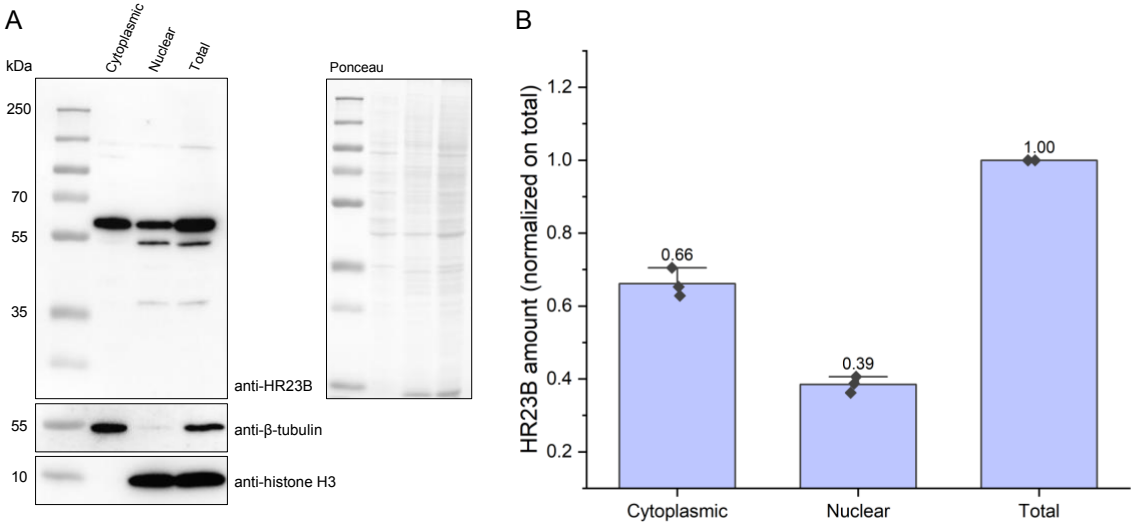

Figure 5: Localization of HR23B using cytoplasmic nuclear extraction assay.

U2OS cells were lysed with different lysis buffers to extract the nuclear and cytoplasmic protein fractions, which were then analyzed in Western Blot using anti-HR23B antibody. Anti-histone-H3 and anti-β-tubulin were used as controls of the nuclear and cytoplasmic fraction. Panel (A) shows respective immunoblots and Ponceau S staining which served as loading control. Estimated protein size of HR23B = 58 kDa. In (B) HR23B signal was quantified and normalized on the total protein. Mean values and standard deviations are depicted (n = 3). For full size immunoblots see appendix (figure 23).

The anti-HR23B immunoblot showed three strong bands at approximately 58 kDa in the nuclear, cytoplasmic, and total protein fraction. In the nuclear and total protein fraction two additional bands that run lower than the estimated protein size could be detected. These lighter bands ran at around 50 kDa and 38 kDa. The HR23B signal in the cytoplasmic protein fraction seemed greater than the one in the nuclear fraction, which

was consistent in all replicates. The quantification of the signals confirmed that HR23B is mostly resided in the cytoplasm with 66% and to a minor degree in the nucleus with 39%. The HR23B signals were normalized on the total protein fraction.
Successful separation of the cytoplasmic and nuclear fractions could be confirmed with anti-β-tubulin and anti-histone-H3 immunoblots. Using Pierce BCA Protein Assay Kit, protein concentrations were measured (3.2.2.2) prior to loading the SDS-gels and consecutive Ponceau S staining proved homogenous application.

4.1.2. Immunofluorescence staining of HR23B in U2OS cells

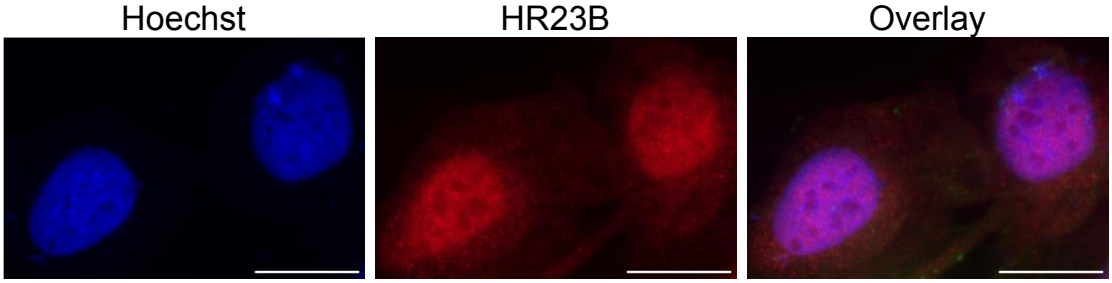

Figure 6: HR23B localisation in U2OS cells using IF staining.

This figure shows IF images of U2OS cells, stained with anti-HR23B antibody (red) and Hoechst (blue) for nuclear detection. The staining was performed according to the protocol (3.2.3.7). Images were visualized using immunofluorescence microscopy and 63x magnification. Scale bar shows 20 µm.

Using the same HR23B-antibody as in 4.1.1, immunofluorescent staining was performed in U2OS cells (protocol 3.2.3.7). Hoechst served as a nuclear stain. In the images depicted in figure 6 HR23B signal was detected in the whole cell, showing the highest intensity in the nucleus. This result again confirms the localization of HR23B in the nuclear and cytoplasmic compartment of U2OS cells, although pattern of distribution seemed to be different from the one observed in 4.1.1.

4.1.3. HR23A and HR23B expression in knockout cell lines

The two proteins HR23A and HR23B have both been shown to be able to facilitate transport of ubiquitinated proteins towards the proteasome (Chen and Madura 2002). Having comparable but not identical structures, it is not yet known to what degree they can replace each other in their function. In this assay, levels of expression of these two proteins in different cell lines were investigated. In this case, U2OS cells as well as knockout cell lines of the two proteins, which were created by Diana Panfilova using CRISPR/Cas9 gene editing technology, were used. These cell lines named HR23A^{KO} and HR23B^{KO} were used in most of the following experiments.

Equal amounts of U2OS, HR23A^{KO} and HR23B^{KO} cells were seeded and harvested at around 85% confluency. The proteins were extracted during cell lysis (protocol 3.2.2.1)

and equal amounts of protein were used for SDS PAGE and consecutive WB analysis (3.2.2.3 and 3.2.2.4). Figure 7 shows anti-HR23A and anti-HR23B immunoblots and Ponceau S staining that served as loading controls. In the anti-HR23A blot, a strong band was detected in WT as well as HR23B^{KO} cells at approximately 56 kDa. In HR23A^{KO} no band could be detected, which confirmed the knockout of the protein. The anti-HR23A signal seemed to be similar or less intense in HR23B^{KO} cells compared to the WT.

The anti-HR23B blot showed multiple bands, the strongest at approximately 58 kDa. There was no signal at this position in the HR23B^{KO} cells, confirming its successful knockout. The band in HR23A^{KO} cells seemed to be stronger compared to the one in the WT. Since this experiment was only performed once, no statistical analysis was carried out.

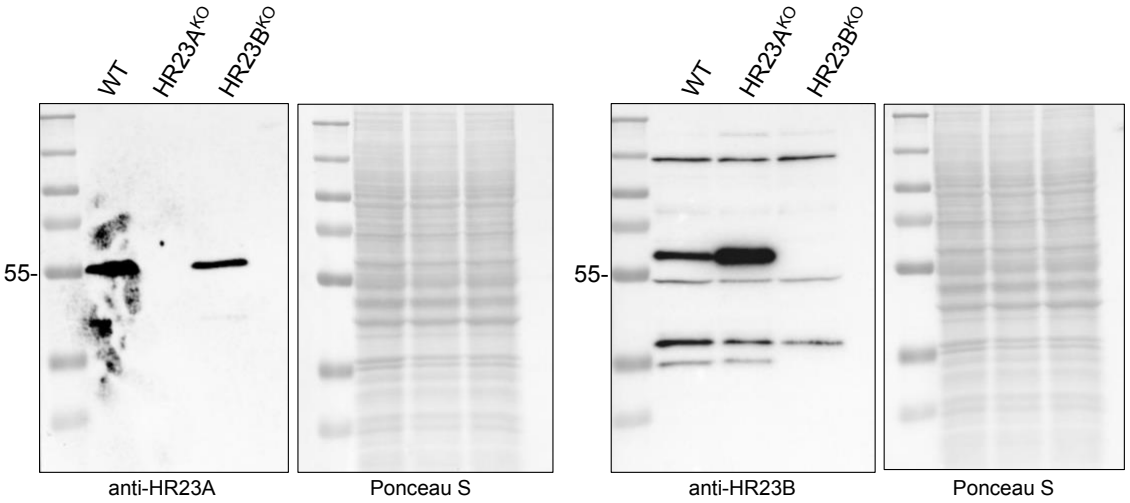

Figure 7: HR23A/B expression in U2OS, HR23A^{KO} and HR23B^{KO}.

In this figure anti-HR23A and anti-HR23B immunoblots, and their corresponding Ponceau S staining are shown. U2OS and HR23A/B^{KO} cells were grown to 85% confluency, harvested, and lysed according to the protocol (see 3.2.2.1). Protein concentrations were measured using BCA assay and equal amounts of protein were loaded onto the SDS gel. Analysis was performed in WB using anti-HR23A and anti-HR23B antibody. Ponceau S staining served as a loading control. N = 1.

4.2. Investigating HR23A and HR23Bs influence on cellular proliferation, cell cycle progression and translatory rate

4.2.1. Nuclear/ cytoplasmic ratio of HR23A/B^{KO} cells

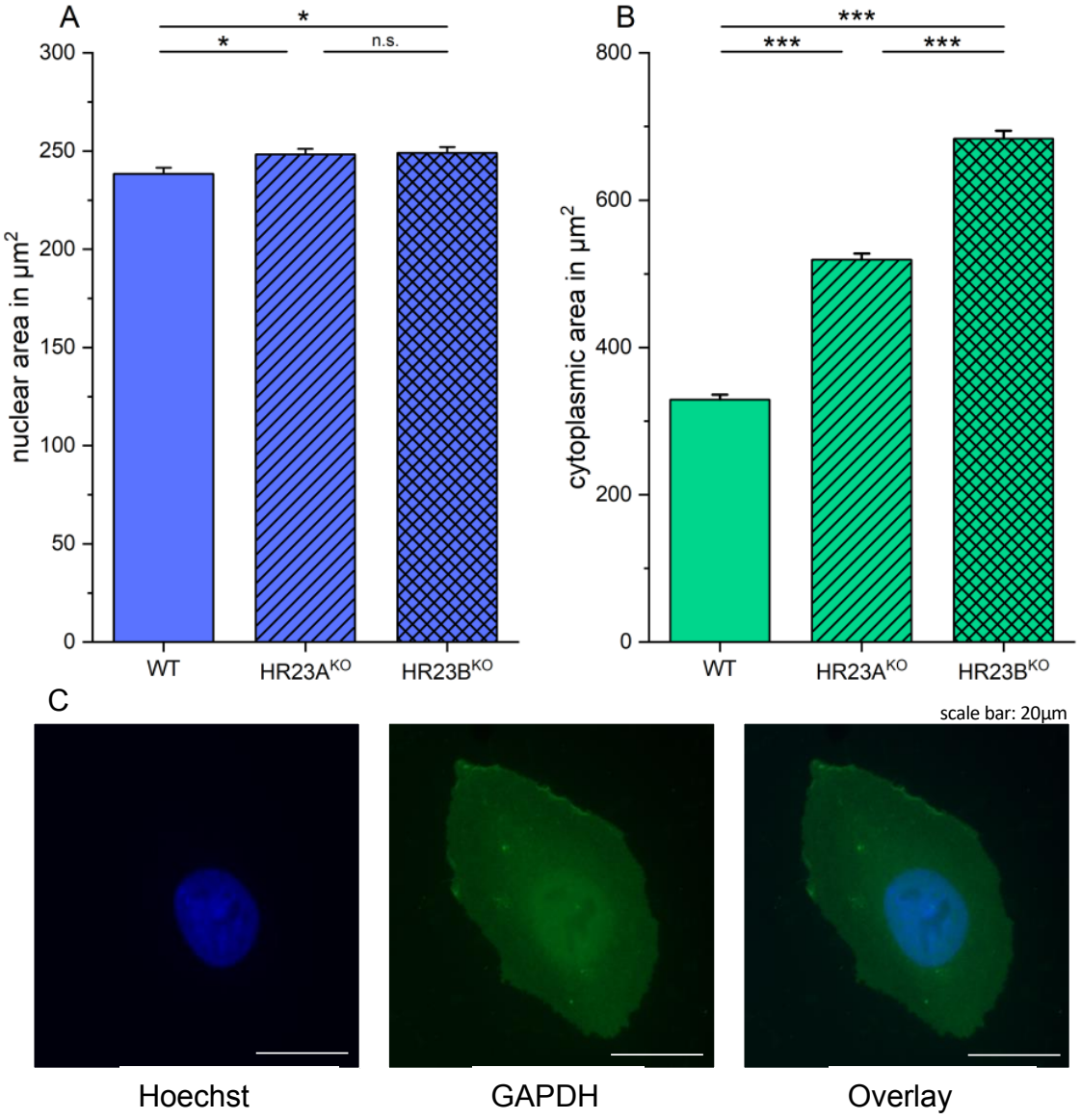

Figure 8: Nuclear and cytoplasmic area of U2OS and HR23A/B^{KO} cells.

U2OS and HR23A/B^{KO} cells were stained using anti-GAPDH and Hoechst (see 3.2.3.7) and visualized using Operetta High content analysis system (see 3.2.3.9). Panel (C) shows an example of the IF staining in U2OS cells. Features “find nuclei” and “find cytoplasm” were used in Harmony high content analysis software to measure cellular and nuclear surface area. The cytoplasmic area was calculated by subtracting nuclear area from cellular area. The cytoplasmic area (A) of HR23A^{KO} and HR23B^{KO} cells increased in comparison to the WT HR23A^{KO} ($p < 0.005$). HR23B^{KO} cells have a larger cytoplasmic area than HR23A^{KO} cells ($p < 0.005$). The nuclear area (B) increased in both HR23A^{KO} and HR23B^{KO} cells comparing to the WT ($p < 0.05$). There was no difference in nuclear area between both knockout cell lines. Mean values and their standard deviations are shown ($n \geq 100$, 3 biological replicates). Statistical analysis was performed using Origin Pro, p-values were calculated using One-way ANOVA and consecutive Tukey test. P-values are indicated by stars, (*) $p < 0.05$, (***) $p < 0.005$. N.s. indicates $p > 0.05$. Scale bar is 20 µm.

While observing U2OS cells and HR23A/B^{KO} cells macroscopically as well as in immunofluorescent staining, a change of cell morphology became apparent. In case of both knockout cell lines, cells appeared to be larger and abnormally proportioned. A change in cell morphology and nuclear/cytoplasmic (N/C) ratio could indicate that the cells are responding to other stimuli related to the knockout.

To quantify this observation, Operetta high content analysis system was used, and the cytoplasmic and nuclear surface area of the cells was measured (see figure 8 and protocol 3.2.3.9). This allowed the calculation of corresponding N/C ratios in the different cell lines. Anti-GAPDH was used to visualize cell borders, Hoechst for nuclear staining as shown in Panel (C). Using Harmony high content analysis software the functions “find nuclei” and “find cytoplasm” were used to identify the cell compartments and measure corresponding surface areas. In another step, the cytoplasmic suface area was calculated by subtracting the nuclear area from the area of the whole cell.

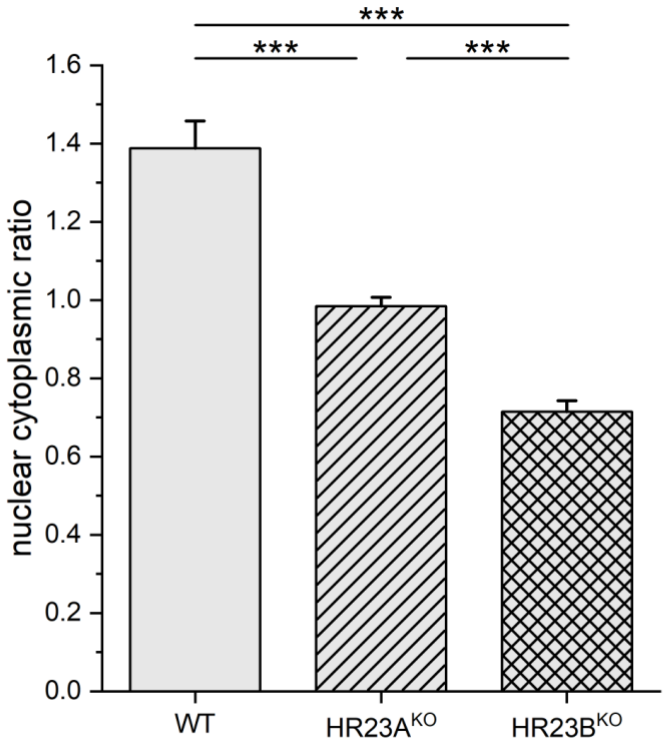

Figure 9: N/C ratio in U2OS, HR23A^{KO} and HR23B^{KO} cells.

The cytoplasmic and nuclear area of U2OS, HR23A^{KO} and HR23B^{KO} cells was measured using Operetta high content analysis (see figure 8 and protocol 3.2.3.9) The N/C ratio was calculated for each measurement. Mean values and their standard deviation are displayed here (n ≥ 100). HR23A and HR23B knockout showed a decreased N/C ratio compared to WT ($p < 0.005$). N/C ratio was lowest in HR23B^{KO} cells. Statistical analysis was performed in Origin Pro. P-values were calculated using One-Way ANOVA and consecutive Tukey test and p-values are indicated by stars, (***) $p < 0.005$.

Figure 8 shows that cytoplasmic area (A) as well as the nuclear area (B) increased in HR23A^{KO} and HR23B^{KO} cells compared to WT ($p < 0.005$). The cytoplasmic area increased to larger extend than the nuclear area, which resulted in a decreased N/C ratio

overall in both HR23A^{KO} and HR23B^{KO} cells (see figure 9). This decrease is statistically relevant compared to WT cells ($p < 0.005$). HR23B^{KO} cells showed the lowest N/C ratio compared to WT and HR23A^{KO} cells.

4.2.2. Cell cycle analysis of HR23A/B^{KO} cells

The difference in N/C ratio in HR23A^{KO} and HR23B^{KO} cells indicated an influence of HR23 proteins on cell morphology and cell growth. To investigate this further, cell cycle analysis of U2OS cells and HR23A/B^{KO} cells was performed. For this experiment, the different cell lines were grown to 85% confluency, then harvested and stained using PI according to the protocol (see 3.2.3.5). Intercalating with the DNA structure, PI signal could be used to measure the DNA content of each cell in flow cytometry (Krishan 1975). The allocation of cells to the different cell cycle phases was then performed as depicted in figure 10 panel (B). Markers were placed in the FL2-A blot, dividing the cells according to their DNA content (protocol see 3.2.3.6).

Figure 10 further shows the results of 5 biological replicates, each measuring 20,000 events. The cell amount of each cell cycle phase was normalized on the total cell count. In G1 phase the relative cell amount of HR23A/B^{KO} cells increased. Here, HR23A^{KO} cells showed a relative increase of around 8% ($p < 0.005$) and HR23B^{KO} of 14% ($p < 0.005$). Regarding the S phase, HR23A^{KO} cells showed a 6% decrease ($p < 0.005$) and HR23B^{KO} cells a 9% decrease ($p < 0.005$) of relative cell amount. In G2 phase relative cell amount reduced by 3% ($p < 0.005$) in HR23A^{KO} and 6% ($p < 0.005$) in HR23B^{KO} compared to WT. In subG1 phase, relative cell amount stayed the same comparing the three cell lines.

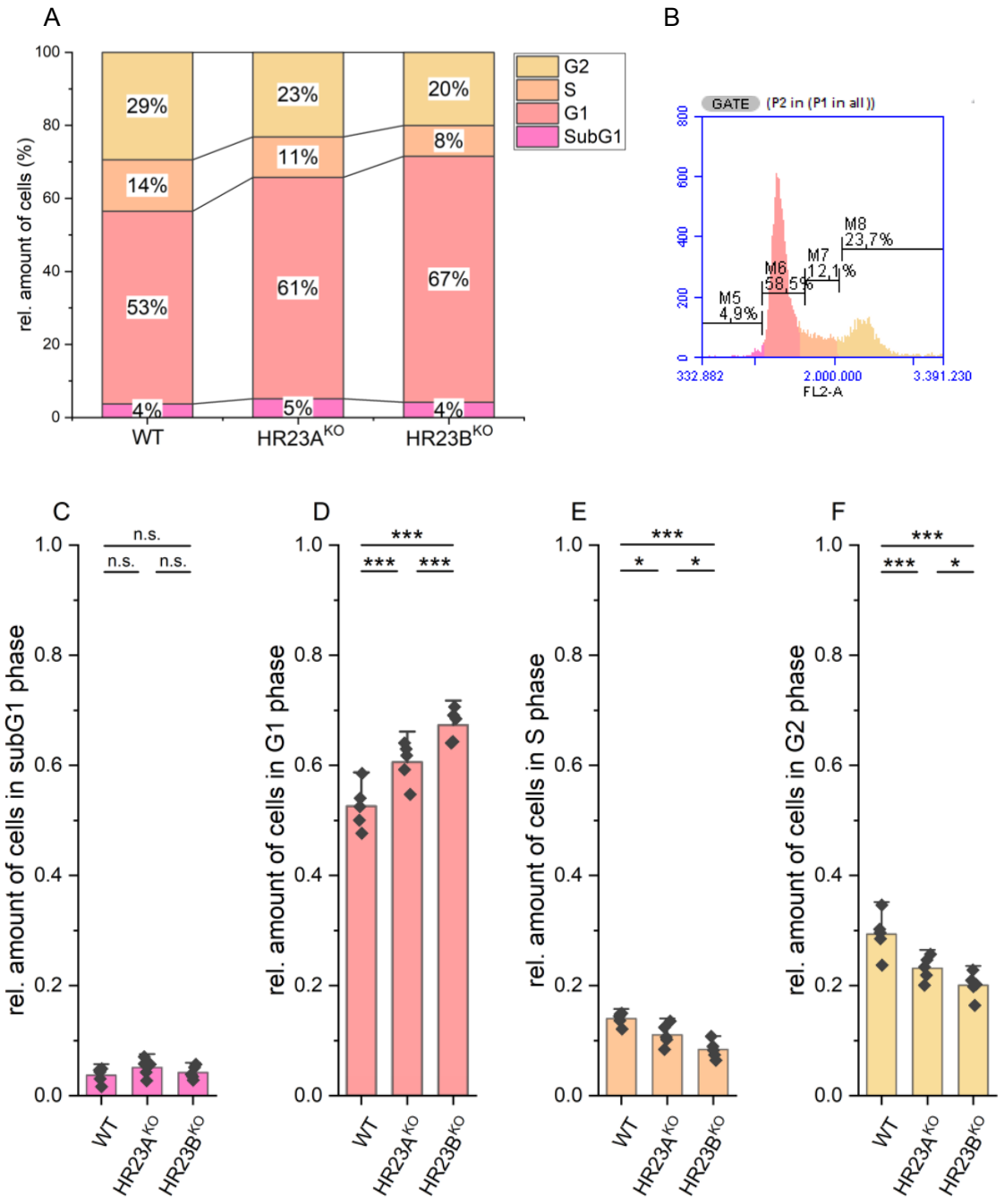

Figure 10: Cell cycle analysis of U2OS cells and HR23A/B^{KO} cells.

U2OS and HR23A/B^{KO} cells were grown up to 85% confluency, harvested and then fixed and stained for cell cycle analysis (3.2.3.5 and 3.2.3.6). The staining was performed using propidium iodide, which intercalates in DNA structures. The DNA content of each cell could then be measured using flow cytometry. The relative cell amounts in each cell cycle phase was measured using BD Accuri C6 Analysis Software. Panel (A) shows the phase-distribution in U2OS and HR23A/B^{KO} cell lines. In (B) the method of dividing the cells according to their DNA content/ PI signal is displayed exemplary. Here channel FL2-A is shown, and markers were set to indicate the following: M5 marks subG1 phase, M6 G1 phase, M7 S phase and M8 G2 phase. The statistical analysis of each cell cycle phase comparing the different cell lines is depicted in (C). Mean values and their standard deviations are shown (n = 5). P values were calculated using Two-Way ANOVA and consecutive Tukey test. P-values are indicated by stars, (*) $p < 0.05$, (**) $p < 0.01$, (***) $p < 0.005$. N.s. indicates $p > 0.05$.

4.2.3. Puromycin incorporation assay of HR23B^{KO} cells

Along with the observations made in 3.2.2, puromycin incorporation assays were performed in order to measure the translatory rate in U2OS and HR23A/B^{KO} cells (see protocol 3.2.2.6). Puromycin has structural similarities of tRNAs and is therefore incorporated into nascent chains at the ribosome depending at the rate of translation. Consequently, the intensity of puromycin is proportional to the amount of synthesized nascent chains and can be used to measure translatory rates (Schmidt et al. 2009).

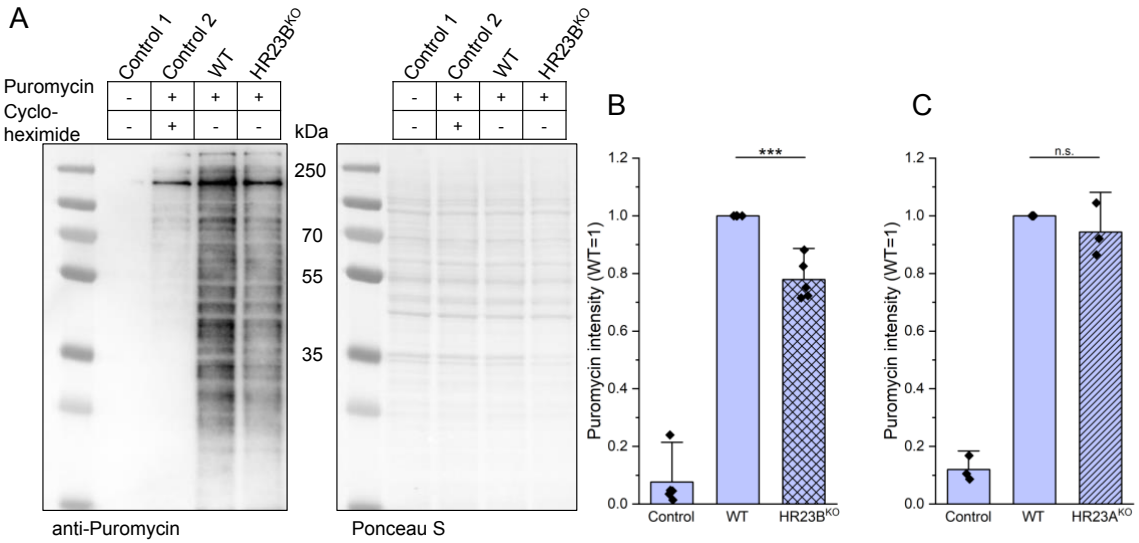

Figure 11: Puromycin incorporation assay of U2OS, HR23B^{KO} and HR23A^{KO} cells.

Equal amounts of U2OS and HR23A/B^{KO} cells were treated with puromycin for 10 min, then lysed and analyzed by WB using anti-Puromycin antibody. Two controls were used, (1) without puromycin incorporation and (2) pre-treated with cycloheximide to inhibit translation. Ponceau S staining served as loading control (see protocol 3.2.2.6). Results were normalized on Ponceau and the puromycin intensity in WT. In panel (A) and (B) the results of WT and HR23B^{KO} cells are shown. Mean values (n = 5) and standard deviations are displayed, p values were calculated using Origin Pro and student's T-test. Panel (C) shows additional results of HR23A^{KO} cells that were conducted in a different experiment involving HDACi treatment (see 4.4.2). Here, mean values (n = 3) and their standard deviations are displayed, statistical analysis was performed in Origin Pro and p values were calculated using Two-way ANOVA and consecutive Tukey test. P-values are indicated by stars, (*) $p < 0.05$, (**) $p < 0.01$, (***) $p < 0.005$. N.s. indicates $p > 0.05$.

In the anti-Puromycin immunoblot a strong signal is detectable over the entire lane in U2OS WT cells (lane 3). In HR23B^{KO} cells (lane 4) the puromycin signal follows the same pattern but the intensity is less strong. Lane 1 and 2 show the negative controls, (1) without puromycin treatment and (2) with pre-treatment using cycloheximide.

The statistical analysis confirmed that puromycin intensity decreases in HR23B^{KO} cells compared to WT ($p < 0.005$), which suggests that the rate of newly translated proteins was lower in this cell line. In a different experiment involving HDACi treatment, translatory rates of HR23A^{KO} cells were tested, which is displayed in panel (C). Here, no significant difference in puromycin intensity and therefore translatory rate could be detected ($p = 0.47$).

4.3. Analysis of Htt in HR23A/B^{KO} cells

4.3.1. Immunofluorescence imaging of Htt constructs in U2OS and HR23A/B^{KO} cells

To investigate the influence of HR23A and HR23B on misfolded proteins that are relevant in neurodegenerative diseases a cell culture-based model for HD was used. The pathologically elongated protein Htt plays a major role in the pathogenesis and progression of this disorder (Group 1993; Rubinsztein et al. 1996).

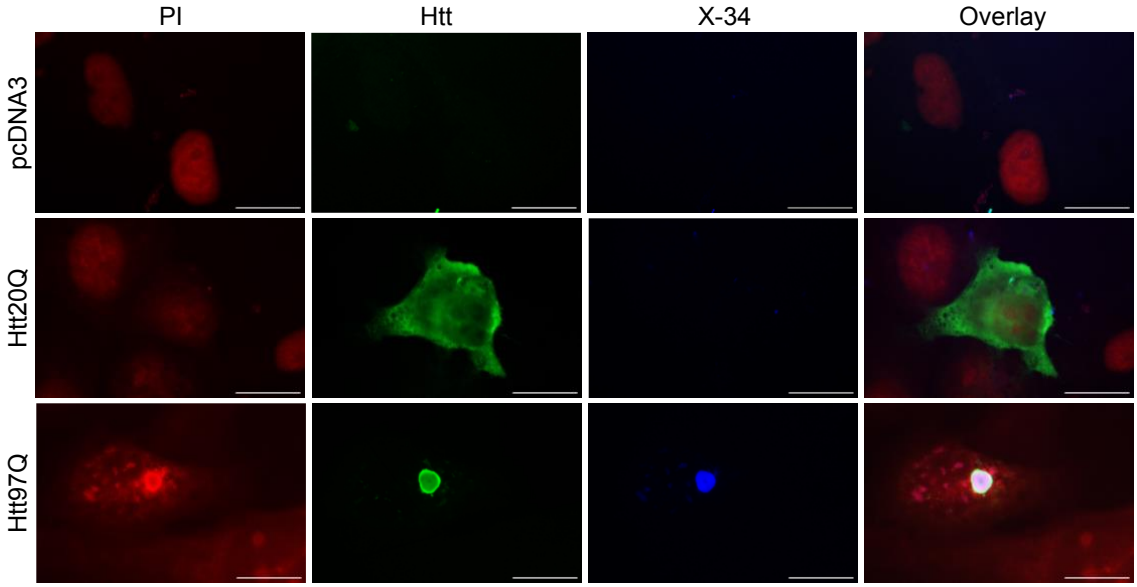

Figure 12: IF staining of Htt constructs in U2OS cells using X-34 aggregate stain.

In this figure, IF staining of U2OS cells is shown, which had been transfected with HA-tagged Htt20Q and Htt97Q via GeneJuice® (protocol 3.2.3.4). Staining was performed using HA-antibody (green), PI served as a nuclear stain (red) and X-34 to visualize aggregates (blue) (protocol 3.2.3.7). As control, pcDNA3 transfected cells were analyzed. Scale bar shows 20 µm.

PcDNA3 plasmids with constructs of HA-tagged exon 1 of Htt and different glutamine repeat lengths were used for our investigations. One with a physiological number of 20 glutamine repeats (Htt20Q), and one with 97 glutamine repeats (Htt97Q), representing pathological elongation. The empty vector pcDNA3 was used as a control.

In the first experiment (figure 12) IF staining of U2OS cells was performed using anti-HA antibody to visualize Htt, PI as a nuclear stain and X-34 to detect β-amyloid structures (protocol 3.2.3.7). The cells had previously been transfected with Htt constructs (Htt20Q, Htt97Q) and the empty vector pcDNA3 as control using GeneJuice® (protocol 3.2.3.4). Cells were visualized using immunofluorescence microscopy and 63x magnification. Here, the different morphologies of Htt in its physiological and pathologically elongated form could be distinguished. Htt20Q showed even distribution within the cell, whereas Htt97Q formed perinuclear structures. The latter colocalized with X-34, which confirmed them as aggregates.

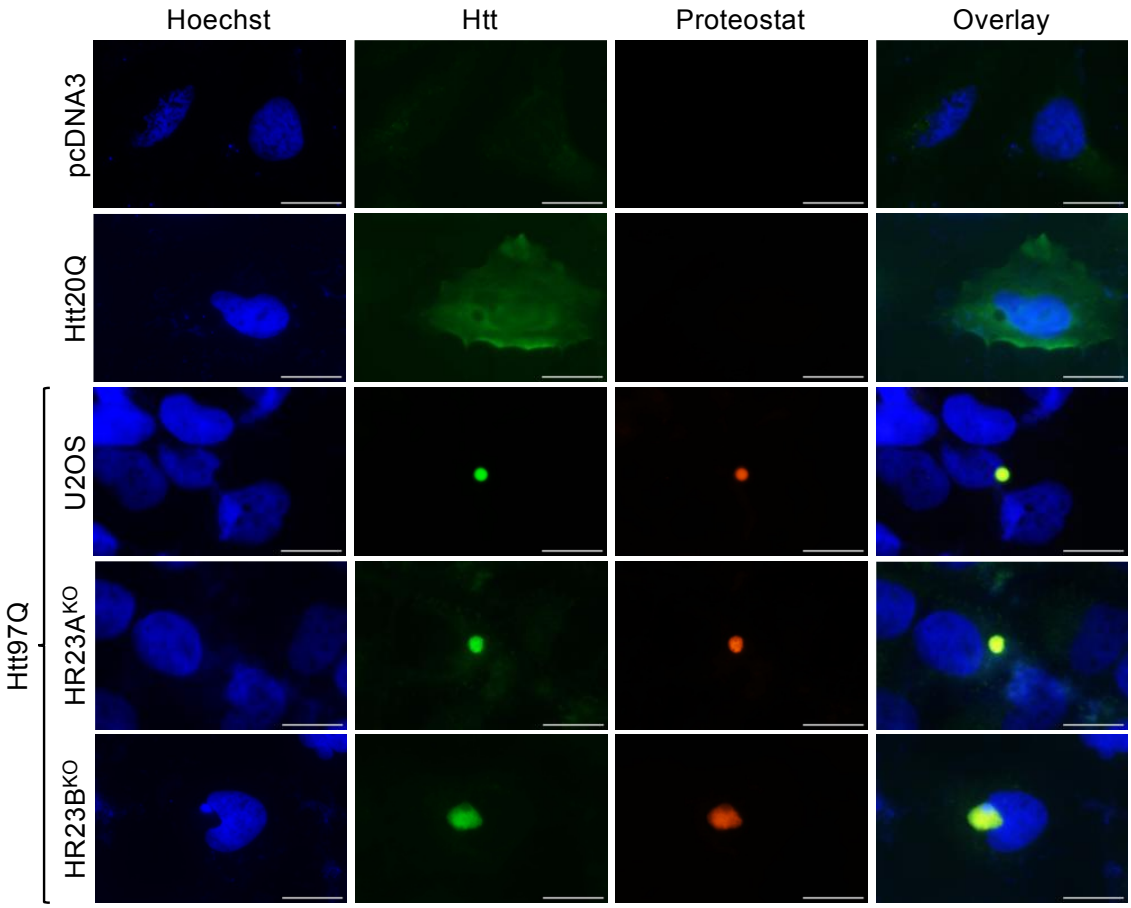

Figure 13: IF staining of Htt constructs in U2OS and HR23A/B^{KO} cells using aggregate stain Proteostat®.

U2OS and HR23A/B^{KO} cells were transfected using GeneJuice® (protocol 3.2.3.4) with HA-tagged Htt 20Q and 97Q as well as the empty vector pcDNA3. IF staining was performed using anti-HA antibody (green), Hoechst (blue) for nuclear staining and Proteostat® aggregate kit (orange) to visualize amyloid structures (protocol 3.2.3.7). Controls were pcDNA3 and Htt20Q transfected cells. Scale bar shows 20 µm.

To validate these findings and investigate the role of HR23A and HR23B in the aggregation behavior of pathological Htt, another experiment involving the HR23A/B knockout cell lines and a different aggregate stain, Proteostat® was performed. U2OS, HR23A^{KO} and HR23B^{KO} cells were transfected using Gene Juice (see protocol in 3.2.3.4) and IF staining performed consecutively (see protocol in 3.2.3.7). In this case, anti-HA antibody (green) was used to visualize Htt and the Proteostat® aggregation kit to detect β-amyloid structures (orange). Hoechst served as a nuclear stain (blue). The samples were visualized using immunofluorescence microscopy and 63x magnification (see figure 13).

Along with the results in figure 12, physiological Htt20Q showed even distribution throughout the cell and Htt97Q formed perinuclear structures. On top of that, the second aggregate stain Proteostat® also confirmed those structures to be aggregates.

Interestingly, it could be observed that aggregates consistently appeared larger and less dense in both HR23A and HR23B knockout cells.

4.3.2. Quantitative analysis of cross-sectional area of Htt 97Q aggregates in HR23A/B^{KO} cells

To look further into the effect of HR23A and HR23B on the aggregation behavior of pathological Htt, the size of the aggregates in the different cell lines was measured. First of all, using IF images obtained in 4.3.1, the cross-sectional area (CSA) of the Htt97Q aggregates in all cell lines was analyzed manually using ImageJ software (protocol see 3.2.3.8). The results are shown in panel (A) of figure 14.

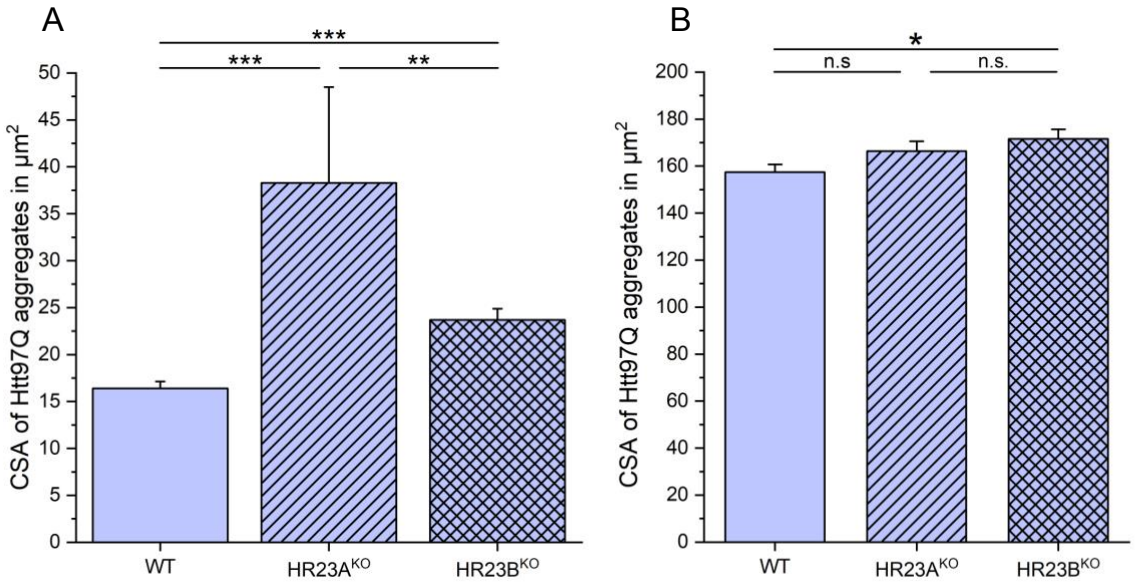

Figure 14: Quantitative analysis of the CSA of Htt97Q aggregates in U2OS and HR23A/B^{KO} cells using two different methods.

The cross-sectional areas of Htt97Q aggregates were measured manually using ImageJ software (A) (protocol 3.2.3.8) and automatically using Operetta Hight content analysis system (B) (3.2.3.9). Mean values and their standard deviations are shown above. In (A) number of aggregates varied between the cell lines (U2OS n = 126, HR23A^{KO} n = 8, HR23B^{KO} n = 58) and in (B) n > 361 (3 biological replicated with a minimum of 361 technical replicated each). P-values were calculated using One-way ANOVA and consecutive Tukey test. The CSA of Htt97Q aggregates is shown to be greater in HR23B^{KO} cells than in U2OS cells using both approaches. Comparing the CSA of Htt97Q aggregates in HR23A^{KO} cells with U2OS and HR23B^{KO} cells showed an increase in the manual approach (A) and no effect in the automated one (B). P-values are indicated by stars, (*) $p < 0.05$, (**) $p < 0.01$, (***) $p < 0.005$. N.s. indicates $p > 0.05$.

Different numbers of aggregates in each cell line were measured using this method (U2OS n = 126, HR23A^{KO} n = 8, HR23B^{KO} n = 58) and statistically analyzed using Origin Pro. The analysis showed that CSA of Htt97Q aggregates increase in both HR23A^{KO} and HR23B^{KO} cells compared to WT, showing the highest mean CSA in HR23A^{KO}.

Having successfully quantified this difference in CSA in the different cell lines, another approach of analysis was used to verify the findings. To achieve a more consistent

number of aggregates measured in each cell line and to automatize the method, the Operetta high content analysis system was used (results shown in figure 14 (B) (protocol see 3.2.3.9). U2OS, HR23A^{KO} and HR23B^{KO} cells were seeded onto a 96 well plate and transfected with HA-tagged exon 1 of Htt20Q and Htt97Q. Cells were stained using anti-HA and Hoechst as nuclear stain. Two IgG controls for both mouse and rabbit secondary antibodies were established to test for unspecific signals. With the Harmony high content analysis software, it was possible to detect the aggregates of Htt97Q using “find spots” and measure the CSA with n > 361 in each of 3 biological replicates.

In HR23B^{KO} cells the mean CSA of Htt97Q aggregates increased compared to WT using both methods of quantification. The increase of CSA in HR23A^{KO} cell lines could only be detected using relatively small (n = 8) number of aggregates in the manual approach. Comparing aggregate CSAs in HR23A^{KO} cells to WT and HR23B^{KO} using Operetta high content analysis system showed no difference.

4.3.3. Analysis of Htt aggregate / cell ratio in U2OS and HR23A/B^{KO} cells

Along with the CSA of the aggregates, the number of aggregates that form per individual cell in the different cell lines was analyzed. To realize this, another experiment using Operetta high content analysis system was carried out. Here, the cells were stained additionally with anti-GAPDH antibody, detecting a housekeeping protein which is distributed evenly in the cell. This allowed identification of the cell borders similarly to the method in 4.2.1 where this approach was used to measure N/C ratios. Since it was possible to identify singular cells using feature “find cells” and Htt97Q aggregates using “find spots”, the ratio of Htt97Q aggregates per cell (aggregate/ cell ratio) could be measured.

Figure 15 (A) shows the results of the statistical analysis and (B) an example of the IF staining of this experiment. It became clear that the aggregate/ cell ratio increased in HR23B^{KO} cells compared to WT ($p < 0.005$) and HR23A^{KO} cells ($p < 0.005$). There was no increase of aggregate/cell ratio in HR23A^{KO} cells compared to WT ($p = 0.62$).

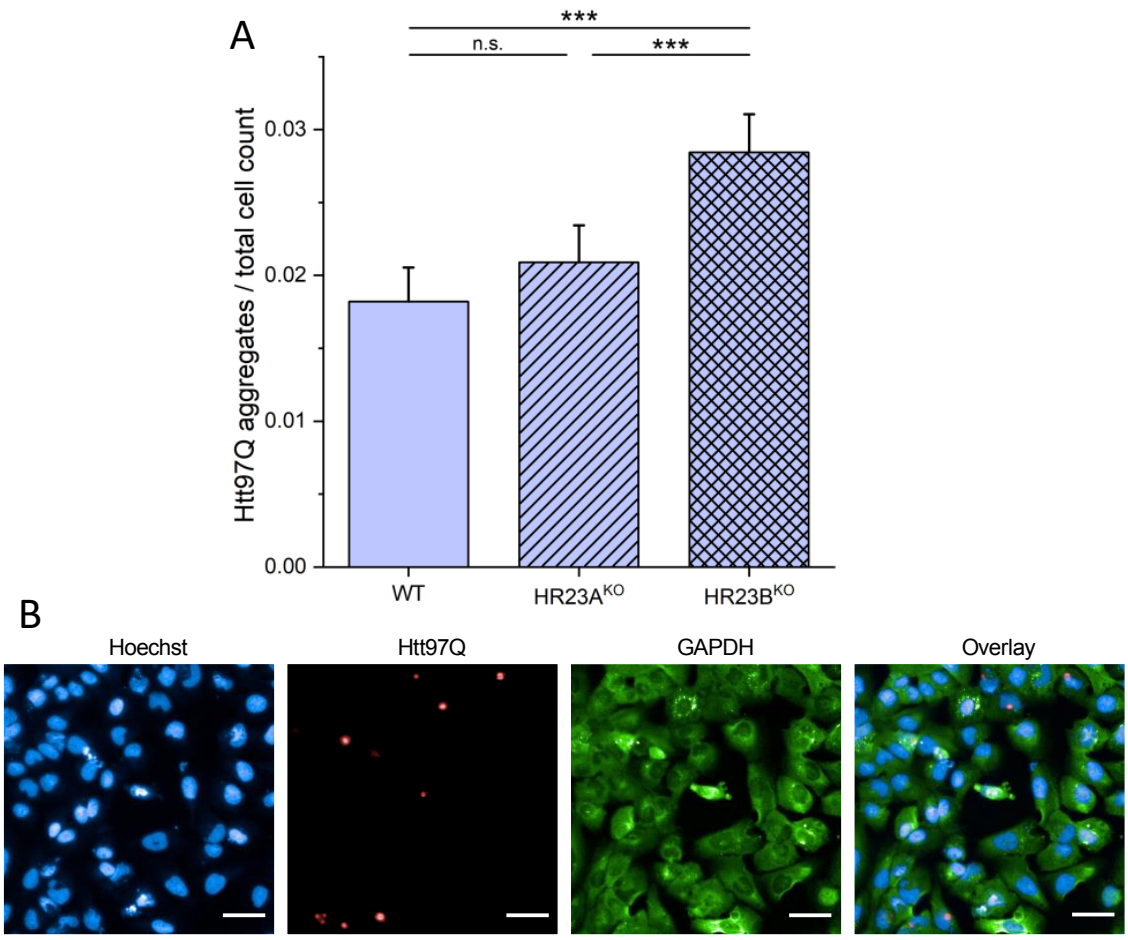

Figure 15: Analysis of aggregate/ cell ratio in U2OS and HR23A/B^{KO} cells.

The aggregate/ cell ratio of Htt97Q in U2OS and HR23A/B^{KO} cells was measured using Operetta high content analysis system (protocol 3.2.3.9). IF staining (B) was obtained using anti-HA to detect Htt97Q aggregates and anti-GAPDH to visualize the cytoplasm/ cell borders. Hoechst was used as a nuclear stain (protocol 3.2.3.7). The aggregate/ cell ratio was calculated and the mean values with their standard deviations are displayed in panel (A) (n = 26). HR23A^{KO} and HR23B^{KO} cells showed an increased aggregate/ cell ratio compared to the WT. The data was statistically analyzed using Origin Pro, p-values were calculated using One-way ANOVA. P-values are indicated by stars, (***) $p < 0.005$. N.s. indicates $p > 0.05$. Scale bar shows 50 µm.

4.3.4. Colocalization of Htt and HR23B using immunofluorescence

In the previous experiments, it was discovered that aggregate size and aggregate/cell ratio of Htt97Q changed in HR23B^{KO} cells. This indicated that HR23B had an impact on the aggregation behavior of pathological Htt. To investigate whether HR23B and Htt97Q might interact with each other, IF staining was performed to colocalize the two proteins. U2OS cells were transfected with pcDNA3, Htt20Q and Htt97Q using GeneJuice® (protocol 3.2.3.4). IF staining was performed using anti-HA (green) to detect Htt, anti-HR23B (red) to visualize HR23B and Hoechst as a nuclear stain (protocol 3.2.3.7). The cells were analyzed using immunofluorescence microscopy with 63x magnification shown in figure 16.

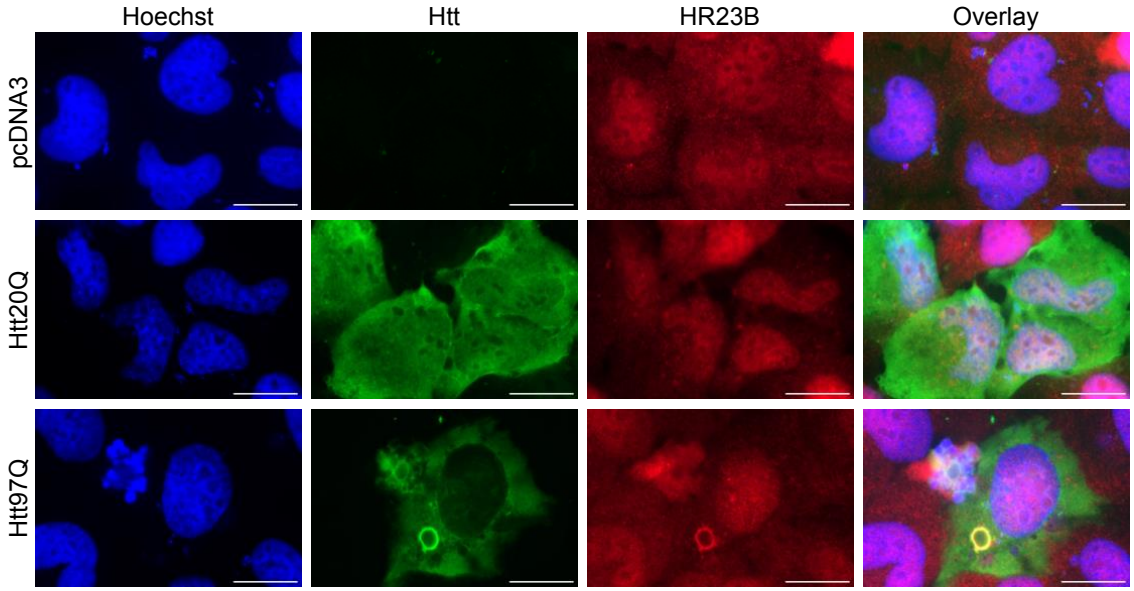

Figure 16: Colocalization of Htt and HR23B using immunofluorescence.

U2OS cells were transfected with HA-tagged Htt20Q and Htt97Q and visualized using immunofluorescence microscopy and 63x magnification. The empty vector pcDNA3 served as control. HR23B could be detected using anti-HR23B (red), Htt with anti-HA (green). Hoechst was used as a nuclear stain (blue). Scale bar shows 20 µm.

As depicted before (see 4.3.1), Htt20Q was distributed evenly in the cell and Htt97Q formed perinuclear aggregates. HR23B was both visible in the cytoplasm and nucleus of the cell, similarly to the observations made in 4.1.2. Observing the IF image of Htt97Q transfected cells an increased intensity of HR23B was noticeable which colocalized with the perinuclear aggregates of Htt97Q.

4.3.5. Co-Immunoprecipitation with GFP-tagged Htt74Q

To further investigate a possible interaction between HR23B and pathological Htt, co-immunoprecipitation (CO-IP) was performed. This method can be used to indicate an indirect interaction between two proteins using an antibody and agarose beads to precipitate the proteins. Kaltenbach et al. had already identified interactors of Htt using this method (Kaltenbach et al. 2007).

Here, a different Htt construct with a GFP tag and 74 glutamine repeats (GFP-Htt74Q) as well as the corresponding GFP-antibody were used in order to perform the pull down of Htt.

U2OS cells were transfected with GFP-Htt74Q and peGFP as a control using GeneJuice® (protocol 3.2.3.4). CO-IP was performed using agarose beads as well as anti-GFP antibody and IgG as control (protocol 3.2.2.7). After successful precipitation, samples were analyzed using WB and anti-HR23B antibody. In figure 17, immunoblots of anti-GFP (A), anti-HR23B (B) and anti-GAPDH (C) are displayed. In the anti-GFP blot, several signals could be detected. In the IP and lysate of peGFP transfected cells (lane

1 and 4), a signal at around 28 kDa and 70 kDa could be observed. The intensity of the signals seemed stronger in the IP, indicating successful pulldown. In GFP-Htt74Q transfected samples (lane 2 and 6) two signals could be observed. One at 28 kDa and one at 55 kDa. The band that ran at 55 kDa showed a strong signal increase comparing lysate to IP sample, also indicating effective precipitation of the protein. Negative controls with IgG showed no signals.

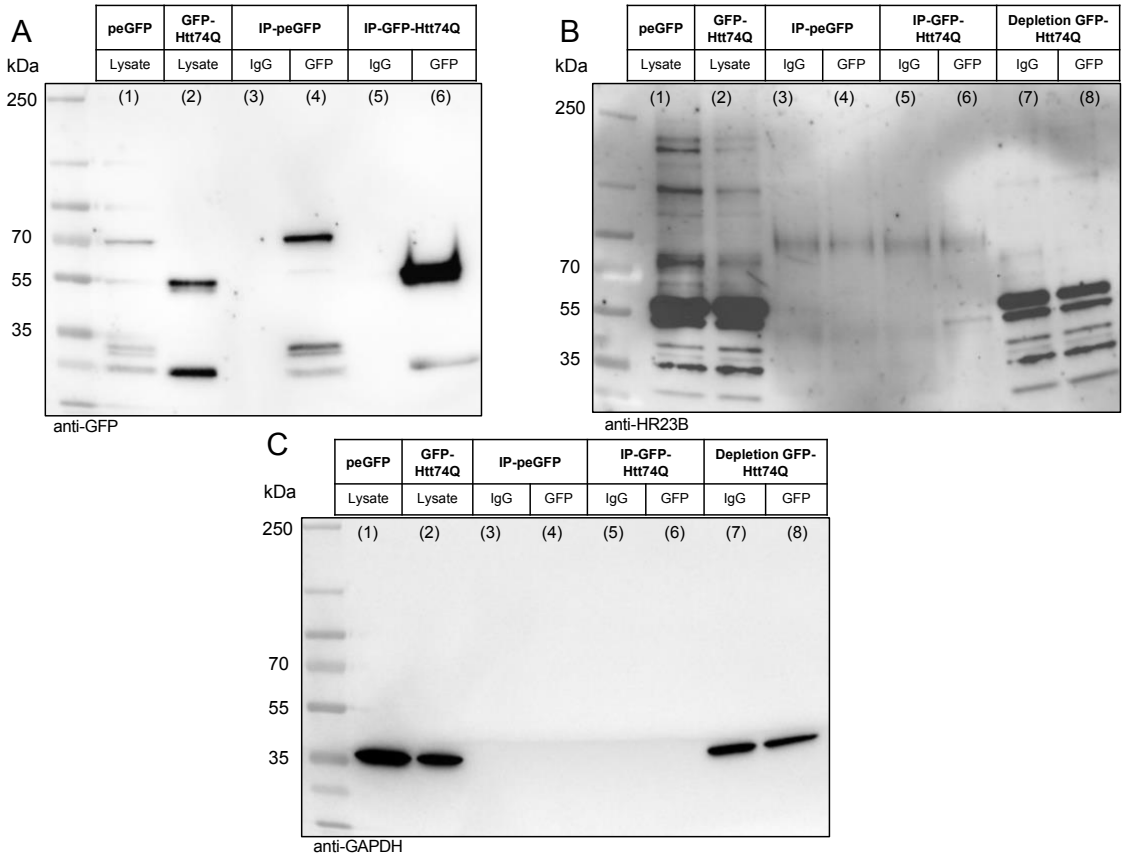

Figure 17: Immunoblots of applied CO-IP of GFP-Htt74Q.

U2OS cells were transfected with GFP-Htt74 and the empty vector peGFP, which served as control (protocol 3.2.3.4). The immunoprecipitation was performed using anti-GFP antibody and IgG as control (protocol 3.2.2.7). The samples were then analyzed in WB and immunoblots were performed using anti-GFP (A), anti-HR23B (B), and anti-GAPDH (C) (protocol 3.2.2.4). In the first and second lane, lysates of peGFP and GFP-Htt74Q transfected cells are shown. In third to sixth lane IPs were applied and seventh and eighth lane showed the depletion. The anti-GFP immunoblot showed the augmented level of GFP-Htt74Q in the IP. HR23B could be detected in both cell lysates and the depletion. In the GFP-Htt74Q-IP there was a light band visible running 5 kDa lower than the estimated protein size of HR23B.

In the anti-HR23B immunoblot (B) multiple bands with different patterns were visible in all lanes. The strongest signals in lysate and depletion samples were detected at around 58 kDa, the estimated protein size of HR23B. Looking at all IP samples (lane 3-6), there was one band at around 100 kDa which appeared in the IP performed with GFP and its negative control. In the IP sample of GFP-Htt74Q transfected cells (lane 6) another lighter band was visible at around 55 kDa, which did not appear in the negative controls. Anti-GAPDH served as a control.

4.4. Influence of acetylation on cell cycle and translatory rate of HR23A/B^{KO} cells

In further investigations, the influence of HDACi treatment on cell cycle progression and translatory rate in U2OS cells as well as HR23A/B^{KO} cells was analyzed. Multiple resources had shown that HR23B can be used as a sensitivity marker for HDACi treatment in tumor therapy. This means that high levels of HR23B in a cell lead to more rapid apoptosis, when treated with HDACi. Low HR23B expression levels, however, correlate with degradation via autophagy (New et al. 2013). We performed the following experiments to investigate the influence of HDACi on cell cycle progression and proteostasis in WT and HR23A/B^{KO} cells. These experiments provide the basis on which further research can be conducted in the future. This might include the interplay of HDACi and the UPS as well as their influence on misfolded proteins.

4.4.1. Cell cycle analysis in U2OS and HR23A/B^{KO} cells upon HDACi treatment

In 4.2.2, cell cycle progression in U2OS and HR23A/B^{KO} cells was investigated, and results showed differences in the pattern of relative cell amounts in G1, S and G2 phase. In this experiment U2OS, HR23A^{KO} and HR23B^{KO} cells were treated with 2.5 µM, 5 µM, and 10 µM of HDACi Vorinostat (SAHA) and DMSO as negative control for 24 h. Subsequently, cells were harvested, fixed and stained with PI and analyzed using flow cytometry (protocol 3.2.3.5). Cell cycle analysis was then performed using BD accuri analysis software, dividing the cells according to their PI signal intensity proportional to DNA content (see protocol 3.2.3.6). The cell amounts were then normalized on the total cell count resulting in relative cell amounts in %.

Figure 18 shows the overall distribution of relative cell amounts in all cell cycle phases, looking at the different cell lines and SAHA concentrations analyzed in the experiment. In this graph, the overall tendencies of change in relative cell amounts could be observed. To perform statistical analysis, the relative cell amounts of each cell line, SAHA concentration and cell cycle phase were normalized on the DMSO treated sample. The results display relative changes of cell amounts of each phase and are shown in figure 19 comparing different HDACi concentrations and comparing the effect in different cell lines in figure 20.

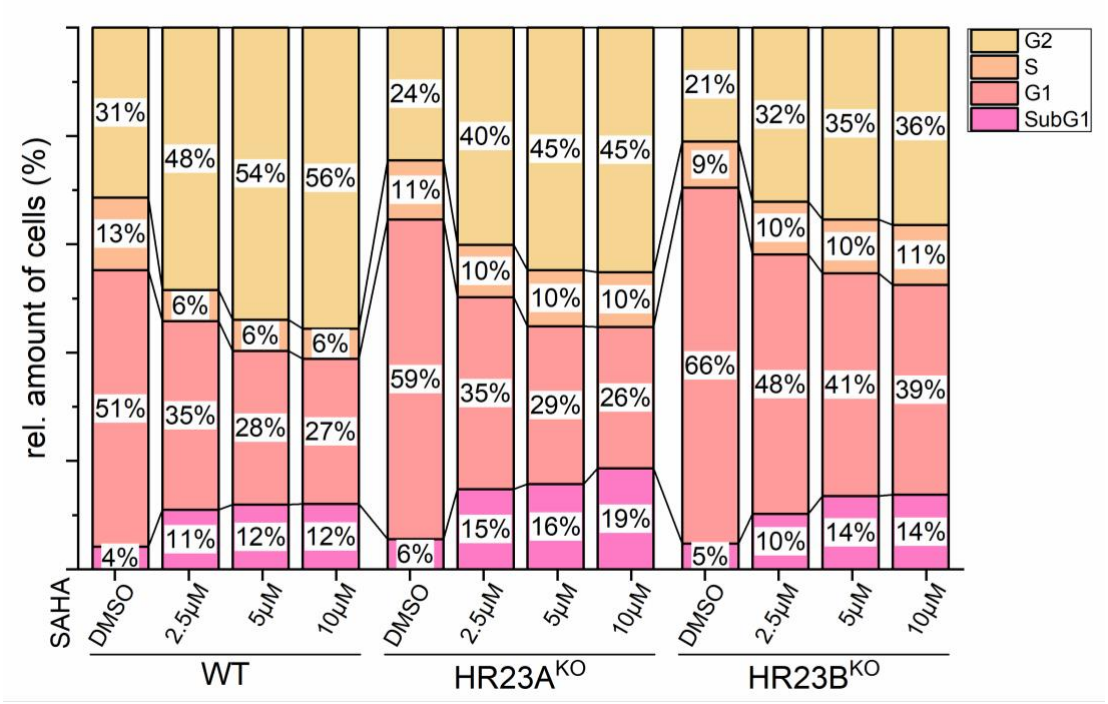

Figure 18: Cell cycle analysis of U2OS, HR23A^{KO} and HR23B^{KO} cells under different HDACi treatments.

U2OS and HR23A/B^{KO} cells were grown to 85% confluency and treated with 2.5 µM, 5 µM, 10 µM SAHA as well as DMSO as control for 24 h. The cells were then harvested and prepared for cell cycle analysis using flow cytometry (see 3.2.3.5 and 3.2.3.6). The DNA content of each cell was measured using PI staining and the cell cycle phases were analyzed accordingly using BD accuri analysis software. Relative cell amounts were calculated using the total cell count and mean values are displayed above (n = 5).

Firstly, cell amounts of each phase within one specific cell line and varying SAHA concentrations were compared (see figure 19). It could be observed that the relative cell amount in subG1 phase increased with rising concentration of HDACi treatment in all cell lines (fig. 19 panel A). Regarding G1 phase, the relative cell amount decreased in each cell line with increasing HDACi concentration (fig. 19 panel B). In S phase, the effect of HDACi treatment on the different cell lines seemed to be most diverse (fig. 19 panel C). In U2OS cells the relative cell amount decreased under HDACi treatment of any concentration ($p < 0.005$). In HR23A/B^{KO} cells the relative cell amount in S phase stayed the same or even increased in HR23B^{KO} cells with 10 µM SAHA treatment ($p < 0.005$). Lastly, in G2 phase the relative cell amounts increased in each cell line under HDACi treatment (fig. 19 panel D).

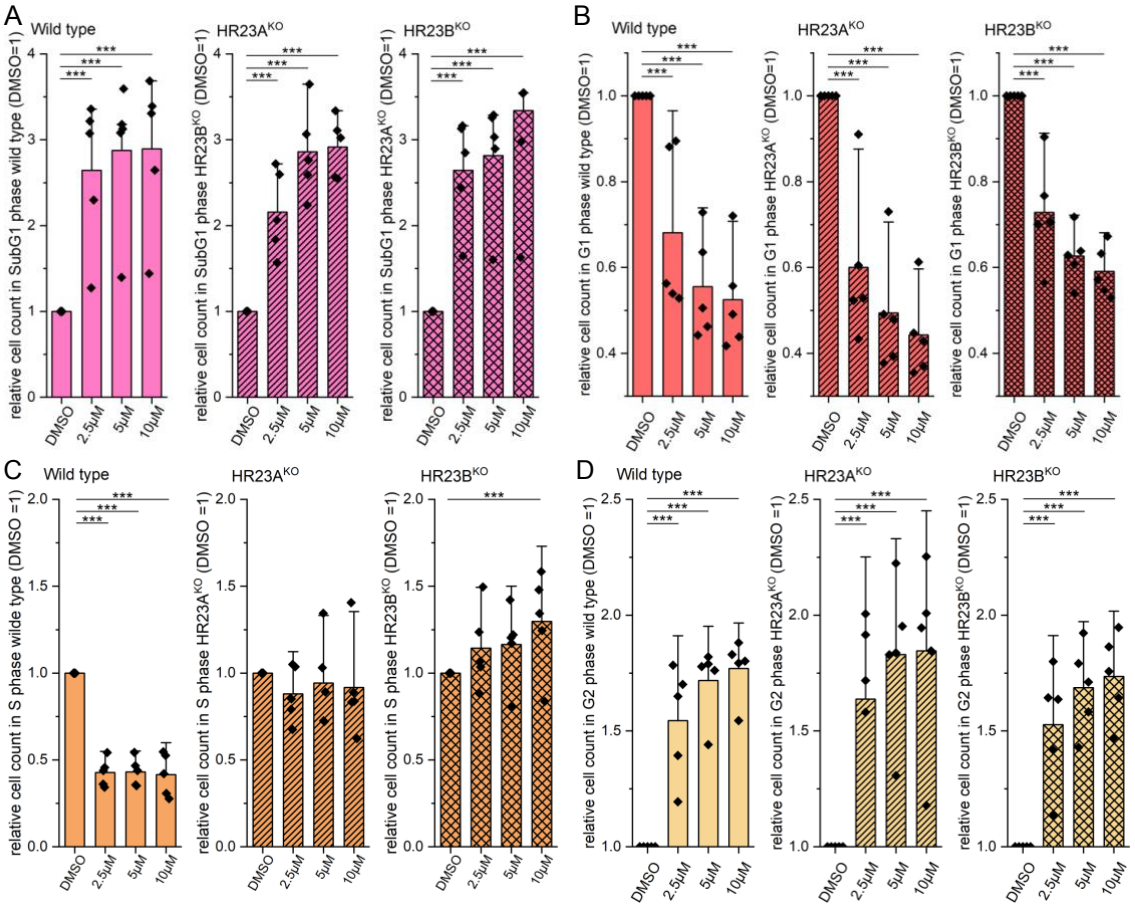

Figure 19: Statistical analysis of cell cycle analysis in U2OS and HR23A/B^{KO} cells under different HDACi treatment concentrations.

This figure shows the statistical analysis of the cell cycle data obtained in 4.4.1. The relative cell amounts of each cell cycle phase and HDACi treatment concentration were normalized on the DMSO treated control of each cell line. Here, this data is shown comparing the relative cell amounts between different levels of HDACi treatments in U2OS, HR23A^{KO} and HR23B^{KO} cells. Mean values and their standard deviations are shown (n = 5). Panel (A) shows the change of relative cell amount in subG1 phase, (B) G1 phase, (C) S phase and (D) G2 phase. P-values were calculated in Origin Pro using Two-way ANOVA and consecutive Tukey test. P-values are indicated by stars, (***) $p < 0.005$. N.s. indicates $p > 0.05$.

In a second analysis, relative cell amounts of each phase in U2OS, HR23A^{KO} and HR23B^{KO} cells were compared in samples with similar HDACi treatment concentration. The results of the statistical analysis are demonstrated in figure 20. Comparing the different cell lines, no difference in relative change of cell amount in subG1 phase could be observed (fig. 20 panel A). In G1 phase, it was noticeable that in HR23B^{KO} cells the cell amount increased to a bigger extent compared to HR23A^{KO} cells ($p < 0.05$) (fig. 20 panel B). Comparing both knockout cell lines to the WT showed no effect. In S phase (fig. 20 panel C), similar to the analysis depicted in figure 19, the relative changes of cell amount deviated in different directions depending on the cell line. In WT cells relative cell amount decreased while it stayed almost the same in HR23A^{KO} and even increased in HR23B^{KO} cells. This pattern could be observed in all levels of HDACi treatment and all

effects in relative change of cell amount showed p-values < 0.005. Lastly, when looking at G2 phase no differences between the cell lines could be observed (fig. 20 panel D).

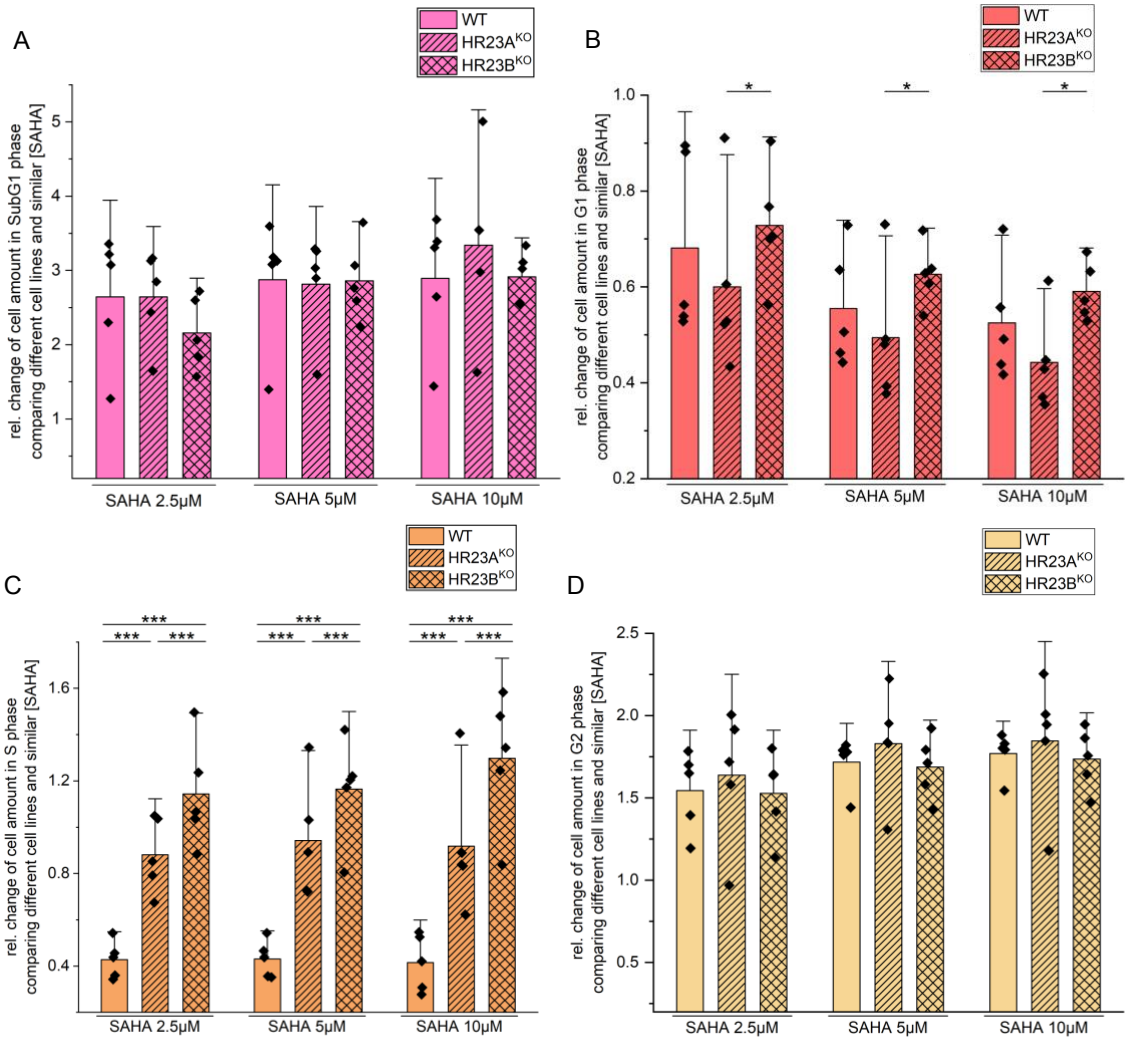

Figure 20: Statistical analysis of cell cycle phases in U2OS and HR23A/B^{KO} cells under HDACi treatment comparing the effect in each cell line.

The change of relative cell amount in each cell cycle phase and HDACi concentration was analyzed and compared between U2OS, HR23A^{KO} and HR23B^{KO} cells. Mean values and their standard deviations (n = 5) are displayed. Panel (A) shows subG1 phase, (B) G1 phase, (C) S phase and (D) the G2 phase. P-values are indicated by stars, (*) $p < 0.05$, (***) $p < 0.005$. N.s. indicates $p > 0.05$.

4.4.2. Puromycin incorporation assay in U2OS and HR23A/B^{KO} cells under HDACi treatment

In addition to analyzing changes in cell cycle progression upon HDACi treatment, translatory rates in U2OS and HR23A/B^{KO} cells were also investigated. To do so, puromycin incorporation assays were performed similarly to 4.2.3 (protocol see 3.2.2.6). In this case, however, cells were treated with 5 µM Vorinostat (SAHA) and DMSO as negative control for 24 h prior to harvest. The level of SAHA concentration was chosen due to the results conducted in cell cycle analysis. Here, 24 h incubation with 5 µM

HDACi treatment showed the greatest effect with the least impact on cell viability, represented by the subG1 phase (see figure 18 and 19).

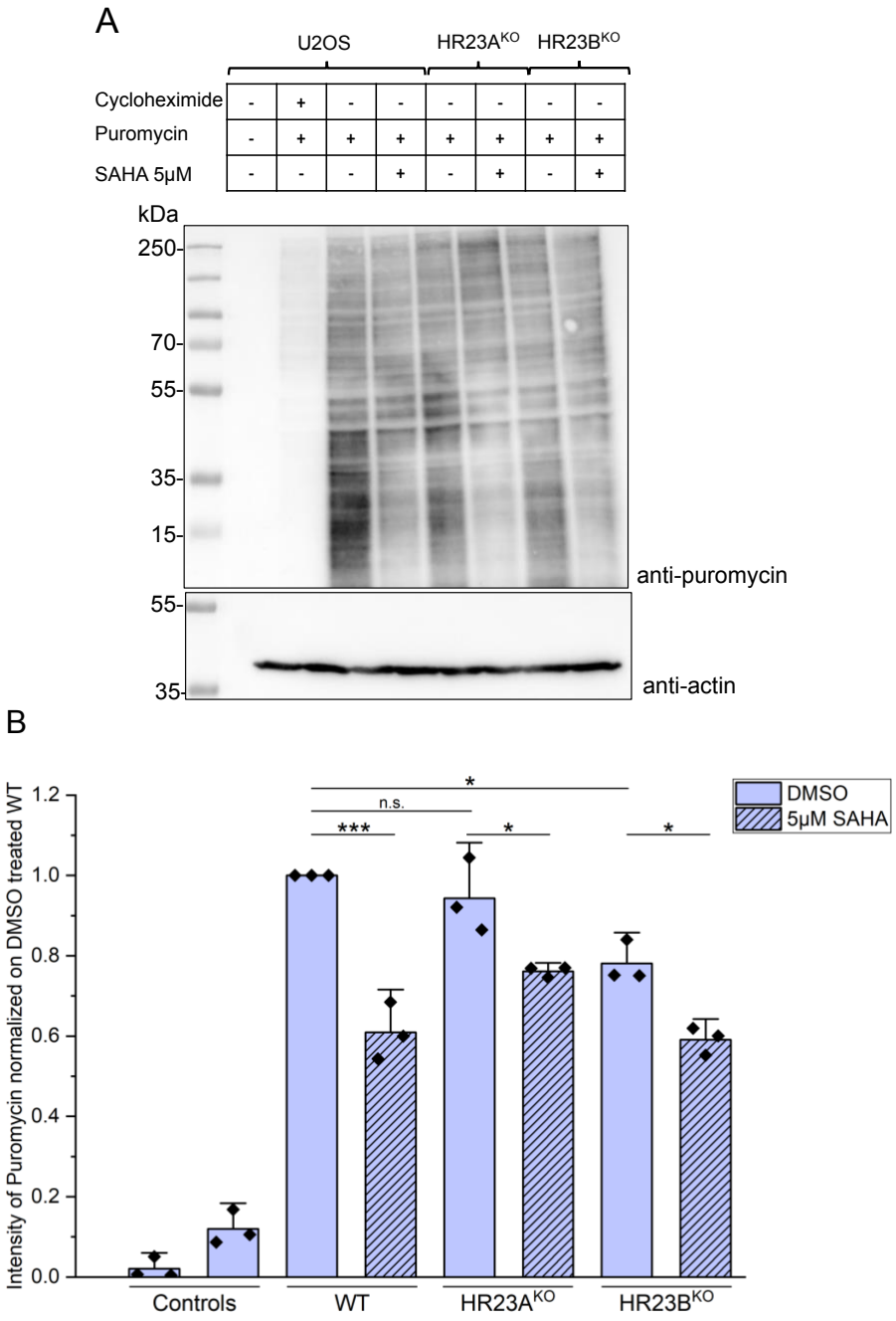

Figure 21: Translatory rates in U2OS and HR23A/B^{KO} cells under HDACi treatment.

U2OS and HR23A/B^{KO} cells were cultivated to 85% confluency. They were treated with 5 µM SAHA or DMSO (control) for 24 h preceding harvest. Afterwards, cells were treated with puromycin. Two controls were carried along, control 1 with no puromycin treatment, control 2 with pre-treatment with cycloheximide (protocol 3.2.2.6). Cells were lysed and analyzed in WB using anti-Puromycin and anti-actin as loading control (protocol 3.2.2.4). Panel A shows the corresponding immunoblots while panel B shows results of the statistical analysis. The puromycin intensity was normalized on Ponceau S staining and puromycin intensity of untreated WT sample. Mean values and their standard deviations are displayed (n = 5). Statistical analysis was performed in Origin Pro using Two-way ANOVA and Tukey test. P-values are indicated by stars, (*) $p < 0.05$, (***) $p < 0.005$. N.s. indicates $p > 0.05$.

As displayed in figure 21 translatory rates decreased in every cell line under HDACi treatment ($p < 0.05$). In 4.2.3, it had already been shown that translatory rates in $HR23B^{KO}$ cells decreased compared to the WT. This result could be replicated in this experiment ($p < 0.02$). However, this was not observed when comparing $HR23A^{KO}$ to WT ($p = 0.47$).

To compare the effect of HDACi treatment on the translatory rate of each cell line, the results were normalized on DMSO treated WT samples and additionally on the DMSO treated control of the correspondent cell line. This way, the relative change of translatory rate under HDACi treatment could be compared between the different cell lines. The results are depicted in figure 22 and show that this calculated ratio of puromycin intensity decreased to a lesser degree in $HR23A^{KO}$ ($p < 0.005$) and $HR23B^{KO}$ cells ($p < 0.05$) compared to WT. There was no effect comparing $HR23A^{KO}$ and $HR23B^{KO}$ cell lines.

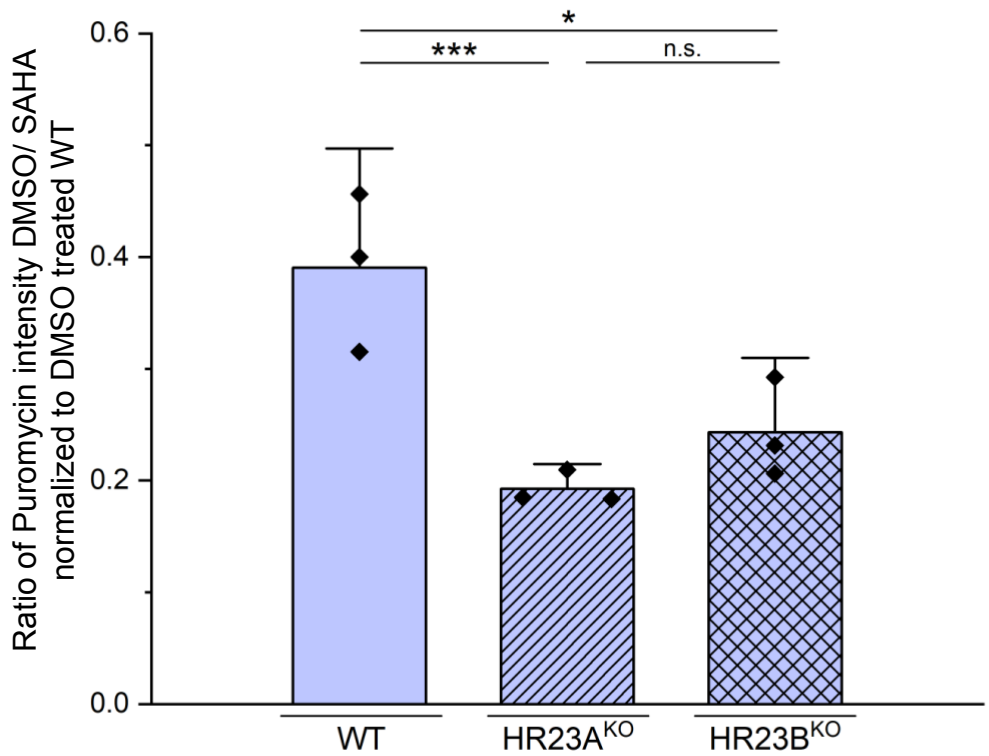

Figure 22: Ratio of puromycin intensity change under HDACi treatment in U2OS, $HR23A^{KO}$ and $HR23B^{KO}$ cells.

This figure shows the relative decrease of puromycin intensity (or calculated ratio) of the investigated cell lines under HDACi treatment. The results were normalized once on DMSO treated WT and then again on the DMSO treated control of the corresponding cell line. This data was statistically analyzed using Origin Pro and One-Way ANOVA with consecutive Tukey test. P-values are indicated by stars, (*) $p < 0.05$, (***) $p < 0.005$. N.s. indicates $p > 0.05$.

5. Discussion

5.1. Proteasome shuttling factors HR23A and HR23B have an impact on cellular morphology, cell cycle progression and proteostasis

5.1.1. Expression of HR23 proteins in U2OS cells

HR23A and HR23B, human homologues of Rad23A and Rad23B which were discovered in *S. cerevisiae*, are proteins with similar but not identical structures. Both contain one UbL and two UbA domains and have been shown to be involved in different cellular functions. These range from NER to nuclear-cytoplasmic transport and protein degradation as part of the UPS. While this study focused mostly on their role as proteasome shuttling factors, it is relevant to investigate where and to what extent these proteins are expressed in the cell culture model used.

Testing the expression levels of HR23A and HR23B in both knockout cell lines and WT U2OS cells showed that HR23B is overexpressed in case of HR23A knockout (see figure 7). However, HR23A levels did not increase in $HR23B^{KO}$ cells. This suggested that HR23B is upregulated in case of HR23A knockout, but not the other way around. If HR23B can replace the entirety of HR23A's functions, its increase in concentration might compensate the effects of HR23A knockout, which might explain the varying effects of HR23A and HR23B knockout in the conducted experiments. It is to be noted that this experiment was only performed once during this study, limiting its significance. However, since finishing this study, Linda Kulka has been able to reproduce these results and verify them through statistical analysis (data not published).

On top of that, Okuda et al. showed that the concentration of HR23B in U2OS cells is on average 10 times higher than the one of HR23A (Okuda et al. 2004). This might further explain the exaggerated effects of HR23B knockout compared to HR23A knockout in most experiments that were conducted in this study. To fully understand whether HR23A and HR23B can replace each other in their function, the cloning of a double-knockout cell line of these proteins has been obtained. These cells are currently investigated and characterized. Moreover, investigating HR23A/B's functions under cellular stress conditions or consecutive of induced DNA damage might help showing the effects more clearly in the future.

In the IF staining performed, the distribution of HR23B could be observed within the cell. It showed that HR23B is present in all cell compartments and IF signal intensity was

highest in the nucleus. These observations were coherent with ones made by different research groups using U2OS and other human cell lines (New et al. 2013; Katiyar, Li, and Lennarz 2004). In the cytoplasmic nuclear extraction assay that was performed, a pattern in which approximately 66% of HR23B resides in the cytoplasm and 39% in the nucleus was observed. These results contradicted the above-mentioned findings in IF imaging. One hypothesis explaining this deviating pattern might be dissimilar methods of measurement in the two experiments. In the extraction assay the total protein amount was measured, independently of the size of the cellular compartment from which it was extracted. In IF, however, the intensity of the fluorescent signal, which is proportional to protein concentration, meaning protein amount per area of the cell, was analyzed. It is possible that a larger amount of HR23B is distributed in the relatively bigger cytoplasm, resulting in lower concentrations while lower HR23B amounts are distributed in the relatively smaller nucleus resulting in higher protein concentrations. To correct this kind of distortion of the data, one would have to normalize the protein amounts measured in the extraction assay on a protein which is known to be expressed equally in the nucleus as in the cytoplasm. Another explanation for the results might be an incomplete lysis of the nucleus, which would explain a decreased protein harvest. To decrease this possibility, it was ascertained that the nuclear membrane was broken up as best as possible performing lysis under harsh conditions and sonifying the samples multiple times.

Katiyar et al. further showed that the localization of HR23B changes depending on the cell cycle. During G1 phase HR23B resides in cytoplasm and nucleus, whereas in S phase HR23B amount in the nucleus is lowest (Katiyar and Lennarz 2005). Since the cell cycle of the cells was not measured prior to performing nuclear cytoplasmic extraction assay there is no way to be certain whether an increase of cells in S phase might have contributed to the results above. We have however performed cell cycle analysis in a different experiment, which showed the highest relative cell amount of U2OS WT cells in G1 phase (53%) under normal cultivating conditions at around 85% confluency. In addition, Linda Kulka had found that the HR23B amount in U2OS cells is highest during the S-phase (data not published).

Regarding the HR23B immunoblot of the cytoplasmic nuclear extraction assay another interesting observation could be made. It was noticeable that the nuclear and total protein fraction show two additional bands, one at 53 kDa and one at 38 kDa. Considering that these bands were not visible in the cytoplasmic protein fraction, it might be assumed that HR23B undergoes additional modification in the nucleus. An interaction with a nuclear

protease or caspase might be part of the explanation. To investigate that further, mass spectrometry might be used in the future to find new interaction partners of HR23B.

In conclusion, it could be shown that HR23B levels rise in HR23A^{KO} cells, but not the other way around. This suggests that the knockout of HR23A triggers HR23B overexpression. It was also shown that HR23B resides both in the nuclear and cytoplasmic compartment with contradicting results regarding the ratio of this distribution. There are different factors including changes in cell cycle that influence the localization of HR23B, which might explain this discrepancy. Lastly, the HR23B immunoblot of the nuclear protein fraction showed additional bands, which suggests that HR23B might be further modified in the nuclear compartment.

5.1.2. HR23A and HR23B impact cell cycle progression, cell morphology and proteostasis

In order to gain deeper understanding of HR23As and HR23Bs role in the progression of the cell cycle, cell cycle analysis in both knockout cell lines and U2OS cells was performed. Here, it was found that in HR23A/B^{KO} cells, the relative cell amount in G1 phase increases, while it decreases in S phase and G2 phase.

Separating G1 and S phase there is an important checkpoint which controls proliferation of a cell (Bertoli, Skotheim, and de Bruin 2013). The distribution of relative cell amounts in the results indicate that due to the knockout of HR23A or HR23B the cell cycle progression is inhibited at this point. Diana Panfilova, who cloned the knockout cell lines had seen similar patterns in her experiments (data not published). This is also coherent with the observations found by Tan et al., who could show that HR23A knockdown hinders cells to pass the G1/S phase checkpoint and inhibits proliferation (Tan, Liang, and Chuang 2015). On top of that, studies in yeast have also shown that Rad23 is involved in the regulation of the cell cycle progression, especially at S phase checkpoint (Clarke et al. 2001; Elder et al. 2002).

The reason why the absence of HR23A and HR23B changes cellular proliferation and cell cycle in U2OS cells remains unclear. One possibility might lie in the function of HR23A and HR23B in NER. It is known that the majority of NER takes place during G1 phase although it happens during all phases (Sarkar et al. 2006). The knockout of HR23A and B might therefore cause a delay of NER and prolong G1 phase. Another theory might be that due to HR23As and HR23Bs function in protein quality control, proteins concentrations change due to the knockout. Any shift in proteostasis might also impact proteins that are involved in cell cycle regulation and then lead to results as described above.

The method which was used to analyze the cell cycle is based on the measurement of PI signal, using flow cytometry. As a result, cell cycle phase distribution patterns were created, and markers were used to quantify the relative cell amounts. The markers were set precisely and were aligned throughout all the samples, but there is still room for inaccuracies due to the manual technique. Small standard deviations, however, showed good reproducibility of the results and the statistical analysis could confirm differences between the cell lines. It's important to note, that the cell cycle analysis performed allowed only to investigate one specific point in time and is therefore ill-suited for interpretation of the true length of each cell cycle phase. For a more precise result, another, more time-consuming method involving 5-bromo-2'-deoxyuridine (BrdU) staining could be performed in the future. Here, the DNA is labelled due to BrdU incorporation and can be measured consecutively using anti-BrdU antibody and flow cytometry (Nowakowski, Lewin, and Miller 1989).

During experiments where U2OS and HR23A/B^{KO} cells were analyzed using IF imaging, a difference in cell morphology became apparent. This observation was quantified using Operetta high content analysis system, analyzing the nuclear and cytoplasmic area as well as the N/C ratio of each cell line. The results showed an overall decrease of N/C ratio in HR23A and HR23B^{KO} cells, mostly due to an increased cytoplasmic area. The N/C ratio generally correlates with the protein amount in each of the cell's compartments. Its dynamic in the knockout cells lines might be due to that fact that HR23A and HR23B can shuttle proteins between nucleus and cytoplasm (Okeke, Chen, and Madura 2020). The absence of those proteins might therefore change overall protein distribution of the cell. A change in N/C ratio may in turn have an impact on metabolic rates and cell cycle progression (Miettinen and Björklund 2017), which could explain the results of cell cycle analysis.

On the other hand, the change in cell cycle progression might also be the reason of the disturbed N/C ratio in HR23A/B^{KO} cells in the first place. Generally, there are two growth phases during the cell cycle, one in G1 and the other in G2 phase. Physiologically, the N/C ratio of a specific cell stays consistent during these processes (von Hertwig 1903). Due to the impact of HR23A/B^{KO} on cell cycle progression however, this regulation might be impaired. To explore this further, real-time analysis of the cell cycle and N/C ratio would need to be performed. The method using Operetta high content analysis system which was used in 4.2.1 had certain strengths and weaknesses. Due to the automated approach and controlled conditions a high number of data points could be gathered, which showed little scattering. This method, however, is rarely used in the literature to measure N/C ratios. The typical method to do this is using flow cytometry. The advantage

of measuring the N/C ratio that way is that in flow cytometry the whole cell and whole nucleus can be analyzed (Sebastian et al. 2021). In IF imaging the data points were calculated using cross sectional areas of the cells and organelles. The dimension in which the cells are visualized could alter the real size of the CSA measured and therefore lead to inaccurate N/C ratios. Considering that over 2,100 cells were measured in 3 different biological replicates makes it likely that this effect could be balanced out.

It is important to look further into this change of nuclear to cytoplasmic ratio because it can indicate certain pathologies. Abnormally regulated N/C ratios can for example lead to cellular malfunction and might facilitate disease. Especially the related decrease of proliferation rates and cell cycle progression can be associated with age-related diseases and cancer (Sung et al. 2014).

Along with cell cycle and N/C ratios the overall rate of translation in the knockout cell lines compared to U2OS cells was investigated. In the puromycin incorporation assays a decrease of translatory rate in HR23B^{KO} cells could be observed.

On the first glance the decrease of translatory rate seemed to be incoherent with the changes in cell cycle progression observed previously. Translatory rate is high in G1 phase and since more cells seem to reside in this phase in HR23B knockout cells a higher level of translation could be expected. Reduced protein synthesis itself, however, can also prevent cells from entering the cell cycle (Øvrebø, Ma, and Edgar 2022). This raises the question in what way these two effects are linked.

Pia Fangmann had already conducted experiments that indicate an interaction between HR23B and ribosomal proteins, which might suggest that it regulated their degradation (data not published). A decreased degradation of those ribosomal proteins might indicate increased translation ability and performance. It is also possible that inhibiting the degradation of ribosomal proteins slows down translatory rates since misfolded or damaged proteins are not eliminated.

Puromycin incorporation assays utilize the structural similarity of puromycin to tRNAs to measure the rate of newly synthesized nascent chains over a given amount of time. To strengthen the specificity of the results, two negative controls were carried along, one without puromycin treatment and one with pre-treatment with cycloheximide, which inhibits translation. This method can be used as an alternative to approaches with radioactive materials and has been shown in the literature to be a good tool for investigating global protein synthesis (Schmidt et al. 2009). In recent studies however, it could be shown that puromycin can accumulate within subcellular locations, outside of active sites of translation making the assays results less accurate (Enam et al. 2020).

This might impact the intensity of puromycin measured overall but should not change the data comparing the different cell lines.

Overall, it was found that HR23A/B^{KO} cells showed changes in the cell cycle analysis compared to U2OS cells, which hint towards cell cycle arrest at the G1/ S checkpoint. On top of that, N/C ratios increased in both knockout cell lines, which might relate to the changes in cell cycle progression. Furthermore, a decrease in translatory rate in HR23B^{KO} cells could be measured.

5.2. HR23B alters the aggregation behavior of pathological Htt

Proteasome shuttling factors like HR23A and HR23B have been shown to interact with ubiquitinated proteins and facilitate their transport towards the proteasome (Chen and Madura 2002). Ubiquitinated proteins are targeted for degradation due to different reasons, one including protein misfolding. Waelter et al. for example demonstrated that impairment of the UPS leads to an accumulation of misfolded exon 1 of the protein Htt (Waelter et al. 2001), which suggests that the UPS is involved in its degradation.

In this study different constructs of exon 1 Htt with pathological (97Q) and physiological (20Q) glutamine repeat lengths were used, which were previously sequenced and tested in Western Blot by Linda Kulka. The aim was to investigate whether HR23A and HR23B are interacting with Htt and analyze how they might influence its morphology and aggregation behavior.

Htt is a very large protein with an estimated size of 350kDa. The mutation which causes increased glutamine repeats and eventually leads to the outbreak of HD is located in exon 1 of the HTT gene. This is why the sole expression of exon 1 has been widely used by the scientific community and is sufficient in creating the pathological phenotype of HD in various models (Bates, Mangiarini, and Davies 1998; Mangiarini et al. 1996).

In the first experiments Htt was visualized using immunofluorescence in U2OS cells. Htt20Q showed to be evenly distributed within the cell, whereas Htt97Q formed perinuclear inclusions. B-amyloid structures could be identified in these inclusions using the two different aggregate-stains X-34 and Proteostat®. X-34 is a fluorescent derivative of congo red and specifically stains amyloid structures (Styren et al. 2000). Proteostat®, however, stains aggregates less specifically, most likely due to their hydrophobic structures (Navarro and Ventura 2014). The results are similar to the ones Waelter et al. found investigating the distribution pattern of pathologically elongated Htt in HEK cells (Waelter et al. 2001).

After successful expression of physiological and pathological Htt in U2OS cells the impact of HR23A and HR23B on their morphology and distribution was investigated. Visualizing the aggregates in U2OS and HR23A/B^{KO} cell lines using IF showed that Htt aggregates appeared larger and less dense in both knockout cell lines. This observation was quantified using two different approaches. With ImageJ software, a different number of aggregates were measured in each cell line. (U2OS n=126, HR23A^{KO} n=8, HR23B^{KO} n=58). It was discovered that the CSA increased in HR23A^{KO} and HR23B^{KO} cell lines. Although the statistical analysis showed relevant changes in CSA, the manual approach made a selection bias likely to have an impact on the results. Also, the differing number of aggregates measured, especially the low number of data points in HR23A^{KO} cells, resulted in higher standard deviations and made a distortion of the results possible.

In the second approach, an automated protocol was established involving Operetta high content analysis system, which resulted in a specific recognition of Htt aggregates. The results verified the increased CSA of Htt97Q aggregates in HR23B^{KO} cell lines but showed no difference in CSA comparing WT and HR23A^{KO} cells.

These data suggest that HR23B has an influence on the morphology of Htt97Q aggregates. This could be due a decreased degradation of misfolded Htt in HR23B^{KO} cells, leading to an increased accumulation of the misfolded species and therefore to larger aggregates. Especially Htt species that are further away from the proteasome might be less likely to be recognized and degraded when HR23B is absent. In HR23A^{KO} cells, however, Htt aggregates showed similar CSAs compared to WT. The results in 4.1.1 suggested that HR23B concentrations might increase in HR23A^{KO}, which could lead to a compensation of the loss of the protein. Another reason for this outcome might be that HR23Bs overall concentration had been shown to be around 10x higher than HR23As (Okuda et al. 2004). The knockout of HR23B might therefore have a larger impact on Htt aggregates.

It remains unclear whether the formation of aggregates in HD is serving as a protective mechanism of the cell or if it leads to disease progression. Therefore, an increase of the CSA of Htt aggregates does not necessarily result in an increased toxicity for the cell. In other neurodegenerative diseases like Parkinson's disease, oligomeric species of α-synuclein have been shown to drive toxicity in numerous studies (Prots et al. 2013; Winner et al. 2011). In Alzheimer's disease smaller fragments of misfolded proteins have also been shown to be more effectively propagated, which leads to faster progression of the illness (Jucker and Walker 2011). The increased CSA of the Htt aggregates could

therefore even have a protective effect on the cell. To investigate that further, cell viability or toxicity assays would need to be performed.

In the next step, the aggregate/cell ratio was measured to investigate whether the number of aggregates per cell changed due to HR23A or HR23B knockout. Using anti-GAPDH antibody, it was possible to visualize the cell borders and the same protocol of Operetta high content analysis system, as mentioned above, was used to detect Htt aggregates for analysis. The results showed an increased aggregate/cell ratio in $HR23B^{KO}$ cells compared to WT and $HR23A^{KO}$ cells. Comparing WT with $HR23A^{KO}$ cells showed no effect. An increased number of aggregates per cell in $HR23B^{KO}$ indicated that in the absence of HR23B either more aggregates are formed or less are degraded. Linda Kulka could also show that overexpression of HR23B achieved the opposite effect and resulted in a decreased aggregate/ cell ratio compared to control conditions. This increase in aggregate frequency could have an impact on the spreading of the disease within the nervous system and therefore on its progression.

To draw a connection between HR23B and pathological Htt, IF staining was performed to colocalize the two proteins. It was visible that in all conditions HR23B is distributed across the whole cell, showing more intense signals in the nucleus. In Htt97Q transfected cells it could be observed that HR23B colocalizes with perinuclear Htt structures. Using a non-confocal microscope, an interference of signals is possible. It is noticeable however that the pattern of HR23B and Htt signals is not identical, which makes a bleed through in between the channels unlikely. Yang et al. could show that HR23B colocalizes in a similar pattern with pathologically elongated Htt (Yang et al. 2018). In models for amyotrophic lateral sclerosis and frontotemporal dementia, HR23B had been shown to colocalize with aggregates of multiple pathogenic proteins (Riemslagh et al. 2019; Zhang et al. 2016). Interestingly, Linda Kulka could show similar colocalization patterns and even show that overexpression of HR23B lead to a change of aggregation behavior of Htt97Q (data not published).

For further analysis of the interaction between HR23B and pathological Htt, CO-IP experiments were performed. In this case, cells were transfected with GFP-tagged Htt and precipitation performed using GFP antibody. The results show that the GFP signal of GFP-Htt74Q increased substantially in the IP sample, which demonstrated a successful pulldown of the Htt construct (see figure 17). Additionally, the anti-HR23B immunoblot showed a faint band at approximately 53 kDa in the IP of GFP-Htt74Q transfected cells. Although this band ran slightly lower than expected, it is interesting to note that it does not appear in the negative controls. This makes it less likely to be an

unspecific signal. However, the experiment was only performed once and would need to be replicated to make a better statement.

If it were a specific signal, the question would remain why it runs lower than the usual HR23B protein. It is possible that HR23B undergoes further proteolytic modification which leads to a smaller variant of the protein. In the immunoblot of the nuclear cytoplasmic extraction assay, a comparable band was visible in the total and nuclear protein fraction, which indicated a possible interaction with a nuclear protease that led to this result.

In addition to the CO-IP experiments, filter retardation assays were performed with the similar aim of detecting an interaction between pathological Htt and HR23B. This method has been used before to detect and quantify different polyglutamine aggregates (Sin et al. 2018). In this case U2OS cells transfected with GFP tagged constructs of Htt74Q, Htt23Q, as well as peGFP and pcDNA3 as controls, were filtered through CA and NC membranes to separate aggregated from non-aggregated proteins. These membranes were analyzed using different antibodies and one example of resulting dot blots is shown in figure 24 (appendix). In the first blot, the successful transfection of GFP tagged constructs could be verified using anti-GFP antibody. Other than expected, however, non-aggregating proteins such as GFP-Htt23Q and peGFP were detected on the CA membrane. It is possible that this is because the protein concentration in the samples was too high, surpassing the filtering capacity of the CA membrane. Also, GFP-Htt74Q signal was detected on the NC membrane, suggesting that not all GFP-Htt74Q species were present in their aggregated form. In the anti-HR23B blot signals could be detected on both membranes in every condition. The intensity of the HR23B signal, however, decreased in the GFP-Htt74Q sample on the NC membrane. This could indicate that HR23B interacts with pathological Htt and is therefore part of aggregate complexes which get filtered by the CA membrane. On the other hand, the anti-GFP blot contradicts this idea, since the GFP signal itself does not decrease on the NC membrane in GFP-Htt74Q transfected samples. Furthermore, the anti-actin blot, used as the control, showed inconsistent signals, indicating varying protein concentrations.

Unfortunately, due to inconsistent results and contradicting signals in the control blot it is not possible to draw any direct conclusion from these experiments. The method itself is promising, however, and in order to produce viable results the method would have to be optimized. One possibility would be to create different lysate dilutions and test for the ideal protein concentration, ensuring strong immunoblot signal while not surpassing the filtering capacity of the CA membrane. On top of that, the protocol for the anti-oligomer

and anti-amyloid fibril blot would have to be adjusted to reduce background and increase specific signal.

The experiments concerning the interaction of the shuttling factors with pathological Htt were first performed only concerning HR23B. Research was able to show, however, that Rad23A, the homologue of HR23A in yeast, interacts with Htt using a yeast two-hybrid screening technique (Haenig et al. 2020). Further investigation of the interaction between HR23A and Htt in a human model would therefore be crucial to be performed in the future.

Regarding all experiments, it could be shown that HR23B and in some cases HR23A influenced the aggregation morphology and frequency of pathological Htt. The cell-based model of HD was first tested and the formation of aggregated was confirmed with two different aggregate stains using IF. Then it was found that the CSA of Htt97Q aggregates increased, as well as the aggregate/ cell ratio increased in HR23B^{KO} cells. In HR23A^{KO} cells the CSA of Htt97 aggregates showed a tendency to be increased in the IF images obtained, however this proved not to be statistically relevant. The aggregate/cell ratio, however, increased significantly. Also, it could be shown that Htt97Q colocalizes with HR23B in IF and one CO-IP experiment hinted towards a direct interaction between the two proteins.

In all the experiments above, U2OS cells served as a model organism. These cells were chosen firstly because the proteins of interest HR23A and HR23B could be easily detected (New et al. 2013) and on top of that due to the larger N/C ratio, which made it easier to detect and quantify subcellular structures. Concerning the applicability of the results, a cell line with neuronal origin would have been a more ideal model for HD. To improve this, Helena Grebenchuck aimed to establish HR23A and HR23B knockout cell lines in neuronal SH-SY5Y cells for experiments in the future.

5.3. HR23B modulates the effect of HDACi treatment on cell cycle and translatory rates of U2OS cells

In another part of this research project, the impact of HDACi treatment on U2OS, HR23A^{KO} and HR23B^{KO} cells and how HR23 proteins modulate this effect was investigated. When treating cells with the HDACi, histone-deacetylases are inhibited which results in hyperacetylation of proteins. This posttranslational modification can occur *N*-terminally or on lysine residues (*K*-acetylation). It could be significant to investigate whether this PTM competes with *K*-ubiquitination and therefore impacts the functioning of the UPS. A change of ubiquitination patterns might have a great impact on the degradation mechanisms in the cell and therefore also on misfolded protein species. In this section preliminary experiments were performed, which targeted the impact of HDACi on the cell cycle and translatory rates of U2OS cells as well as HR23A/B^{KO} cells. These results might be used as a basis for further investigations of the impact of HDACi on the UPS and the role of HR23 proteins in this context in the future.

In the first experiment performed with HDACi treatment 4.4.1, cell cycle analysis of SAHA (Vorinostat) treated cells was carried out. Vorinostat is a pan-HDACi, which inhibits a broad range of histone deacetylases and was approved for clinical use in cutaneous t-cell lymphoma in 2006 (Mann et al. 2007). It is not fully understood what drives the anti-cancer effect of HDACi treatment. It is suggested however, that altered acetylation patterns of cytoplasmic proteins might reveal more targets for PQC systems such as molecular chaperones and the UPS. It has also been shown that HDACi can induce apoptosis and promote protein misfolding (Kulka et al. 2020), which may lead to increased cancer cell death. Vorinostat has been tested in multiple clinical trials for different cancer therapies and as a therapeutic agent in neurodegenerative disorders.

Similar to the cell cycle analysis in 4.2.2, U2OS, HR23A^{KO} and HR23B^{KO} cells were used and different concentrations of SAHA were added for 24 h. It was noticeable that with rising concentration of HDACi treatment, the distribution of cells in the different cell cycle phases changed. The number of cells in subG1 phase which represented debris and dead cells rose with increasing SAHA concentration. This is coherent with studies of HDACi treatment that showed increased cell toxicity and cell cycle arrest (Natarajan et al. 2019). Comparing this effect between HR23A/B^{KO} and WT cells indicated no difference. This suggests that the knockout of HR23 proteins does not impact the overall rate of apoptosis under HDACi treatment. Especially in HR23B^{KO} cells, a desensitization against HDACi would have been expected since it had been found that cell toxicity of SAHA/ Vorinostat was HR23B-dependent in some cancer types (Hurwitz et al. 2012).

HR23B had also been found to serve as a sensitivity biomarker for HDACi induced apoptosis (Khan et al. 2010). It is possible that analyzing the subG1 phase and correlating it to the rate of apoptosis does not create results that are sensitive enough to demonstrate this dependency. In the subG1 population the DNA is fragmented, which is often a result of apoptosis, but can also represent aneuploid cells. To measure the rate of apoptosis more precisely, an additional staining with annexin V for example could be performed in the future (van Engeland et al. 1998).

Looking at G1 and S phase, the quality of the effect of HDACi treatment changed comparing the two knockout cell lines and the WT. In G1 phase, an exaggerated decrease of relative cell amounts in HR23A^{KO} compared to HR23B^{KO} cells in all SAHA concentrations could be observed. Interestingly, comparing either knockout cell line to the WT showed no effect. It is possible that this is due to the effect that was observed in 4.1.3. Here, HR23B expression levels seemed to be higher following the HR23A knockout compared to the WT. This might explain the greater effect when comparing the two knockout cell lines with each other rather than with the WT. Since finishing this study, the results of 4.1.3 could be statistically verified by Linda Kulka (data not published).

The change of relative cell amount under HDACi treatment was most diverse during S-phase. Here, in HR23B^{KO} cells the relative cell amount increased (see fig. 16), while the relative cell amounts in HR23A^{KO} stayed the same and even decreased in U2OS cells. The increase of relative cell amounts in S phase of HR23B^{KO} cells was only statistically relevant in the condition with the highest concentration of SAHA (10µM). In HR23A^{KO} a slight tendency of increase of cells in S phase could be observed, although the data points vary too much to verify this statistically. The question remains, why this tendency is so diverse to what is observed in U2OS cell under HDACi treatment. In 4.2.2 it had been observed that the knockout of HR23 proteins led to cell cycle arrest or inhibition at G1/S phase checkpoint. Looking at the results from 4.4.1 it seems as though HDACi treatment might reverse this effect. One hypothesis might be that the degradation of certain cell cycle inhibitors is dependent on HR23 proteins, which may lead to their accumulation upon knockout. Treatment with HDACi, which enhances acetylation, may then interfere on the same residues of ubiquitination, and target them for degradation via ubiquitin-independent routes leading to disinhibition of the cell cycle.

Drawing information from the cell cycle analysis, it was established that HDACi treatment with 5 µM SAHA for 24 h was the appropriate concentration to show the greatest effect with the least amount of cell loss due to toxicity. This is why this concentration was used to repeat puromycin incorporation assays and investigate the translatory rates of U2OS

and HR23A/B^{KO} cells under the treatment. It was found that incubating the cells with HDACi lead to a decrease in overall translatory rates in all cell lines. The control conditions that were treated with DMSO showed similar results, comparing the different cell lines as in 4.2.3, which further verified these findings and the impact of HR23B knockout on translatory rates of the cell. When comparing the relative decrease of translatory rates in the different cell lines it could be observed that in HR23B^{KO} cells translatory rates were overall lower but less impacted by HDACi treatment. As mentioned before, it had been shown that the toxicity of HDACi is dependent on HR23B (Hurwitz et al. 2012). The knockout of the protein might therefore also lead to decreased impact of HDACi translatory rates of the cells.

In summary, it could be observed that HDACi treatment impacts both cell cycle progression and translatory rate in U2OS and HR23A/B^{KO} cells. In case of HR23B^{KO}, the relative number of cells in S phase increased under 10 µM SAHA treatment, whereas it decreased in U2OS cells or stayed the same in HR23A^{KO}. Also, the decrease of translatory rate under HDACi treatment was less intense in HR23A^{KO} and HR23B^{KO}, compared to U2OS cells.

As mentioned before, these experiments were conducted as groundwork to investigate the impact of HDACi on the UPS in the context of protein misfolding and neurodegenerative diseases. Going along with this, Linda Kulka had already performed IF staining of Htt97Q transfected U2OS cells under HR23B overexpression and consecutive HDACi treatment. The results showed that Htt97Q aggregates could be dissolved under HR23B overexpression and treatment with an HDACi could reverse this effect (data not published). This result suggests that there might be a connection between the role of HR23B and HDACi treatment in the context of protein misfolding, which would need to be investigated further.

6. Conclusion

The aim of this work was to investigate the influence of proteasome shuttling factors HR23A and HR23B on misfolded Htt, specifically focusing on aggregate morphology and distribution as well as protein-protein interaction. First, using IF, Htt could be visualized in U2OS cells, showing that pathological Htt forms aggregates, whereas physiological Htt was distributed evenly in the cell. The formation of Htt aggregates could here be verified using two different aggregate stains Proteostat® and X-34. On top of that, when visualizing HR23B in IF, co-localization of the proteasome shuttling factor and Htt aggregates could be observed. Then, in one CO-IP experiment, a small amount of HR23B in the precipitate of pathological Htt could be observed.

Having verified the accurate expression of the Htt constructs, the morphology and frequency of Htt aggregates was then analyzed in HR23A/B^{KO} cells. Using two different approaches, the CSA of Htt aggregates was measured. Both showed an increase of CSA in HR23B^{KO} cells. In HR23A^{KO} cells, the aggregates also showed a tendency to have increased CSAs, which could be quantified in only one of the two experimental approaches. Additionally, an increase in aggregate/cell ratio could be observed in HR23B^{KO} cells. This showed that the absence of HR23B might modulate aggregate formation and distribution of pathological Htt. What is not known yet is whether the increase of CSA correlates with higher or lower toxicity of the aggregates and whether the aggregates might also be less dense compared to WT. To answer these questions more research will have to be made.

Another major part of this work was the further characterization of HR23A's and HR23B's. function, primarily focusing on the effect of their knockout on cell cycle, cell morphology and translatory rate. It could be observed in WB that HR23B expression levels rise in HR23A^{KO} cells, which might explain the phenomenon that HR23A^{KO} showed less effect in many experiments and might suggest that HR23B can replace HR23A in its function. In cell cycle analysis it was observed that in HR23A^{KO} and HR23B^{KO} cells the relative cell amount in G1 phase increases, while it decreases in S phase and G2 phase. This might lead to the inhibition of cell cycle progression, and therefore cell proliferation. In the Operetta experiment it could further be shown that the N/C ratio decreases in HR23A^{KO} and HR23B^{KO}. Any change in N/C ratio can be a sign of pathology in a cell and is likely to correlate with lower proliferation rates. Along with this, using puromycin incorporation assays, it could be shown that also the translatory rate decreases in HR23B knockout. In conclusion, HR23B^{KO} seems to lead to a decrease of cellular proliferation and overall protein synthesis. What mechanism is behind those

effects remains unclear. Elucidating their role in cellular homeostasis, however, is crucial for example in predicting possible side effects of future therapeutic interventions.

In the third part of the project, the effects of HDACi Vorinostat on cell cycle and translatory rates in U2OS and HR23A/B^{KO} cells were investigated. These experiments served as preliminary data for further research on the effect of acetylation on the UPS and on misfolded proteins. HDACi treatment led to decreased translatory rates in all cell lines, however, HR23A/B^{KO} cells showed lower levels of translatory decline. This might suggest that the absence of HR23A and HR23B might lead to decreased HDACi efficacy. In cell cycle analysis the most diverse effect was observed during S phase, HDACi treatment led to a decrease in relative cell amount in WT cells, but in increase in HR23B^{KO}. Why this effect is obtained will need to be investigated in further research.

This study has shown that proteasome shuttling factors HR23A and HR23B modulate the aggregation behavior of pathological Htt in a cellular model and their knockout leads to significant changes in protein homeostasis of a cell. To gain more insight and to improve the applicability of these results further experiments in neuronal cell lines should be continued. On top of that, it is important to investigate whether the change of aggregation behavior in Htt is beneficial or toxic for the cell and for disease propagation. Nonetheless, these results shed light on the abundance of mechanisms that shape protein quality control and might be used in the future to create new therapeutic strategies for age-related neurodegenerative disease like HD.

7. Literature

Andrew, S. E. 1993. "The relationship between trinucleotide {CAG) repeat length and clinical features of Huntington's disease."

Anfinsen, C. B. 1973. "Principles that Govern the Folding of Protein Chains." *Science* 181 (4096):223-230.

Araki, Marito, Chikahide Masutani, Mitsuyo Takemura, Akio Uchida, Kaoru Sugasawa, Jun Kondoh, Yoshiaki Ohkuma, and Fumio Hanaoka. 2001. "Centrosome Protein Centrin 2/Caltractin 1 Is Part of the Xeroderma Pigmentosum Group C Complex That Initiates Global Genome Nucleotide Excision Repair *." *Journal of Biological Chemistry* 276 (22):18665-18672. doi: 10.1074/jbc.M100855200.

Arrasate, Montserrat, Siddhartha Mitra, Erik S. Schweitzer, Mark R. Segal, and Steven Finkbeiner. 2004. "Inclusion body formation reduces levels of mutant huntingtin and the risk of neuronal death." *Nature* 431 (7010):805-810. doi: 10.1038/nature02998.

Barron, J. C., E. P. Hurley, and M. P. Parsons. 2021. "Huntingtin and the Synapse." *Front Cell Neurosci* 15:689332. doi: 10.3389/fncel.2021.689332.

Bates, G. P., L. Mangiarini, and S. W. Davies. 1998. "Transgenic mice in the study of polyglutamine repeat expansion diseases." *Brain Pathol* 8 (4):699-714. doi: 10.1111/j.1750-3639.1998.tb00196.x.

Bertoli, C., J. M. Skotheim, and R. A. de Bruin. 2013. "Control of cell cycle transcription during G1 and S phases." *Nat Rev Mol Cell Biol* 14 (8):518-28. doi: 10.1038/nrm3629.

Burnette, W. Neal. 1981. "“Western Blotting”: Electrophoretic transfer of proteins from sodium dodecyl sulfate-polyacrylamide gels to unmodified nitrocellulose and radiographic detection with antibody and radioiodinated protein A." *Analytical Biochemistry* 112 (2):195-203. doi: https://doi.org/10.1016/0003-2697(81)90281-5.

Chen, Li, and Kiran Madura. 2002. "Rad23 Promotes the Targeting of Proteolytic Substrates to the Proteasome." *Molecular and Cellular Biology* 22 (13):4902-4913. doi: 10.1128/MCB.22.13.4902-4913.2002.

Chen, M., and P. G. Wolynes. 2017. "Aggregation landscapes of Huntingtin exon 1 protein fragments and the critical repeat length for the onset of Huntington's disease." *Proc Natl Acad Sci U S A* 114 (17):4406-4411. doi: 10.1073/pnas.1702237114.

Clark, P. L. 2004. "Protein folding in the cell: reshaping the folding funnel." *Trends Biochem Sci* 29 (10):527-34. doi: 10.1016/j.tibs.2004.08.008.

Clarke, D. J., G. Mondesert, M. Segal, B. L. Bertolaet, S. Jensen, M. Wolff, M. Henze, and S. I. Reed. 2001. "Dosage suppressors of pds1 implicate ubiquitin-associated domains in checkpoint control." *Mol Cell Biol* 21 (6):1997-2007. doi: 10.1128/mcb.21.6.1997-2007.2001.

Collins, G. A., and A. L. Goldberg. 2020. "Proteins containing ubiquitin-like (Ubl) domains not only bind to 26S proteasomes but also induce their activation." *Proc Natl Acad Sci U S A* 117 (9):4664-4674. doi: 10.1073/pnas.1915534117.

Elder, Robert T., Xiang-qian Song, Mingzhong Chen, Kevin M. Hopkins, Howard B. Lieberman, and Yuqi Zhao. 2002. "Involvement of rhp23, a Schizosaccharomyces pombe homolog of the human HHR23A and Saccharomyces cerevisiaeRAD23 nucleotide excision repair genes, in cell cycle control and protein ubiquitination." *Nucleic Acids Research* 30 (2):581-591. doi: 10.1093/nar/30.2.581.

Elsasser, Suzanne, Devin Chandler-Militello, Britta Müller, John Hanna, and Daniel Finley. 2004. "Rad23 and Rpn10 Serve as Alternative Ubiquitin Receptors for the Proteasome *." *Journal of Biological Chemistry* 279 (26):26817-26822. doi: 10.1074/jbc.M404020200.

Enam, Syed Usman, Boris Zinshteyn, Daniel H. Goldman, Madeline Cassani, Nathan M. Livingston, Geraldine Seydoux, and Rachel Green. 2020. "Puromycin reactivity does not

accurately localize translation at the subcellular level." *eLife* 9:e60303. doi: 10.7554/eLife.60303.

Group, Huntington's Disease Collaborative Research. 1993. "A novel gene containing a trinucleotide repeat that is expanded and unstable on Huntington's disease chromosomes. The Huntington's Disease Collaborative Research Group." *Cell* 72 (6):971-83. doi: 10.1016/0092-8674(93)90585-e.

Haenig, C., N. Atias, A. K. Taylor, A. Mazza, M. H. Schaefer, J. Russ, S. P. Riechers, S. Jain, M. Coughlin, J. F. Fontaine, B. D. Freibaum, L. Brusendorf, M. Zenkner, P. Porras, M. Stroedicke, S. Schnoegl, K. Arnsburg, A. Boeddrich, L. Pigazzini, P. Heutink, J. P. Taylor, J. Kirstein, M. A. Andrade-Navarro, R. Sharan, and E. E. Wanker. 2020. "Interactome Mapping Provides a Network of Neurodegenerative Disease Proteins and Uncovers Widespread Protein Aggregation in Affected Brains." *Cell Rep* 32 (7):108050. doi: 10.1016/j.celrep.2020.108050.

Hartl, F. U. 1996. "Molecular chaperones in cellular protein folding." *Nature* 381 (6583):571-9. doi: 10.1038/381571a0.

Heinen, Christian, Klàra Ács, Deborah Hoogstraten, and Nico P. Dantuma. 2011. "C-terminal UBA domains protect ubiquitin receptors by preventing initiation of protein degradation." *Nature Communications* 2 (1):191. doi: 10.1038/ncomms1179.

Hurwitz, J. L., I. Stasik, E. M. Kerr, C. Holohan, K. M. Redmond, K. M. McLaughlin, S. Busacca, D. Barbone, V. C. Broaddus, S. G. Gray, K. J. O'Byrne, P. G. Johnston, D. A. Fennell, and D. B. Longley. 2012. "Vorinostat/SAHA-induced apoptosis in malignant mesothelioma is FLIP/caspase 8-dependent and HR23B-independent." *Eur J Cancer* 48 (7):1096-107. doi: 10.1016/j.ejca.2011.11.009.

Jucker, M., and L. C. Walker. 2011. "Pathogenic protein seeding in Alzheimer disease and other neurodegenerative disorders." *Ann Neurol* 70 (4):532-40. doi: 10.1002/ana.22615.

Kaltenbach, Linda, Eliana Romero, Robert Becklin, Rakesh Chettier, Russell Bell, Amit Phansalkar, Andrew Strand, Cameron Torcassi, Justin Savage, Anthony Hurlburt, Guang-Ho Cha, Lubna Ukani, Cindy Chepanoske, Yuejun Zhen, Sudhir Sahasrabudhe, James Olson, Cornelia Kurschner, Lisa Ellerby, John Peltier, and Robert Hughes. 2007. "Huntingtin Interacting Proteins Are Genetic Modifiers of Neurodegeneration." *PLoS genetics* 3:e82. doi: 10.1371/journal.pgen.0030082.

Katiyar, S., G. Li, and W. J. Lennarz. 2004. "A complex between peptide:N-glycanase and two proteasome-linked proteins suggests a mechanism for the degradation of misfolded glycoproteins." *Proc Natl Acad Sci U S A* 101 (38):13774-9. doi: 10.1073/pnas.0405663101.

Katiyar, Samiksha, and William J. Lennarz. 2005. "Studies on the intracellular localization of hHR23B." *Biochemical and Biophysical Research Communications* 337 (4):1296-1300. doi: https://doi.org/10.1016/j.bbrc.2005.09.192.

Khan, O., S. Fotheringham, V. Wood, L. Stimson, C. Zhang, F. Pezzella, M. Duvic, D. J. Kerr, and N. B. La Thangue. 2010. "HR23B is a biomarker for tumor sensitivity to HDAC inhibitor-based therapy." *Proc Natl Acad Sci U S A* 107 (14):6532-7. doi: 10.1073/pnas.0913912107.

Kim, Byoungkook, Kyoung-Seok Ryu, Hyun-Jin Kim, Sung-Jae Cho, and Byong-Seok Choi. 2005. "Solution structure and backbone dynamics of the XPC-binding domain of the human DNA repair protein hHR23B." *The FEBS Journal* 272 (10):2467-2476. doi: https://doi.org/10.1111/j.1742-4658.2005.04667.x.

Komander, D., and M. Rape. 2012. "The ubiquitin code." *Annu Rev Biochem* 81:203-29. doi: 10.1146/annurev-biochem-060310-170328.

Krishan, A. 1975. "Rapid flow cytofluorometric analysis of mammalian cell cycle by propidium iodide staining." *J Cell Biol* 66 (1):188-93. doi: 10.1083/jcb.66.1.188.

Kulka, L. A. M., P. V. Fangmann, D. Panfilova, and H. Olzscha. 2020. "Impact of HDAC Inhibitors on Protein Quality Control Systems: Consequences for Precision Medicine in Malignant Disease." *Front Cell Dev Biol* 8:425. doi: 10.3389/fcell.2020.00425.

Laemmli, U. K. 1970. "Cleavage of structural proteins during the assembly of the head of bacteriophage T4." *Nature* 227 (5259):680-5. doi: 10.1038/227680a0.

Lashuel, Hilal A., Benjamin M. Petre, Joseph Wall, Martha Simon, Richard J. Nowak, Thomas Walz, and Peter T. Lansbury. 2002. "α-Synuclein, Especially the Parkinson's Disease-associated Mutants, Forms Pore-like Annular and Tubular Protofibrils." *Journal of Molecular Biology* 322 (5):1089-1102. doi: https://doi.org/10.1016/S0022-2836(02)00735-0.

Liu, Yanshun, and David Eisenberg. 2002. "3D domain swapping: as domains continue to swap." *Protein science : a publication of the Protein Society* 11 (6):1285-1299. doi: 10.1110/ps.0201402.

Mangiarini, L., K. Sathasivam, M. Seller, B. Cozens, A. Harper, C. Hetherington, M. Lawton, Y. Trottier, H. Lehrach, S. W. Davies, and G. P. Bates. 1996. "Exon 1 of the HD gene with an expanded CAG repeat is sufficient to cause a progressive neurological phenotype in transgenic mice." *Cell* 87 (3):493-506. doi: 10.1016/s0092-8674(00)81369-0.

Mann, B. S., J. R. Johnson, M. H. Cohen, R. Justice, and R. Pazdur. 2007. "FDA approval summary: vorinostat for treatment of advanced primary cutaneous T-cell lymphoma." *Oncologist* 12 (10):1247-52. doi: 10.1634/theoncologist.12-10-1247.

Miettinen, T. P., and M. Björklund. 2017. "Mitochondrial Function and Cell Size: An Allometric Relationship." *Trends Cell Biol* 27 (6):393-402. doi: 10.1016/j.tcb.2017.02.006.

Nasir, J., S. B. Floresco, J. R. O'Kusky, V. M. Diewert, J. M. Richman, J. Zeisler, A. Borowski, J. D. Marth, A. G. Phillips, and M. R. Hayden. 1995. "Targeted disruption of the Huntington's disease gene results in embryonic lethality and behavioral and morphological changes in heterozygotes." *Cell* 81 (5):811-23. doi: 10.1016/0092-8674(95)90542-1.

Natarajan, U., T. Venkatesan, V. Radhakrishnan, S. Samuel, P. Rasappan, and A. Rathinavelu. 2019. "Cell Cycle Arrest and Cytotoxic Effects of SAHA and RG7388 Mediated through p21(WAF1/CIP1) and p27(KIP1) in Cancer Cells." *Medicina (Kaunas)* 55 (2). doi: 10.3390/medicina55020030.

Navarro, Susanna, and Salvador Ventura. 2014. "Fluorescent dye ProteoStat to detect and discriminate intracellular amyloid-like aggregates in Escherichia coli." *Biotechnology Journal* 9 (10):1259-1266. doi: https://doi.org/10.1002/biot.201400291.

New, M., H. Olzscha, G. Liu, O. Khan, L. Stimson, J. McGouran, D. Kerr, A. Coutts, B. Kessler, M. Middleton, and N. B. La Thangue. 2013. "A regulatory circuit that involves HR23B and HDAC6 governs the biological response to HDAC inhibitors." *Cell Death Differ* 20 (10):1306-16. doi: 10.1038/cdd.2013.47.

Nowakowski, R. S., S. B. Lewin, and M. W. Miller. 1989. "Bromodeoxyuridine immunohistochemical determination of the lengths of the cell cycle and the DNA-synthetic phase for an anatomically defined population." *J Neurocytol* 18 (3):311-8. doi: 10.1007/bf01190834.

Okeke, Evelyn, Li Chen, and Kiran Madura. 2020. "The Cellular Location of Rad23, a Polyubiquitin Chain-Binding Protein, Plays a Key Role in Its Interaction with Substrates of the Proteasome." *Journal of Molecular Biology* 432 (7):2388-2404. doi: https://doi.org/10.1016/j.jmb.2020.03.001.

Okuda, Y., R. Nishi, J. M. Ng, W. Vermeulen, G. T. van der Horst, T. Mori, J. H. Hoeijmakers, F. Hanaoka, and K. Sugasawa. 2004. "Relative levels of the two mammalian Rad23 homologs determine composition and stability of the xeroderma pigmentosum group C protein complex." *DNA Repair (Amst)* 3 (10):1285-95. doi: 10.1016/j.dnarep.2004.06.010.

Olzscha, H., O. Fedorov, B. M. Kessler, S. Knapp, and N. B. La Thangue. 2017. "CBP/p300 Bromodomains Regulate Amyloid-like Protein Aggregation upon Aberrant Lysine Acetylation." *Cell Chem Biol* 24 (1):9-23. doi: 10.1016/j.chembiol.2016.11.009.

Øvrebø, J. I., Y. Ma, and B. A. Edgar. 2022. "Cell growth and the cell cycle: New insights about persistent questions." *Bioessays* 44 (11):e2200150. doi: 10.1002/bies.202200150.

Pickart, Cecile M. 2001. "Mechanisms Underlying Ubiquitination." *Annual Review of Biochemistry* 70 (1):503-533. doi: 10.1146/annurev.biochem.70.1.503.

Prots, I., V. Veber, S. Brey, S. Campioni, K. Buder, R. Riek, K. J. Böhm, and B. Winner. 2013. "α-Synuclein oligomers impair neuronal microtubule-kinesin interplay." *J Biol Chem* 288 (30):21742-54. doi: 10.1074/jbc.M113.451815.

Riemslagh, Frederike W., Hannes Lans, Harro Seelaar, Lies-Anne W. F. M. Severijnen, Shamiram Melhem, Wim Vermeulen, Eleonora Aronica, R. Jeroen Pasterkamp, John C. van Swieten, and Rob Willemsen. 2019. "HR23B pathology preferentially co-localizes with p62, pTDP-43 and poly-GA in C9ORF72-linked frontotemporal dementia and amyotrophic lateral sclerosis." *Acta Neuropathologica Communications* 7 (1):39. doi: 10.1186/s40478-019-0694-6.

Ross, C. A., and C. M. Pickart. 2004. "The ubiquitin-proteasome pathway in Parkinson's disease and other neurodegenerative diseases." *Trends Cell Biol* 14 (12):703-11. doi: 10.1016/j.tcb.2004.10.006.

Rubinsztein, D. C., J. Leggo, R. Coles, E. Almqvist, V. Biancalana, J. J. Cassiman, K. Chotai, M. Connarty, D. Crauford, A. Curtis, D. Curtis, M. J. Davidson, A. M. Differ, C. Dode, A. Dodge, M. Frontali, N. G. Ranen, O. C. Stine, M. Sherr, M. H. Abbott, M. L. Franz, C. A. Graham, P. S. Harper, J. C. Hedreen, M. R. Hayden, and et al. 1996. "Phenotypic characterization of individuals with 30-40 CAG repeats in the Huntington disease (HD) gene reveals HD cases with 36 repeats and apparently normal elderly individuals with 36-39 repeats." *Am J Hum Genet* 59 (1):16-22.

Sarkar, S., A. A. Davies, H. D. Ulrich, and P. J. McHugh. 2006. "DNA interstrand crosslink repair during G1 involves nucleotide excision repair and DNA polymerase zeta." *Embo j* 25 (6):1285-94. doi: 10.1038/sj.emboj.7600993.

Saudou, F., S. Finkbeiner, D. Devys, and M. E. Greenberg. 1998. "Huntingtin acts in the nucleus to induce apoptosis but death does not correlate with the formation of intranuclear inclusions." *Cell* 95 (1):55-66. doi: 10.1016/s0092-8674(00)81782-1.

Schmidt, Enrico K., Giovanna Clavarino, Maurizio Ceppi, and Philippe Pierre. 2009. "SUnSET, a nonradioactive method to monitor protein synthesis." *Nature Methods* 6 (4):275-277. doi: 10.1038/nmeth.1314.

Sebastian, J. A., M. J. Moore, E. S. L. Berndl, and M. C. Kolios. 2021. "An image-based flow cytometric approach to the assessment of the nucleus-to-cytoplasm ratio." *PLoS One* 16 (6):e0253439. doi: 10.1371/journal.pone.0253439.

Shacham, T., N. Sharma, and G. Z. Lederkremer. 2019. "Protein Misfolding and ER Stress in Huntington's Disease." *Front Mol Biosci* 6:20. doi: 10.3389/fmolb.2019.00020.

Sin, O., A. Mata-Cabana, R. I. Seinstra, and E. A. A. Nollen. 2018. "Filter Retardation Assay for Detecting and Quantifying Polyglutamine Aggregates Using Caenorhabditis elegans Lysates." *Bio Protoc* 8 (19). doi: 10.21769/BioProtoc.3042.

Styren, S. D., R. L. Hamilton, G. C. Styren, and W. E. Klunk. 2000. "X-34, a fluorescent derivative of Congo red: a novel histochemical stain for Alzheimer's disease pathology." *J Histochem Cytochem* 48 (9):1223-32. doi: 10.1177/002215540004800906.

Su, V., and A. F. Lau. 2009. "Ubiquitin-like and ubiquitin-associated domain proteins: significance in proteasomal degradation." *Cell Mol Life Sci* 66 (17):2819-33. doi: 10.1007/s00018-009-0048-9.

Sugasawa, K., C. Masutani, A. Uchida, T. Maekawa, P. J. van der Spek, D. Bootsma, J. H. Hoeijmakers, and F. Hanaoka. 1996. "HHR23B, a human Rad23 homolog, stimulates

XPC protein in nucleotide excision repair in vitro." *Mol Cell Biol* 16 (9):4852-61. doi: 10.1128/mcb.16.9.4852.

Sung, W. W., Y. M. Lin, P. R. Wu, H. H. Yen, H. W. Lai, T. C. Su, R. H. Huang, C. K. Wen, C. Y. Chen, C. J. Chen, and K. T. Yeh. 2014. "High nuclear/cytoplasmic ratio of Cdk1 expression predicts poor prognosis in colorectal cancer patients." *BMC Cancer* 14:951. doi: 10.1186/1471-2407-14-951.

Sweeney, Patrick, Hyunsun Park, Marc Baumann, John Dunlop, Judith Frydman, Ron Kopito, Alexander McCampbell, Gabrielle Leblanc, Anjli Venkateswaran, Antti Nurmi, and Robert Hodgson. 2017. "Protein misfolding in neurodegenerative diseases: implications and strategies." *Translational Neurodegeneration* 6 (1):6. doi: 10.1186/s40035-017-0077-5.

Tan, Xiaotong, Ruei-Yue Liang, and Show-Mei Chuang. 2015. "hHR23A is required to control the basal turnover of Chk1." *Cellular Signalling* 27 (11):2304-2313. doi: https://doi.org/10.1016/j.cellsig.2015.08.010.

van Engeland, M., L. J. Nieland, F. C. Ramaekers, B. Schutte, and C. P. Reutelingsperger. 1998. "Annexin V-affinity assay: a review on an apoptosis detection system based on phosphatidylserine exposure." *Cytometry* 31 (1):1-9. doi: 10.1002/(sici)1097-0320(19980101)31:1<1::aid-cyto1>3.0.co;2-r.

Varela, A. E., K. A. England, and S. Cavagnero. 2019. "Kinetic trapping in protein folding." *Protein Eng Des Sel* 32 (2):103-108. doi: 10.1093/protein/gzz018.

von Hertwig, Richard. 1903. *Über Korrelation von Zell-und Kerngröße und ihre Bedeutung für die geschlechtliche Differenzeierung und die Teilung der Zelle*.

Waelter, S., A. Boeddrich, R. Lurz, E. Scherzinger, G. Lueder, H. Lehrach, and E. E. Wanker. 2001. "Accumulation of mutant huntingtin fragments in aggresome-like inclusion bodies as a result of insufficient protein degradation." *Mol Biol Cell* 12 (5):1393-407. doi: 10.1091/mbc.12.5.1393.

Winner, B., R. Jappelli, S. K. Maji, P. A. Desplats, L. Boyer, S. Aigner, C. Hetzer, T. Loher, M. Vilar, S. Campioni, C. Tzitzilonis, A. Soragni, S. Jessberger, H. Mira, A. Consiglio, E. Pham, E. Masliah, F. H. Gage, and R. Riek. 2011. "In vivo demonstration that alpha-synuclein oligomers are toxic." *Proc Natl Acad Sci U S A* 108 (10):4194-9. doi: 10.1073/pnas.1100976108.

Yang, Hui, Hong-Wei Yue, Wen-Tian He, Jun-Ye Hong, Lei-Lei Jiang, and Hong-Yu Hu. 2018. "PolyQ-expanded huntingtin and ataxin-3 sequester ubiquitin adaptors hHR23B and UBQLN2 into aggregates via conjugated ubiquitin." *The FASEB Journal* 32 (6):2923-2933. doi: https://doi.org/10.1096/fj.201700801RR.

Yokoi, Masayuki, and Fumio Hanaoka. 2017. "Two mammalian homologs of yeast Rad23, HR23A and HR23B, as multifunctional proteins." *Gene* 597:1-9. doi: https://doi.org/10.1016/j.gene.2016.10.027.

Zhang, Y. J., T. F. Gendron, J. C. Grima, H. Sasaguri, K. Jansen-West, Y. F. Xu, R. B. Katzman, J. Gass, M. E. Murray, M. Shinohara, W. L. Lin, A. Garrett, J. N. Stankowski, L. Daughrity, J. Tong, E. A. Perkerson, M. Yue, J. Chew, M. Castanedes-Casey, A. Kurti, Z. S. Wang, A. M. Liesinger, J. D. Baker, J. Jiang, C. Lagier-Tourenne, D. Edbauer, D. W. Cleveland, R. Rademakers, K. B. Boylan, G. Bu, C. D. Link, C. A. Dickey, J. D. Rothstein, D. W. Dickson, J. D. Fryer, and L. Petrucelli. 2016. "C9ORF72 poly(GA) aggregates sequester and impair HR23 and nucleocytoplasmic transport proteins." *Nat Neurosci* 19 (5):668-677. doi: 10.1038/nn.4272.

8. Research theses

I. HR23B is expressed in both cytoplasm and nucleus of U2OS cells.

II. HR23B expression levels increase in HR23A^{KO} cells.

III. HR23B and HR23A knockout leads to the inhibition of cell cycle progression at the G1/S checkpoint, signified by relative accumulation of cells in G1 phase and decrease in S and G2 phase in U2OS cells.

IV. HR23B knockout leads to decreased translatory rates in U2OS cells.

V. Pathologically elongated Htt forms perinuclear aggregates in U2OS cells, whereas physiological Htt is distributed evenly.

VI. HR23B and pathological Htt colocalize in IF imaging in U2OS cells.

VII. HR23B knockout leads to increased CSA of pathologically elongated Htt in U2OS cells.

VIII. HR23B knockout leads to increased aggregate/ cell ratio of pathologically elongated Htt in U2OS cells.

IX. HR23A and HR23B knockout decrease the effect of HDACi treatment on cell cycle progression in U2OS cells.

X. HR23A and HR23B knockout decrease the effect of HDACi treatment on translatory rates in U2OS cells.

III. Acknowledgments

I extend my deepest gratitude to my grandparents Ingeborg Klein and Uwe Georg Klein for their unwavering love, encouragement, and belief in me throughout this journey. Your constant support has been my anchor, empowering me to pursue my dreams with determination and resilience.

I am also profoundly grateful to my supervisors Prof. Heidi Olzscha and Prof. Rüdiger Horstkorte for their invaluable guidance, expertise, and mentorship. Your insights and encouragement have been instrumental in shaping my research and academic growth.

I would like to express my gratitude to my friend and colleague Dr. Linda Kulka for her friendship, collaboration, and support. Your enthusiasm and positivity have made this academic journey truly fulfilling and enjoyable.

Heartfelt thanks also go to my mother Angela-Christiane Riemer and sister Almut-Christiane Riemer for their endless love and belief in my abilities. Your encouragement and support have inspired me to overcome any challenges and stay true to myself during this time.

To all those who have contributed to my thesis, whether through guidance, encouragement, or simply being there for me, I offer my sincerest thanks. Your support has been instrumental in making this journey a rewarding and transformative experience.

IV. Appendix

i. Full-size immunoblots of 4.1.1

In 4.1.1 nuclear cytoplasmic extraction assays were performed to localize HR23B within the cell compartments. Here, the controls of the nuclear and cytoplasmic protein fractions are depicted in full size alongside with their Ponceau staining. To verify the purity of the nuclear protein fraction anti-Histone H3 antibody was used, for the cytoplasmic protein fraction anti-β-tubulin antibody was used.

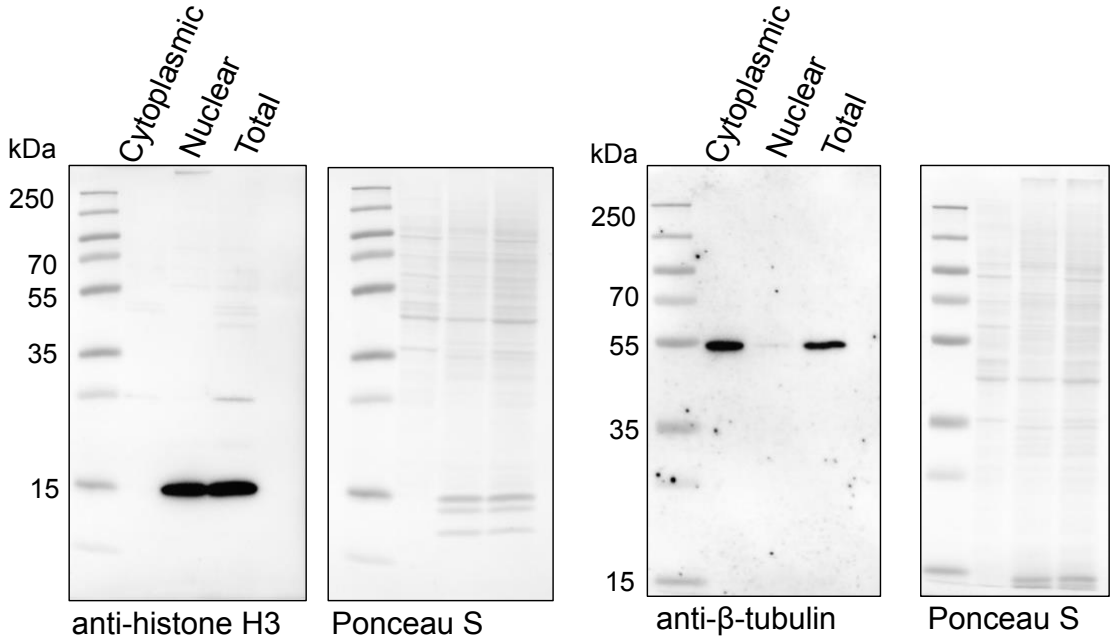

Figure 23: Full size control immunoblots of 4.1.1.

In this figure anti-histone H3 immunoblot, and anti-β-tubulin immunoblots and their corresponding Ponceau S staining are depicted in full size.

ii. Filter retardation assay of Htt constructs

In addition to the CO-IP (see 4.3.5) that was performed to detect an interaction between GFP-Htt74Q and HR23B, filter retardation assays were carried out with similar intention. Here, cell lysates were filtered through a CA membrane to separate aggregated proteins from non-aggregated proteins. On top of that, the aim was to investigate whether HR23B and pathological Htt could both be detected within those aggregates using dot blot.

In this experiment, U2OS cells were transfected with GFP tagged Htt constructs (GFP-Htt74Q, GFP-Htt23Q as well as peGFP and pcDNA3 as a control) using GeneJuice® (see protocol 3.2.3.4). The cells were then lysed, and equal amounts of protein were used to perform the filter retardation assay (protocol 3.2.2.8). The two different membranes were then analyzed using primary and secondary antibodies with similar

concentrations as in Western Blot. Here, anti-GFP, anti-HR23B, anti-oligomer and anti-amyloid fibril were used to detect the corresponding proteins and anti-actin was used as a control. In the anti-GFP blot, a strong signal was detected in all conditions except the pcDNA3 control. GFP-Htt74Q could be detected on both CA and NC membrane. Aggregated GFP-Htt74Q was detected on the CA membrane, as well as the NC membrane. Other than expected non-aggregating proteins such as GFP-Htt23Q and peGFP were also detected on the CA membrane. HR23B could be visualized in all samples on the CA and NC membrane. The anti-HR23B dot blot of Htt7Q transfected sample seemed less intense on the NC than the CA membrane.

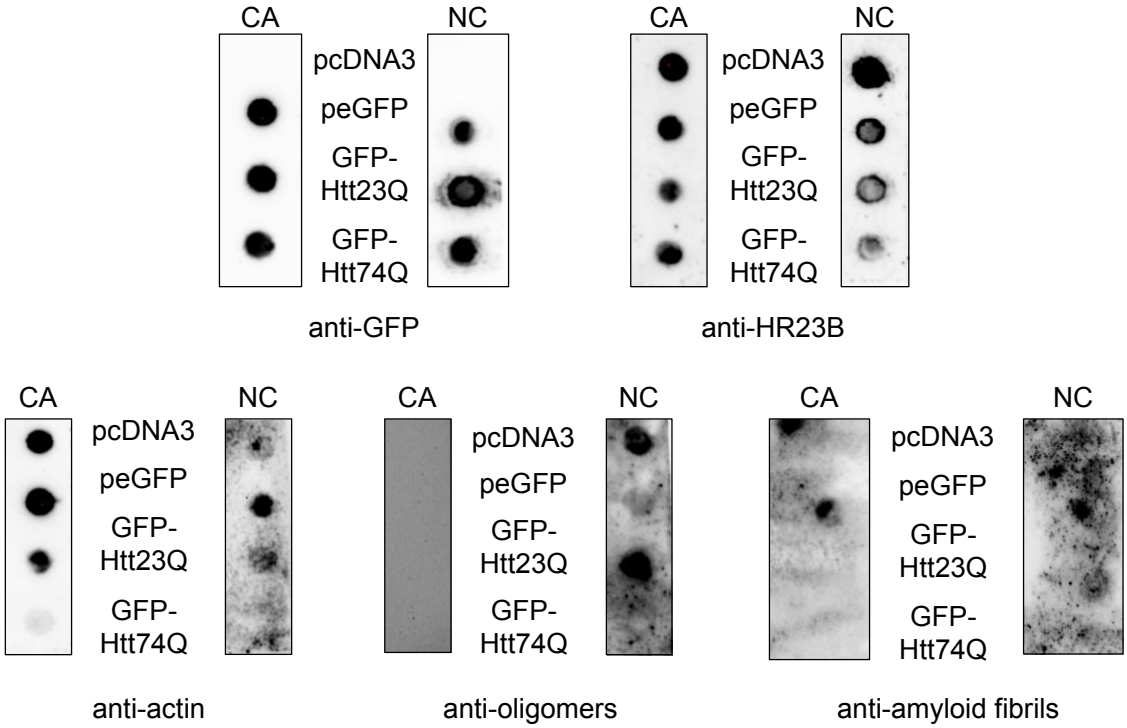

Figure 24: Dot blot of filter retardation assay using U2OS cells transfected with GFP-tagged Htt constructs.

U2OS cells were transfected with GFP-tagged GFP-Htt23Q and GFP-Htt74Q as well as the empty vectors peGFP and pcDNA3 as controls. Cells were lysed and filter retardation assay with a CA and NC membrane was performed (protocol see 3.2.2.8). Samples were filtered through both membranes using vacuum. Both membranes were afterwards analyzed using anti-GFP, anti-HR23B, anti-oligomer and anti-amyloid fibrils antibody (concentrations see 3.1.9.1). Anti-actin served as a control.

The anti-oligomers immunoblot showed that no oligomeric species could be detected on the CA membrane. On the NC membrane, oligomers could be visualized in samples pcDNA3 and GFP-Htt23Q. The anti-amyloid fibrils showed high background and no clear signals in any of the samples and both membranes. The CA membrane anti-actin control showed clear signals in all samples except GFP-Htt74Q. On the NC membrane, anti-actin signals were less clear, but the same pattern could be detected.

Erklärungen

(1) Ich erkläre, dass ich mich an keiner anderen Hochschule einem Promotionsverfahren unterzogen bzw. eine Promotion begonnen habe.

(2) Ich erkläre, die Angaben wahrheitsgemäß gemacht und die wissenschaftliche Arbeit an keiner anderen wissenschaftlichen Einrichtung zur Erlangung eines akademischen Grades eingereicht zu haben.

(3) Ich erkläre an Eides statt, dass ich die Arbeit selbstständig und ohne fremde Hilfe verfasst habe. Alle Regeln der guten wissenschaftlichen Praxis wurden eingehalten; es wurden keine anderen als die von mir angegebenen Quellen und Hilfsmittel benutzt und die den benutzten Werken wörtlich oder inhaltlich entnommenen Stellen als solche kenntlich gemacht.

Korfu (Griechenland), 05.05.24